

1     **Copernicus Atmosphere Monitoring Service - Regional Air Quality Production System v1.0**

2     Augustin Colette<sup>1</sup>, Gaëlle Collin<sup>2</sup>, François Besson<sup>2</sup>, Etienne Blot<sup>2</sup>, Vincent Guidard<sup>2,14</sup>, Frédéric Meleux<sup>1</sup>, Adrien Royer<sup>2</sup>,  
3     Valentin Petiot<sup>2,14</sup>, Claire Miller<sup>2</sup>, Oihana Fermond<sup>2</sup>, Alizé Jeant<sup>2</sup>, Mario Adani<sup>5,16</sup>, Joaquim Arteta<sup>14</sup>, Anna Benedictow<sup>10</sup>,  
4     Robert Bergström<sup>11</sup>, Dene Bowdalo<sup>8</sup>, Jorgen Brandt<sup>4</sup>, Gino Briganti<sup>5</sup>, Ana. C. Carvalho<sup>11</sup>, Jesper Heile Christensen<sup>4</sup>, Florian  
5     Couvidat<sup>1</sup>, Ilaria D’Elia<sup>5</sup>, Massimo D’Isidoro<sup>5</sup>, Hugo Denier van der Gon<sup>12</sup>, Gaël Descombes<sup>1</sup>, Enza Di Tomaso<sup>3, 8</sup>, John  
6     Douros<sup>13</sup>, Jeronimo Escribano<sup>8</sup>, Henk Eskes<sup>13</sup>, Hilde Fagerli<sup>10</sup>, Yalda Fatahi<sup>9</sup>, Johannes Flemming<sup>3</sup>, Elmar Friese<sup>6</sup>, Lise Frohn<sup>4</sup>,  
7     Michael Gauss<sup>10</sup>, Camilla. Geels<sup>4</sup>, Guido Guarnieri<sup>5</sup>, Marc Guevara<sup>8</sup>, Antoine Guion<sup>1</sup>, Jonathan Guth<sup>14</sup>, Risto Hänninen<sup>9</sup>, Kaj  
8     Hansen<sup>4</sup>, Ulas Im<sup>4</sup>, Ruud Janssen<sup>12</sup>, Marine Jeoffrion<sup>2</sup>, Mathieu Joly<sup>14</sup>, Luke Jones<sup>3</sup>, Oriol Jorba<sup>8</sup>, Evgeni Kadantsev<sup>9</sup>, Michael  
9     Kahnert<sup>11</sup>, Jacek W. Kaminski<sup>7</sup>, Rostislav Kouznetsov<sup>9</sup>, Richard Kranenburg<sup>12</sup>, Jeroen Kuenen<sup>12</sup>, Anne Caroline Lange<sup>6</sup>,  
10    Joachim Langner<sup>11</sup>, Victor Lannuque<sup>1</sup>, Francesca Macchia<sup>8</sup>, Astrid Manders<sup>12</sup>, Mihaela Mircea<sup>5</sup>, Agnes Nyiri<sup>10</sup>, Miriam Olid<sup>8</sup>,  
11    Carlos Pérez García-Pando<sup>8,15</sup>, Julia Palamarchuk<sup>9</sup>, Antonio Piersanti<sup>5</sup>, Blandine Raux<sup>1</sup>, Miha Razinger<sup>3</sup>, Lennard Robertson<sup>11</sup>,  
12    Arjo Segers<sup>12</sup>, Martijn Schaap<sup>12</sup>, Pilvi Siljamo<sup>9</sup>, David Simpson<sup>10</sup>, Mikhail Sofiev<sup>9</sup>, Anders Stangel<sup>9</sup>, Joanna Struzewska<sup>7</sup>,  
13    Carles Tena<sup>8</sup>, Renske Timmermans<sup>12</sup>, Thanos Tsikerdekis<sup>13</sup>, Svetlana Tsyro<sup>10</sup>, Svyatoslav Tyuryakov<sup>9</sup>, Anthony Ung<sup>1</sup>,  
14    Andreas Uppstu<sup>9</sup>, Alvaro Valdebenito<sup>10</sup>, Peter van Velthoven<sup>13</sup>, Lina Vitali<sup>5</sup>, Zhuyun Ye<sup>4</sup>, Vincent-Henri Peuch<sup>3</sup>, Laurence  
15    Rouil<sup>1, ^a</sup>

16    <sup>1</sup>INERIS: Institut National de l’Environnement Industriel et des Risques, Verneuil en Halatte, 60550, France

17    <sup>2</sup>Météo-France, Saint-Mandé, 94165, France

18    <sup>3</sup>ECMWF: European Centre for Medium-Range Weather Forecasts, Reading, RG2 9AX, United Kingdom

19    <sup>4</sup>Aarhus University: Roskilde, 4000, Denmark

20    <sup>5</sup>ENEA: Italian National Agency for New Technologies, Energy and Sustainable Economic Development, Bologna, 40129,  
21    Italy

22    <sup>6</sup>Forschungszentrum Jülich GmbH, ICE-3, Institute of Climate and Energy Systems - Troposphere, 52428 Jülich, Germany

23    <sup>7</sup>IEP-NRI: Institute of Environmental Protection - National Research Institute, Warsaw, 00-001, Poland

24    <sup>8</sup>BSC: Barcelona Supercomputing Center, Barcelona, 08034, Spain

25    <sup>9</sup>FMI, Finnish Meteorological Institute, Helsinki, 00-001, Finland

26    <sup>10</sup>MET Norway: Norwegian Meteorological Institute, Oslo, 0372, Norway

27    <sup>11</sup>SMHI: Swedish Meteorological and Hydrological Institute. Norrköping, SE-601 76, Sweden

28    <sup>12</sup>TNO: Netherlands Organisation for applied scientific research, Utrecht, 3584, The Netherlands

- 29 <sup>13</sup> KNMI: Royal Netherlands Meteorological Institute, De Bilt, 3730, The Netherlands
- 30 <sup>14</sup>: Centre National de Recherches Météorologiques - UMR 3589 CNRS/Météo-France, Toulouse, 31000, France
- 31 <sup>15</sup>. Catalan Institution for Research and Advanced Studies (ICREA), 08010, Barcelona, Spain
- 32 <sup>16</sup>Centro Euro-Mediterraneo sui Cambiamenti Climatici, 40127 Bologna, Italy
- 33 ^a: now at: ECMWF: European Centre for Medium-Range Weather Forecasts, Reading, RG2 9AX, United Kingdom
- 34 *Correspondence to:* Augustin Colette (augustin.colette@ineris.fr)

35

## 36    **Abstract**

37    The Copernicus Atmosphere Monitoring Service (CAMS) delivers a wide range of free and open products in relation to  
38    atmospheric composition at global and regional scales. The CAMS Regional Service produces daily forecasts, analyses, and  
39    reanalyses of air quality in Europe. This Service relies on a distributed modelling production by eleven teams in ten European  
40    countries: CHIMERE (France), DEHM (Denmark), EMEP (Norway), EURAD-IM (Germany), GEM-AQ (Poland), LOTOS-  
41    EUROS (The Netherlands), MATCH (Sweden), MINNI (Italy), MOCAGE (France), MONARCH (Spain), and SILAM  
42    (Finland). The project management and coordination of the service is devoted to a Centralised Regional Production Unit. Each  
43    model produces every day 24h analyses for the previous day and 97h forecasts for 19 chemical species over a spatial domain  
44    at 0.1x0.1 degree resolution (approximately 10km x 10km) with 420 points in latitude and 700 in longitude and 10 vertical  
45    levels. Six pollen species are also delivered for the surface forecasts. The eleven individual models are then combined into an  
46    ENSEMBLE median. In total, more than 82 billion data points are made available for public use on a daily basis.

47    The design of the system follows clear technical requirements in terms of consistency in the model setup and forcing fields  
48    (meteorology, surface anthropogenic emission fluxes, and chemical boundary conditions). But it also benefits from a diversity  
49    in the description of atmospheric processes through the design of the eleven European Chemistry Transport Model (CTM)  
50    involved.

51    The present article aims to provide a comprehensive technical documentation, both for the setup as well as for the diversity of  
52    CTMs involved in the Service. We also include an overview of the main output products, their public dissemination and the  
53    related evaluation and quality control strategy.

## 54    **1    Introduction**

55    The Copernicus Atmosphere Monitoring Service (CAMS, [atmosphere.copernicus.eu/](https://atmosphere.copernicus.eu/)) is the core global and regional  
56    atmospheric environmental service operated by the European Centre for Medium-Range Weather Forecast (ECMWF) within  
57    the European Union Copernicus Earth Observation Programme. It provides a wide range of free, open, and quality assured  
58    products in relation to global and regional air quality, inventory-based emissions, observation-based surface fluxes of  
59    greenhouse gases and from biomass burning, solar energy, ozone and UV radiation, and climate forcings (Peuch et al., 2022).

60    We focus here on the regional production service (<https://atmosphere.copernicus.eu/european-air-quality-forecast-plots/>)  
61    which provides daily 4-day forecasts of the main air quality species and analyses of the day before, as well as posterior re-  
62    analyses using the latest observation datasets available for assimilation. It constitutes today the reference air quality forecasting  
63    system at European scale by building upon a distributed production of eleven chemistry transport models operated in ten  
64    European countries, with a Centralised Regional Production Unit to ensure a consistent implementation. Such a comprehensive  
65    air quality forecasting system operated at continental scale has no equivalent in the world.

66    Air quality monitoring and forecasting constitute an essential activity to improve the knowledge of atmospheric composition  
67    and air pollution patterns and identify short and long-term mitigation strategies. In the European legislation, the Directive (Ec,  
68    2008) on ambient air quality and cleaner air for Europe of the European Parliament and of the European Council, defines limit  
69    and target values for regulatory ambient air concentrations and improvement of ambient air quality to avoid, prevent or reduce  
70    harmful effects on human health and the environment. To this end, it sets out the methodological requirements for the  
71    assessment of ambient air quality in Member States which are based on the implementation of adequate monitoring systems,  
72    typically relying on reference and standardised instruments operated at air quality monitoring stations whose data are reported  
73    to the Air Quality e-reporting database maintained by the European Environment Agency (which subsequently makes the data  
74    publicly available). A revision of the Ambient Air Quality Directive was adopted by the European Council in October 2024,  
75    the revision includes amongst other features, a stronger emphasis on the use of air quality models as well as an explicit reference  
76    to the Copernicus Atmosphere Monitoring Service as a trusted source of information products and supplementary tools to  
77    support reporting activities in relation to forecasting and management of air pollution episodes.

78    Modelling comes as a complementary information on ambient air quality. Fitness for forecasting purposes of air quality  
79    modelling has been widely documented (Zhang et al., 2012a, b), but air quality models are also essential to produce exposure  
80    maps through data assimilation or data fusion. In such processes, the prior modelled estimates of surface air concentrations of  
81    the main air pollutants are combined with in situ or remote sensing observations to produce improved mapping of air pollution,  
82    typically for use in health impact assessment or epidemiological studies (Shaddick et al., 2020). Air quality modelling and  
83    reanalyses are also typically used to anticipate ex-ante and assess ex-post the effectiveness of policy mitigation strategies. The

84 projections and hindcasts performed in the framework of the Convention on Long Range Transboundary Air Pollution  
85 (CLRTAP) of the United Nations Economic Commission for Europe Geneva Air Convention and its Gothenburg Protocol  
86 constitute a good example of atmospheric modelling activities in support of policy decisions at European scale (Maas and  
87 Grennfelt 2016).

88 Whereas several European countries or selected metropolitan areas operate their own air quality modelling system, there is  
89 also a need to produce air quality forecasts and analyses over the whole European continent: to provide background data for  
90 those local systems (chemical boundary conditions), for the areas not covered by any national system, or just as complementary  
91 information. The Copernicus Atmosphere Monitoring Service has played that role since 2015. It builds upon the earlier  
92 research and development phases initiated since 2005 through European collaborative research and innovation projects: GEMS  
93 (Hollingsworth, 2008) and MACC, MACC-II, and MACC-III (Marécal et al., 2015; Peuch et al., 2014).

94 The unique setup of the system allows it to reach an unprecedented level of quality and robustness by relying on a set of  
95 stringent common requirements combined with a large variety of Chemistry-Transport Models (CTMs). Since 2022, an  
96 ensemble of eleven CTMs have been used: CHIMERE (INERIS, France), DEHM (Aarhus Univ., Denmark), EMEP (Met  
97 Norway), EURAD-IM (Forschungszentrum Juelich, Germany), GEM-AQ (IEP-NRI, Poland), LOTOS-EUROS (TNO and  
98 KNMI, The Netherlands), MATCH (SMHI, Sweden), MINNI (ENEA, Italy), MOCAGE (Météo-France, France),  
99 MONARCH (BSC, Spain), and SILAM (FMI, Finland). Using an ensemble of CTMs allows at the same time to minimize the  
100 risk of failure in the daily operational production, and to increase the skill of the forecast (Galmarini et al., 2013). But  
101 consistency in the implementation is key to ensure the continuous improvement of the system, hence the crucial role of the  
102 CAMS Regional Central Production Unit led by Météo-France and INERIS.

103 Each model delivers every day 24h analyses and 97h forecast for 19 chemical species over a spatial domain at 0.1x0.1 degree  
104 resolution (approximately 10km x 10km) with 420 points in latitude and 700 in longitude and 10 vertical levels. Additionally,  
105 surface forecasts of six pollen species are delivered. With the 11 individual models and one ENSEMBLE median, it is a total  
106 of almost 82 billion data point made available for public use every day.

107 The results of the CAMS Regional Service are made publicly available as quick looks on the website  
108 [atmosphere.copernicus.eu/european-air-quality-forecast-plots](https://atmosphere.copernicus.eu/european-air-quality-forecast-plots) and the numerical outputs are disseminated on the Copernicus  
109 Atmosphere Data Store (ADS): [ads.atmosphere.copernicus.eu](https://ads.atmosphere.copernicus.eu). The typical use of the forecasts is as background information  
110 used by national and local air quality agencies, in addition to their knowledge about specific local air pollution sources. This  
111 can be done either qualitatively by the consultation of available online viewers, or by using the numerical data to feed  
112 downstream chemistry-transport, gaussian, or machine-learning models. The use of reanalyses is rather for policy applications

113 (for regulatory reporting obligations or to assess the impact policy interventions through trends analyses) or exposure  
114 assessment in health impact studies.

115 The aim of the present article is to provide a transparent and detailed documentation to serve as a reference for the user of  
116 CAMS Regional Air quality Products. It constitutes an update of the previous similar article devoted to the MACC regional  
117 forecast system (Marécal et al., 2015), whereas the system was still in research mode at the time and not fully operational. A  
118 focus on regional activities within the overall CAMS portfolio was also described in (Peuch et al., 2022). The CAMS Regional  
119 production system has evolved continuously over the past. In the present article, we provide a detailed description of the system  
120 as it stands in 2024. But since the near real time production of forecast and analysis remains available for public use with a 3-  
121 year retention time, and reanalysis data remain available since the beginning of the production, we also provide some  
122 information about the major evolutions in the recent past.

123 The main characteristics of the centralised production system are introduced in Section 2. This section covers the overall  
124 production workflow, but also the common features and requirements which apply to the distributed production of individual  
125 modelling teams such as the common external forcing data. Since the use of an ensemble of eleven different chemistry transport  
126 models is an important specificity of the service, we devote a large part of the paper in Section 3 to summarize the formulation  
127 of each model and how they adapt specifically to the requirement of the CAMS Regional Production System. The post-  
128 processing as well as some elements regarding the evaluation and quality control or the main uses of the production are  
129 presented in Section 4. In the conclusion (Section 5) we refer to the short and long-term development priorities to ensure the  
130 performance and sustainability of the system over the long term.

## 131    **2    Centralised Regional Production Unit**

### 132    **2.1    Organisation of the production system**

133    The CAMS regional production relies on a quite unique ensemble of 11 individual models whose daily operation is distributed  
134    amongst 11 modelling centres in ten European countries. The coordination is handled by the Central Regional Production Unit  
135    (CRPU) which is led by Météo-France, with the support of INERIS for model development matters and reanalysis production  
136    (Figure 1).

137    The CRPU defines the design of the regional production system under the auspices of ECMWF. This includes setting the  
138    guidance and requirements for the implementation of individual models as well as continuous evolution in order to maintain  
139    the system within the state of the art. The CRPU is also in charge of contractual matters and relations with the providers of  
140    input data as well as the delivery of model results to the Atmosphere Data Store for public use (Section 4.3).

141    In earlier MACC phases and the first CAMS regional project, only 7 models were contributing to the distributed operational  
142    production: CHIMERE, EMEP, EURAD-IM, LOTOS-EUROS, MATCH, MOCAGE, and SILAM. As of October 2019,  
143    DEHM and GEM-AQ joined the operational system. As of June 2022, MINNI and MONARCH joined the production.

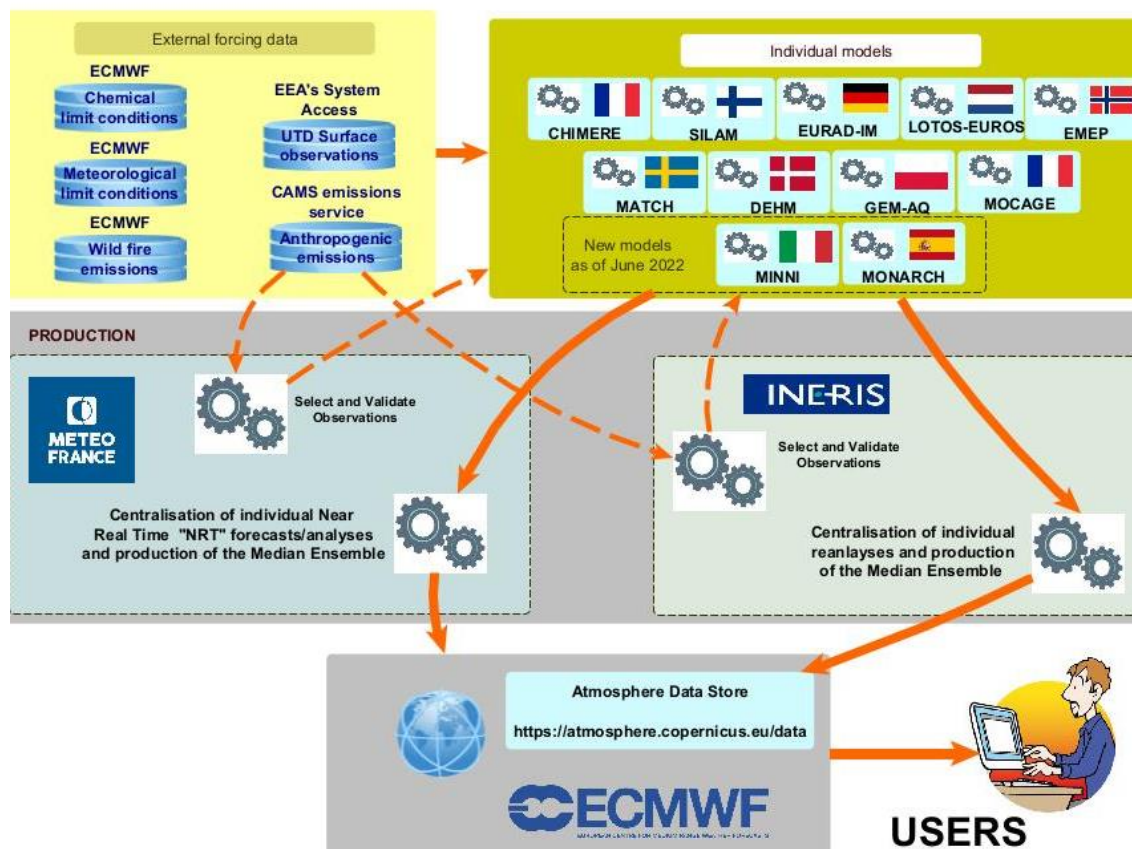


Figure 1: Schematic of the CAMS Regional Production workflow. Top-left the external forcings (anthropogenic emissions, meteorology, boundary conditions) and in-situ observations for assimilation and evaluation. Top right: eleven regional chemistry-transport model operated in ten European countries. Middle: Meteo-France (for the near real time) and INERIS (for the reanalysis) centralise the individual productions. Bottom: the results are disseminated to the Atmosphere Data Store.

## 2.2 Modelling products

The CAMS regional system includes both daily 4-days forecasts and several analysis products. All of them are provided from both eleven individual CTMs results and an ENSEMBLE product which is constituted by the median of individual models at each grid point (See also Section 4 on post-processing).

Hourly near-real time forecasts (NRT/FC) are released every day with a 4 days horizon (from 0 to 96hrs forecasts). They rely on chemistry-transport outputs, some of which are initialised on the basis of the previous analysis (see details in Section 3). The ENSEMBLE NRT/FC fields are made available publicly each day at 08:00 UTC for forecast horizon 0 to 48hrs (day 1



and day 2), and at 10:00 UTC for forecast horizon 49 to 96hrs (day 3 and days 4). All the forecasts are initiated at 00 UTC, the differentiated timing for the 48hr or 96hr lead time is only to account for longer production times.

The list of output species has been expanding gradually over the years. The choice of selected species accounts for user requests, especially with regards to downstream modelling needs (in the case where the CAMS regional system is used as forcing boundary conditions for smaller scale nested models), understanding air pollution episodes, and availability of observation data for evaluation and quality control (which is essentially focusing on PM<sub>10</sub>, PM<sub>2.5</sub>, NO<sub>2</sub>, O<sub>3</sub> and pollens at present, but research grade measurement of the EMEP Monitoring Programme or the ACTRIS European Research Infrastructure are considered to strengthen the quality control procedures).

As of April 2025, the list of species in the NRT/FC includes the following gases: ozone (O<sub>3</sub>), nitrogen oxide (NO), nitrogen dioxide (NO<sub>2</sub>), carbon monoxide (CO), sulphur dioxide (SO<sub>2</sub>), glyoxal (CHOCHO), formaldehyde (HCHO), ammonia (NH<sub>3</sub>), total Non-Methane Volatile Organic Compounds (NMVOC, defined as the sum of the mass of the carbon atoms of all the VOC species of the chemical scheme of the model, excluding the methane and PANs species, and expressed in unit µg/m<sup>3</sup> of carbon atoms), and total Peroxy-Acetyl Nitrates (PANs). Particulate matter (PM) are included as : PM<sub>2.5</sub> (smaller than 2.5µm), PM<sub>10</sub> (smaller than 10µm). The following tracers in the PM<sub>2.5</sub> fraction are also provided: sulphate (SO<sub>4</sub><sup>2-</sup>), nitrate (NO<sub>3</sub><sup>-</sup>), ammonium (NH<sub>4</sub><sup>+</sup>), total secondary inorganic aerosols (SIA), total elemental carbon (EC), EC fraction related to residential emissions, total organic matter. In the PM<sub>10</sub> fraction, the tracers include desert dust, sea salt and wildfires. In addition, six pollen species are included: birch, olive, grass, alder, mugwort and ragweed.

Hourly near-real time analysis (NRT/AN) are released each day by 12:00 UTC for the previous day. Here, each individual model is corrected to minimise error with observed air pollutant concentrations over Europe. For the latest reanalysis available on the ADS as of January 2024 (covering the year 2021), the list of species is: for O<sub>3</sub>, NO, NO<sub>2</sub>, CO, NH<sub>3</sub>, NMVOC, PM<sub>10</sub>, PM<sub>2.5</sub>, PM<sub>10</sub> wildfires, PM<sub>10</sub> dust, EC total, EC residential, PAN, SIA, SO<sub>2</sub>. For earlier years, not all of these species are available, and in the future the list will continue expanding to catch up with the full species set in the daily forecast production. Note that observations are available for assimilation only for NO<sub>2</sub>, O<sub>3</sub>, PM<sub>10</sub>, and PM<sub>2.5</sub>. Individual components contributing to the total PM<sub>10</sub> or PM<sub>2.5</sub> mass are scaled according to the assimilation of total PM<sub>10</sub> or PM<sub>2.5</sub> measurements, and pollen species are not assimilated.

The daily analyses products are supplemented by an interim reanalysis (IRA) and a validated reanalysis (VRA). Both rely on the same modelling tools as the NRT production, including assimilation strategy. But the observations taken into account differ. Acknowledging that for the NRT/AN production some observations can be missing or not validated, daily analyses are reproduced with a 20 days delay in the IRA. This time gap is considered sufficient to fix most failures in NRT data flows and maximise the number of available measurement data. The interim reanalysis is subsequently consolidated and delivered in the

186 first months of Y+1. Since all observations are only definitively validated by European member states by the end of the  
187 following year (Y+1), the full year Y is reprocessed in Y+2 to produce the VRA of the corresponding year. As for NRT, the  
188 production of IRA/VRA is also distributed across individual modelling teams which operate their own modelling system. The  
189 CRPU (INERIS in the case of reanalyses) defines the common requirements in terms of model setup, input data (meteorology,  
190 emissions, and assimilated observations) and centralised the verification and production of the ENSEMBLE product.

### 191 **2.3 Air quality observations**

192 The gathering, filtering and selection of observations is centralised by the CRPU and subsequently disseminated to individual  
193 modelling teams which apply different assimilation algorithms even though the exact same stations are assimilated by each  
194 model (see details in Section 3). All observation data are obtained from the Air Quality e-reporting database<sup>1</sup> maintained by  
195 the European Environment Agency where near real time “up-to-date” (UTD) and validated observations are reported, in  
196 particular for countries of the European Union which are expected to do so with respect to the European Directives.

197 An important step lies in the filtering and selection of data. For the NRT production (both FC and AN), the stations are clustered  
198 using an objective classification which consists in building classes of stations which exhibit similar patterns of temporal  
199 variability to differentiate background and proximity stations (Joly and Peuch, 2012). Originally (when the model had a  
200 resolution of approximately 20x20km<sup>2</sup>), only the stations corresponding broadly to suburban and rural typologies were  
201 included. But since November 2020, all stations falling in classes 1-7 of the Joly & Peuch classification are included, which  
202 means broadly that urban background sites are taken into account while traffic and industrial sites are excluded. This way,  
203 even if the spatial resolution of the CAMS Regional Production is 10x10km, we ensure the relevance of the modelling setup  
204 to capture urban background air quality.

205 The design and use of this objective classification is particularly useful in NRT applications, which includes more outlying  
206 data than the reanalyses. Such NRT applications are also less used for regulatory applications for which reanalyses are  
207 preferred. This is why, the station classification in IRA and VRA follows the standard typology declared by the member states  
208 in their reporting (even if it is admitted that it is not exempt from misclassification). In VRA and IRA, stations labelled as  
209 traffic and industrial are strictly excluded and only background (urban, suburban, and rural) stations are included.

210 Approximately 2-third of the stations’ data are distributed by the CRPU for assimilation (both for NRT/AN and IRA&VRA),  
211 while the rest of the data are kept for evaluation (see Section 4.2).

---

<sup>1</sup> <https://www.eea.europa.eu/data-and-maps/data/aqereporting-9>, last accessed 30/10/2024

212 This splitting is first performed using the station list used for VRA and IRA, therefore using only the sites for which member  
213 states declared the typology as “background” that are available for the previous years (year-1 for IRA (Y-1) and year-2 for  
214 VRA (Y-2)). Stations with less than 1 months of data are removed. The first prerequisite is to treat collocated stations together  
215 for the pollutant pairs NO<sub>2</sub>/O<sub>3</sub> and PM<sub>10</sub>/PM<sub>2.5</sub>. This prevents, for example, having the same station for NO<sub>2</sub> assimilation and  
216 O<sub>3</sub> evaluation. The second prerequisite is to use a random selection process to ensure a good spatial coverage of stations in the  
217 two listings. However, the construction of the assimilation and validation station sets is not entirely random: evaluation stations  
218 are always selected near assimilation stations, while spatially isolated stations (typically in remote areas of Europe) are used  
219 for assimilation. This classification is revised on an annual basis for each new production cycle of IRA and VRA to take into  
220 account the evolution of the network.

221 The splitting obtained for the VRA and IRA production is subsequently translated for the NRT production. All the stations  
222 from classes 1 to 7 belonging to the set of evaluation of VRA/IRA are tagged for NRT evaluation and all the stations that do  
223 not belong to the evaluation of VRA/IRA are tagged for NRT assimilation (AN).

224 At present there is no centralisation of the dissemination of any satellite observation of atmospheric composition even if many  
225 individual modelling teams already assimilate satellite data, and this is expected to further develop in the coming years (See  
226 details in the presentation of individual models in Section 3).

## 227 **2.4 Modelling domain**

228 The modelling domain covers Europe within 25°W to 45°E longitude and 30°N to 72°N latitude at a 0.1°x0.1° resolution.  
229 Whereas in earlier phases of the project some individual models were operating at slightly lower resolution (about 0.2°), today  
230 all models operate on a native resolution of about 0.1°. Covering the whole region is a strong requirement, and all models  
231 deliver data over the entire domain, which means that some of them perform the forecast on a slightly larger domain in order  
232 to include a buffer area or cope with differing geographic projection (see details in Section 3). The spatial extent has evolved  
233 marginally in recent years, it was only reaching up to 70°N until June 2019.

234 The strategy for the vertical discretisation is left open for individual contributing models, but there is a common requirement  
235 in the delivery of model results on common vertical levels. As of January 2024, the complete list of vertical levels is: surface,  
236 50m, 100m, 250m, 500m, 750m, 1000m, 2000m, 3000m, and 5000m above ground. This has evolved substantially in recent  
237 years, only surface concentrations were provided in the earlier phases of CAMS, and different lists of vertical levels have been  
238 archived in the past for near real time forecast, analyses, and reanalysis products.

## 239    **2.5    Meteorology and chemical boundary conditions**

240    The meteorological fields used to force the individual operational CTMs are from the European Centre for Medium-Range  
241    Weather Forecasts (ECMWF) operational meteorological forecasts at high resolution based on the IFS model (Integrated  
242    Forecasting System). The spatial resolution of the IFS forecast has increased in time, it is about 9km as of 2024. The exact list  
243    of meteorological parameters used to drive the individual CTMs differs depending on the models (see details in Section 3).  
244    Most of them use the forecast starting at 12:00 UTC on D–1 but there might also be some deviations to account for operational  
245    constraints.

246    The chemical boundary conditions are also obtained from ECMWF but using the configuration including chemistry of the IFS:  
247    IFS-COMPO referred to as CAMS-Global in this article (Flemming et al., 2015; Rémy et al., 2019) operating at approximately  
248    40km spatial resolution. CAMS-Global runs forecasts twice daily from 00 and 12 UTC and the data are available every hour  
249    (for surface fields) and every 3 hours (for above surface model- and pressure-level fields). The model results are made available  
250    for further use as boundary conditions of regional models through different dissemination routes including the MARS archive  
251    server of ECMWF, a dedicated ftp access for the regional CAMS operational models, and the atmosphere data store (ADS) of  
252    Copernicus.

253    The list of species used as boundary conditions for the regional CAMS models is given in Table 2. Further details are available  
254    through the CAMS User Support website<sup>2</sup> and (Morcrette et al., 2009). All aerosol species are provided as dry PM, except for  
255    sea salt, whose mass and size is provided at a relative humidity of 80%. The mass of the corresponding dry sea salt is 1/4.3  
256    smaller and the radius is half of the sea salt at relative humidity of 80%.

## 257    **2.6    Surface emissions**

### 258    **2.6.1    Anthropogenic emissions**

259    Using identical anthropogenic emissions in all the eleven individual models is essential for the consistency of the CAMS  
260    Regional products. The so-called TNO-MACC-III (Kuenen et al., 2014) emission inventory was used for several years in the  
261    past. Since June 2019, it has been replaced by the CAMS-REG emissions inventory, which is regularly updated (Kuenen et  
262    al., 2022). The CAMS-REG inventory is based on official national totals of air pollutant emissions reported in compliance  
263    with the European Directive on National Emission Reduction Commitments (2016/2284/EU) and the Gothenburg Protocol of  
264    the LRTAP Convention. Additional processing is applied to ensure consistency in the dataset by making corrections and  
265    performing some gap-filling where information is missing. A consistent spatial distribution for gridded emission datasets is

---

<sup>2</sup>    <https://confluence.ecmwf.int/display/CKB/CAMS%3A+Global+atmospheric+composition+forecast+data+documentation>  
(last accessed 30/10/2024)

266 applied at  $0.05^\circ \times 0.1^\circ$  resolution. Since June 2021, the CAMS Regional production has used an improved version of the  
267 CAMS-REG inventory which substituted national estimates of wood burning emission in order to cope with a well-established  
268 inconsistency in the reporting of condensable emissions (Denier Van Der Gon et al., 2015).

269 The use of officially reported emissions induces a subsequent delay in the successive updates of the emission datasets. The  
270 Emissions for year Y, are reported in March Y+2. Then they undergo verification, gap filling and spatialisation before being  
271 considered for implementation in the CAMS Regional production. The emissions being used for the day-to-day forecasts are  
272 thus generally based on national emissions reported about 3 years earlier. In order to cope with this limitation, the CAMS-  
273 REG emission inventory developed a methodology to extrapolate the officially reported emissions to the most recent historical  
274 year. The methodology basically consists in two steps. First, early available relevant activity data for different sectors are used  
275 to extrapolate the trend in the activity, which are used to adjust future emissions. Second, for the historical years for which  
276 emission data are available from CAMS-REG the trend in these is compared to the trend in the activities. If a significant trend  
277 is found (here defined as  $>3\%$  per year) the trend in the implied emission factor is determined by taking the ratio of the trend  
278 in emissions and in activities, which is then projected into the future. The methodology has been validated for historical years  
279 and overall works well, but such a method has also limitations, for instance it is not possible to predict sudden events such as  
280 closure of power plants or industrial facilities, or implementation of emission reduction techniques in large facilities. This way,  
281 the emission implemented in late 2024 in the regional production could be based on an estimate for the year 2023 (CAMS-  
282 REG v7.1).

283 The common requirement to use CAMS-REG emissions in all CTMs is strictly enforced for the forecast. For the analysis, in  
284 one of the models (Table 1) analysed concentrations are pulled away from the state that is physically related to the emissions  
285 and therefore will not be strictly relatable anymore to specified required emissions. But none of the models use inverse  
286 modelled emissions based on observation in the forecast.

287 Only the spatialised annual fluxes of  $\text{NO}_x$ ,  $\text{SO}_x$ , NMVOCs,  $\text{NH}_3$ , CO,  $\text{PM}_{10}$  and  $\text{PM}_{2.5}$  emissions are prescribed for all models.  
288 The subsequent disaggregation required in CTMs in terms of (i) hourly/daily/weekly/monthly profiles, (ii) vertical injection  
289 height, and (iii) mapping towards model chemical species is left open for individual modelling teams. Default information is  
290 nevertheless provided regarding the temporal disaggregation (Guevara et al., 2021) as well as the speciation of total VOC or  
291 total PM on individual VOC species or aerosol species, respectively. NMVOC emissions in CAMS-REG are provided with  
292 year-, sector- and country-dependent speciation profiles to breakdown total NMVOC to the 25 Global Emission Initiative  
293 (GEIA) species, originally defined under the REanalysis of the TROpospheric chemical composition (RETRO) project  
294 (Schultz et al., 2007). Each CAMS individual modelling team performs a remapping of the 25 GEIA NMVOC species to the  
295 species of their corresponding gas phase chemical mechanism. Concerning PM, the default profiles provided in CAMS-REG  
296 allow splitting coarse and fine PM emissions to primary organic carbon, elemental carbon, sulphates, sodium and others.

297     **2.6.2     Biogenic, natural and wildfire emissions**

298     Biogenic emissions are left to the choice of individual operational models, most of which include their own online calculation  
299     of emissions from vegetation and other natural sources. They include soil emissions for (i) mineral dust resuspension, (ii) soil  
300     NO<sub>x</sub> or even (iii) sea salt within the European domain, but the agriculture related NH<sub>3</sub> emissions are issued from the  
301     anthropogenic emission inventory.

302     The only coordination regarding ecosystem emissions concerns wildfires where all models are expected to use the Global Fire  
303     Assimilation System (GFAS) product (Kaiser et al., 2012) provided by CAMS. GFAS is based on fire radiative power retrievals  
304     from data of the Moderate Resolution Imaging Spectroradiometer (MODIS) instruments aboard the Terra and Aqua satellites.  
305     GFAS provides hourly emission data with a 8-hr delay compared to real time. Each individual modelling team retrieves GFAS  
306     emission when initiating their forecast. As the individual forecasts are initiated between 12:00 D-1 and 03:00 D+0 depending  
307     on the regional systems, the only full day where GFAS wildfire emissions are available is D-2, and some systems also include  
308     part of D-1 emissions. Each system therefore reconstructs a 24hr cycle of emission based either on D-2 only or also including  
309     part of D-1 emissions. This cycle is used by all models for their analysis of D-1. For the forecast, persistence of this daily cycle  
310     of emission is only maintained for D+0 and D+1 considering that the vast majority of wildfires in Europe are not persisting  
311     for longer time periods.

312     **2.6.3     Pollen emission and dispersion**

313     The following pollen species are included in the CAMS Regional production: birch, grass, olive, ragweed, alder, and mugwort.  
314     Their implementation in the individual operational CAMS models differ in terms of advection and deposition strategies, but  
315     as for the anthropogenic air pollutants, the emission terms are coordinated following the original documentation of (Sofiev et  
316     al., 2013) and subsequent updates for additional species. The pollen species differ in terms of their geographic distribution  
317     (source masks), total amount of available pollen grains, start and end date of the season (heatsum thresholds), and the shape  
318     of the season (source strength as function of time). The alder pollen emission model is similar to that of birch and olive, while  
319     the mugwort source is a variation of the grass source. However, mugwort is implemented as five different sub-species, each  
320     with its own spatially gridded start and end dates of the flowering season. Ragweed pollen follows the method described in  
321     (Prank et al., 2013).

322     Once emitted, pollen species are advected in the model in the same way as other chemically inert species and are subject to  
323     gravitational settling and wet scavenging over time.

## 3 Individual Model Description

### 3.1 CHIMERE

#### 3.1.1 Model Overview

CHIMERE is a multi-scale CTM developed jointly by INERIS and CNRS (Menut et al., 2021). Its development was initiated in the early 2000s (Bessagnet et al., 2004; Vautard et al., 2005) and it has since then pioneered operational national air quality forecasting in France (Rouil et al., 2009). It is also extensively used for long-term simulations for emission control scenarios (Colette et al., 2013; Meleux et al., 2007; Colette et al., 2015). It runs over a range of spatial scale from the hemispheric to the urban scale, with resolutions from 100km to 1km (Colette et al., 2014; Bessagnet et al., 2017). The exact model version used since June 2021 in the CAMS Regional Production is CHIMERE v2020r1.

#### 3.1.2 Model geometry

For the CAMS regional forecasts, CHIMERE uses a regular latitude-longitude grid with a  $0.1^\circ \times 0.1^\circ$  resolution which covers  $25^\circ\text{W}$  to  $45^\circ\text{E}$  and  $30^\circ\text{N}$  to  $72^\circ\text{N}$  and 9 vertical levels, extending from the surface up to 500 hPa, a lowermost layer about 20m deep and about 7 layers below 2 km. No vertical downscaling is applied and concentrations in the lowermost model layer are considered representative of the surface.

#### 3.1.3 Forcing Meteorology

The forcing meteorology is retrieved from the IFS model vertical layers covering the CHIMERE vertical extent on a  $0.1^\circ \times 0.1^\circ$  horizontal grid resolution with a temporal resolution of 3 hours. The forecast released at 00:00UTC of the previous days is used. The three-dimensional meteorological parameters included to force the CHIMERE forecast are horizontal wind components, temperature, specific humidity, orography, rain water/snow mixing ratios, cloud liquid and ice water contents. The 2D variables included are: surface temperature, surface pressure, large scale and convective precipitations, boundary layer height, sensible and latent heat fluxes at surface, surface solar radiation downwards, soil parameters (water and temperature) for 4 layers (0-7 cm, 7-28 cm, 28-100 cm, 100-255 cm), sea ice cover, and snow depth.

#### 3.1.4 Chemical initial and boundary conditions

Lateral and top boundary conditions are taken from chemical species available in CAMS-Global forecast model of the previous day at 3hr temporal resolution. The full list of species used from CAMS-Global is given in Table 2. The forecasts are initialised by the CHIMERE forecasts of the previous day.

### 351   **3.1.5   Emissions**

352   The common annual anthropogenic emissions CAMS-REG are implemented as explained in Section 2.5.1. Temporal  
353   disaggregation is based on TNO time profiles provided with CAMS-REG. Chemical disaggregation for VOCs is based on  
354   (Passant, 2002). PM components are speciated using the splits provided with the CAMS-REG database.

355   Biogenic VOC emissions are computed online with the MEGAN 2.10 algorithm (Guenther et al., 2012) implemented in  
356   CHIMERE and using high spatiotemporal data LAI (30 arcsec every 8 days) generated from MODIS (Yuan et al., 2011).  
357   Biogenic emission factors are estimated based on the 30 arcsec USGS (US Geophysical Survey) land-use database and the  
358   emission factors provided for each functional type by (Guenther et al., 2012).

359   The hourly GFAS wildfire emission for D-2 (i.e. the last full day available when launching the forecast system) are used for  
360   the analysis (D-1) and the first two days of the forecast (D+0 and D+1). Fire emissions are set to zero for the remainder of the  
361   forecast horizon.

362   Dust production within the European domain is included (Alfaro and Gomes, 2001). It is based on a scheme for saltation and  
363   a vertical flux estimate using cohesion kinetic energies scheme (Marticorena and Bergametti, 1995).

### 364   **3.1.6   Solver, advection and mixing**

365   The numerical time solver is based on a splitting operator which solves separately transport (including deposition and  
366   emissions), chemistry and aerosol formation.

367   Advection is based on the Piecewise Parabolic Method 3d order scheme (Colella and Woodward, 1984). Vertical turbulent  
368   mixing takes place only in the boundary layer. The formulation uses K-diffusion parameterisation (Troen and Mahrt, 1986),  
369   without counter-gradient term.

### 370   **3.1.7   Deposition**

371   Dry deposition of gaseous and particle species is parameterised as a downward flux out of the lowest model layer where the  
372   deposition velocity is described through a resistance analogy (Wesely, 1989). Wet deposition of particles and gases are  
373   computed by using a polydisperse distribution of rain droplets based on (Willis and Tattelman, 1989) and by computing the  
374   efficiency of the collision. Below-cloud scavenging of gases is assumed irreversible and is therefore only accounted for the  
375   most soluble compounds ( $\text{HNO}_3$ ,  $\text{H}_2\text{O}_2$ ,  $\text{HCl}$ ,  $\text{SO}_2$  and  $\text{NH}_3$ ). In-cloud scavenging is accounted for all gases by computing the  
376   gaseous and aqueous phases partitioning based on Henry's law constants and the pH of the clouds. Scavenging by snow is also  
377   accounted for and is based on (Chang, 1984) for gases and on (Wang et al., 2014) for particles.



### 378    **3.1.8    Chemistry and aerosols**

379    In order to optimise computing time, the reduced MELCHIOR2 mechanism with 44 species and about 120 reactions is derived  
380    from the full mechanism MELCHIOR (Derognat et al., 2003). The sectional aerosol module accounts for 7 species and 10 bins  
381    from 10nm to 40µm (primary particle material, nitrate, sulphate, ammonium, biogenic secondary organic aerosol SOA,  
382    anthropogenic SOA and water). Photolytic rates are attenuated using liquid water and relative humidity. The aerosol module  
383    is described in great details in (Couvidat et al., 2018) and accounts for condensation, nucleation, and condensation/evaporation.  
384    Aerosol thermodynamic equilibrium is achieved using the ISORROPIA model version 2.1. The secondary organic aerosol  
385    formation mechanism used in the operational forecasting version of CHIMERE is described in (Bessagnet et al., 2008).

### 386    **3.1.9    Assimilation system**

387    The CHIMERE assimilation for operational purposes relies on a kriging based approach to assimilate hourly concentration  
388    values for correcting the raw model results. For the analysis period, linear regression between a selected set of observations  
389    (excluding mountain and proximity sites) and the raw CHIMERE model is performed (in moving neighbourhood). The  
390    experimental variogram of the regression residuals is then computed and a variogram model is fitted; the model adequacy is  
391    checked by cross validation. Ultimately, observations are kriged with the CHIMERE model as external drift (in moving  
392    neighbourhood). This method is applied for O<sub>3</sub> and NO<sub>2</sub>. For PM<sub>10</sub> and PM<sub>2.5</sub>, an ordinary co-kriging of the observations (main  
393    variable) and CHIMERE (secondary variable) is applied to ensure consistency between both pollutants. Only in-situ surface  
394    observations are used.

395    Further evolution of the CHIMERE assimilation system using an ensemble Kalman Filter approach is under development, in  
396    particular to pave the way for assimilation of satellite data. It is has however not yet demonstrated to provide better skill score  
397    than the geostatistical method.

398

## 399    **3.2    DEHM**

### 400    **3.2.1    Model Overview**

401    The Danish Eulerian Hemispheric Model (DEHM) is a 3-dimensional, offline, large-scale, Eulerian, atmospheric chemistry  
402    transport model developed to study long-range transport of air pollution in the Northern Hemisphere. DEHM was originally  
403    developed in the early 1990's in order to study the atmospheric transport of sulphur-dioxide and sulphate into the Arctic  
404    (Christensen, 1997; Heidam et al., 2004). The model has been modified, extended and updated continuously since then and  
405    now includes a flexible setup with the possibility for nested domains with higher resolutions over targeted areas (Brandt et al.,  
406    2012; Geels et al., 2021). Apart from standard air pollution components and pollen, the DEHM model also includes mercury  
407    (Christensen et al., 2004), CO<sub>2</sub> (Lansø et al., 2019) and POPs (Hansen et al., 2008).

### 408    **3.2.2    Model geometry**

409    The horizontal domain is defined on a regular latitude-longitude grid of 0.1° resolution with grid centre points covering  
410    longitude 24.95°W to 44.95°E and latitude 30.05°N to 71.95°N. The vertical discretization is defined on 29 terrain-following  
411    sigma levels up to about 100hPa. The 12 lowest layers are within the lowest 1 km of the atmosphere and the thickness of the  
412    lowest layer is about 20m. The model includes an option for downscaling to the surface, but this is not applied in the operational  
413    setup.

### 414    **3.2.3    Forcing Meteorology**

415    The forcing meteorology is retrieved from the IFS model vertical layers covering the DEHM vertical extent on a 0.2°x0.2°  
416    horizontal grid resolution with a temporal resolution of 3 hours. The forecast released at 12:00 UTC of the previous days is  
417    used. The meteorological parameters included to force the DEHM forecast are: 3D fields of the horizontal wind components  
418    (U,V), temperature, specific humidity, cloud liquid water contents, cloud ice water contents, rain water contents, snow water  
419    contents and fraction of cloud cover. The 2D fields are land-sea mask, surface pressure, geopotential height, skin temperature,  
420    Ustar, large scale and convective rain, snow depth, sensible heat flux, latent heat flux, net solar radiation, boundary layer  
421    height, 2 m temperature, 2 m dew point temperature, 10 m wind (U,V), albedo, sea ice area fraction and surface roughness.

### 422    **3.2.4    Chemical initial and boundary conditions**

423    Lateral and top boundary conditions are taken from chemical species available in CAMS-Global forecast model of the previous  
424    day at 3 hr temporal resolution. The full list of species used from CAMS-Global is given in Table 2. The DEHM forecasts are  
425    initialised by the DEHM forecasts of the previous day.

### 426   **3.2.5   Emissions**

427   The common annual anthropogenic emissions CAMS-REG are implemented as explained in Section 2.5.1. Originally the  
428   temporal disaggregation was based on the GENEMIS tables, using a GNFR to SNAP matrix. From 2021 the new CAMS-  
429   TEMPO (Guevara et al., 2021) profiles for annual, monthly, weekly and daily distribution of emissions have been included in  
430   the operational version of DEHM. PM components are speciated using the splits provided with the CAMS-REG emissions.  
431   The speciation of VOCs from the emission input of total non-methane VOCs is based on the global speciated NMVOC  
432   emission database EDGAR 4.3.2 (Huang et al., 2017).

433   Natural emissions of the Biogenic Volatile Organic Compounds (BVOCs) isoprene and monoterpenes are estimated in the  
434   DEHM model based on the MEGAN model (Zare et al., 2012). The production of sea salt aerosols at the ocean surface is  
435   based on two parameterisation schemes describing the bubble-mediated sea spray production of smaller and larger aerosols.  
436   In each time step, the production is calculated for 10 size bins and thereafter summed up to give an aggregated production of  
437   fine (with dry diameters <1.3  $\mu\text{m}$ ) and coarse (with dry diameters ranging 1.3-6 $\mu\text{m}$ ) aerosols (Soares et al., 2016). NO<sub>x</sub>  
438   emissions from soil are based on data from the Global Emissions Inventory Activity (Yienger and Levy, 1995) and from  
439   lightning they are from (Price et al., 1997).

440   The hourly GFAS wildfire emissions are retrieved as soon as they are available (i.e. with a 8-hr delay from real time) in order  
441   to obtain a recent 24hr cycle spanning over D-2 and D-1. This cycle is used for the analysis (D-1) and the first two days of the  
442   forecast (D+0 and D+1). Fire emissions are set to zero for the remainder of the forecast horizon. Hourly injection heights are  
443   calculated based on the hourly data of ‘Mean altitude of maximum injection’ and ‘Altitude of plume top’.

### 444   **3.2.6   Solver, advection and mixing**

445   The horizontal advection is solved numerically using the higher order Accurate Space Derivatives scheme, documented to be  
446   very accurate (Dabdub and Seinfeld, 1994), especially when implemented in combination with a Forester filter (Forester,  
447   1977). The vertical advection as well as the dispersion sub-models is solved using a finite elements scheme (Pepper et al.,  
448   1979) for the spatial discretization. For the temporal integration of the dispersion, the q-method (Lambert, 1991) is applied and  
449   the temporal integration of the 3-dimensional advection is carried out using a Taylor series expansion to third order. Time  
450   integration of the advection is controlled by the Courant-Friedrich-Lewy (CFL) stability criterion. A wind adjustment is  
451   included in order to ensure mass conservation.

452   The vertical diffusion is configured by K<sub>z</sub> profiles (Hertel et al., 1995), based on Monin-Obukhov similarity theory for the  
453   surface layer. This K<sub>z</sub> profile is extended to the whole boundary layer by using a simple extrapolation, which ensures that K<sub>z</sub>

454 is decreasing in the upper part of the boundary layer. The planetary boundary layer (PBL) height is obtained directly from the  
455 IFS meteorology.

### 456 **3.2.7 Deposition**

457 Gaseous and aerosol dry-deposition velocities are calculated based on the resistance method for 16 different land-use types  
458 and are configured similar to the EMEP model (Emberson et al., 2000b; Simpson et al., 2003), except for the dry deposition  
459 of species on water surfaces, where the deposition depends on the solubility of the chemical species and the wind speed (Hertel  
460 et al., 1995).

461 Wet deposition includes in-cloud and below-cloud scavenging and is calculated as the product of scavenging coefficients and  
462 the concentration of gases and particles in air (Simpson et al., 2003). The in-cloud scavenging coefficients are dependent on  
463 Henry's law constants and the rate at which precipitation is formed.

### 464 **3.2.8 Chemistry and aerosols**

465 The basic chemical scheme in DEHM now includes 74 different species and 158 reactions. It is based on the original scheme  
466 by (Strand and Hov, 1994). The original Strand and Hov scheme has been modified in order to improve the description of,  
467 amongst other things, the transformations of nitrogen containing compounds. The chemical scheme has been extended with a  
468 detailed description of the ammonia chemistry through the inclusion of ammonia ( $\text{NH}_3$ ) and related species: ammonium-nitrate  
469 ( $\text{NH}_4\text{NO}_3$ ), ammonium bisulphate ( $\text{NH}_4\text{HSO}_4$ ), ammonium sulphate ( $(\text{NH}_4)_2\text{SO}_4$ ) and particulate nitrate ( $\text{NO}_3$ ) formed from  
470 nitric acid ( $\text{HNO}_3$ ) using an aerosol equilibrium approach with reaction rates dependent on the equilibrium (Frohn, 2004).  
471 Furthermore, reactions concerning the wet-phase production of particulate sulphate have been included. The photolysis rates  
472 are calculated by using a 2-stream version of the Phodis model (Kylling et al., 1995). The original rates for inorganic and  
473 organic chemistry have been updated with rates from the chemical scheme applied in the EMEP model (Simpson et al., 2003).  
474 SOA formation is included via a VBS-based approach (Bergström et al., 2012b; Zare et al., 2014). In total, DEHM includes  
475 nine classes of particulate matter ( $\text{PM}_{2.5}$ ,  $\text{PM}_{10}$ , TSP, seasalt < 2.5 mm, sea-salt > 2.5 mm, smoke from wood stoves, fresh black  
476 carbon, aged black carbon, and organic carbon).

### 477 **3.2.9 Assimilation system**

478 Since the system upgrade in November 2020, the assimilation in DEHM has been based on an updated version of the  
479 comprehensive 3D-var data assimilation scheme previously described in (Silver et al., 2016). The NMC method (Kahnert,  
480 2008; Parrish and Derber, 1992) is used to estimate the background error covariance matrix. Two 1-year runs of DEHM using  
481 analysed and forecasted ECMWF weather data are performed and their differences are used to estimate the background errors

482 in spectral space for O<sub>3</sub>, NO<sub>2</sub>, SO<sub>2</sub>, CO, PM<sub>2.5</sub>, and PM<sub>10</sub>. For the analysis and reanalysis runs, surface in-situ observations of  
483 the six species are assimilated at an hourly basis in DEHM.

### 484   **3.3    EMEP**

#### 485   **3.3.1    Model Overview**

486   The EMEP MSC-W (European Monitoring and Evaluation Programme Meteorological Synthesizing Centre-West) model is a  
487   chemical transport model developed at the Norwegian Meteorological Institute under the EMEP programme of the United  
488   Nations Geneva Convention on Long-range Transboundary Air Pollution. The EMEP MSC-W model system allows several  
489   options with regard to the chemical schemes used and the possibility of including aerosol dynamics. (Simpson et al., 2012)  
490   described an early version of the EMEP MSC-W model in detail, while updates to the model since 2012 have been documented  
491   and evaluated in the annual status reports of EMEP (see (Emep, 2023) and references therein). The forecast version of the  
492   EMEP MSC-W model (EMEP-CWF) has been in operation since June 2006. The scheduled model updates in CAMS ensure  
493   that the model version stays as close as possible to the official EMEP Open Source version<sup>3</sup>. Nevertheless, the EMEP-CWF  
494   results and performances in CAMS might differ from those presented in the annual EMEP Status Reports, because of different  
495   input data (emissions and meteorological driver) and model configurations (Forecast in EMEP-CWF versus Hindcast in EMEP  
496   Status Reports).

#### 497   **3.3.2    Model geometry**

498   The EMEP-CWF covers the European domain [30°N-76°N] x [30°W-45°E] on a geographic projection with a horizontal  
499   resolution of 0.1° x 0.1° (longitude-latitude). Vertically the model uses 20 levels defined as hybrid coordinates. The 10 lowest  
500   model levels are within the PBL, and the top of the model domain is at 100 hPa. The lowermost layer has a thickness of  
501   approximately 50 meters. Vertical downscaling is used to derive surface concentrations at 3 meters altitude, as described in  
502   (Simpson et al., 2012).

#### 503   **3.3.3    Forcing Meteorology**

504   The forcing meteorology is retrieved from the IFS model vertical layers covering the EMEP vertical extent on a 0.1°x0.1°  
505   horizontal grid resolution with a temporal resolution of 3 hours. The forecast released at 12:00UTC of the previous days is  
506   used. The meteorological parameters included to force the EMEP forecast are: 3D fields of the horizontal wind components  
507   (U,V), potential temperature, specific humidity, and cloud fraction. The 2D fields are land-sea mask, surface pressure, friction  
508   velocity (u\*), large scale and convective precipitation, soil water, snow depth, fraction of snow cover, fraction of ice cover,  
509   sensible heat flux, latent heat flux, sea surface temperature, 2m temperature and 2m relative humidity. The IFS forecasts do  
510   not include 3D precipitation, which is needed by the EMEP-CWF model. Therefore, a 3D precipitation estimate is derived  
511   from large-scale precipitation and convective precipitation (surface variables).

---

<sup>3</sup> <https://github.com/metno/emep-ctm> (last accessed 30/10/2024)

### 512   **3.3.4   Chemical initial and boundary conditions**

513   Boundary conditions are taken from chemical species available in the CAMS-Global forecast model of the previous day at 3hr  
514   temporal resolution (Table 2). In cases where CAMS-Global chemical boundary conditions are not available, default boundary  
515   conditions are specified for O<sub>3</sub>, CO, NO, NO<sub>2</sub>, CH<sub>4</sub>, HNO<sub>3</sub>, PAN, SO<sub>2</sub>, isoprene, C<sub>2</sub>H<sub>6</sub>, some VOCs, Sea salt, Saharan dust  
516   and SO<sub>4</sub>, as annual mean concentrations along with a set of parameters for each species describing seasonal, latitudinal and  
517   vertical distributions. It should be noted however that unavailability of CAMS-Global is very exceptional (less than once a  
518   year), and in general due to data transfer issues. The EMEP forecasts are initialised by the EMEP 3D VAR analysis of the  
519   previous day.

### 520   **3.3.5   Emissions**

521   The common annual anthropogenic emissions CAMS-REG are implemented as explained in Section 2.5.1. Temporal  
522   disaggregation is based on CAMS-REG-TEMPO v4.1. Chemical disaggregation for PM species follows the tables that come  
523   with CAMS-REG while VOC emissions are speciated for each source-sector based on a lumped-species approach as described  
524   in (Simpson et al., 2012; Bergström et al., 2022) .

525   The hourly GFAS wildfire emission for D-2 (i.e. the last full day available when launching the forecast system) are used for  
526   the analysis (D-1) and the first two days of the forecast (D+0 and D+1). Fire emissions are set to zero for the remainder of the  
527   forecast horizon.

528   The mineral dust source in the EMEP model is based on (Alfaro and Gomes, 2001; Fécan et al., 1998; Gomes et al., 2003;  
529   Marticorena and Bergametti, 1995; Marticorena et al., 1997).

530   Natural emissions of Biogenic Volatile Organic Compounds (BVOCs) are based on Table 3 of (Simpson et al., 2012).

### 531   **3.3.6   Solver, advection and mixing**

532   The numerical solution of the advection terms of the continuity equation is based on the scheme of (Bott, 1989). The fourth  
533   order scheme is utilized in the horizontal directions. In the vertical direction, a second order version applicable to variable grid  
534   distances is employed.

535   The turbulent diffusion coefficients (K<sub>z</sub>) are first calculated for the whole 3D model domain on the basis of local Richardson  
536   numbers. The planetary boundary layer (PBL) height is then calculated using methods described in (Simpson et al., 2012). For  
537   stable conditions, K<sub>z</sub> values are retained. For unstable situations, new K<sub>z</sub> values are calculated for layers below the mixing  
538   height using the O'Brien interpolation.

### 539   **3.3.7   Deposition**

540   Parameterisation of dry deposition is based on a resistance formulation. The deposition module makes use of a stomatal  
541   conductance algorithm which was originally developed for ozone fluxes, but which is now applied to all gaseous pollutants  
542   when stomatal control is important (Emberson et al., 2000a; Simpson et al., 2003; Tuovinen et al., 2004). Non-stomatal  
543   deposition for  $\text{NH}_3$  is parameterised as a function of temperature, humidity, and the molar ratio  $\text{SO}_2/\text{NH}_3$ .

544   Both gaseous and particulate nitrogen species are scavenged in the EMEP model according to their wet scavenging ratios and  
545   collection efficiencies listed in Table S20 of (Simpson et al., 2012). In-cloud and sub-cloud scavenging ratios are considered  
546   for gases and in-cloud scavenging ratios and sub-cloud scavenging efficiencies for particles.

### 547   **3.3.8   Chemistry and aerosols**

548   The EmChem19 chemical scheme couples the sulphur and nitrogen chemistry to the photochemistry and organic aerosol  
549   formation using about 200 reactions between ca. 130 species (Bergström et al., 2022; Simpson et al., 2020b; Andersson-Sköld  
550   and Simpson, 1999). The standard model version distinguishes 2 size fractions for aerosols, fine aerosol ( $\text{PM}_{2.5}$ ) and coarse  
551   aerosol ( $\text{PM}_{2.5-10}$ ). The aerosol components presently accounted for are  $\text{SO}_4$ ,  $\text{NO}_3$ ,  $\text{NH}_4$ , anthropogenic primary PM, organic  
552   aerosols, and sea salt. Also aerosol water is calculated. Dry deposition parameterisation for aerosols follows standard  
553   resistance-formulations, accounting for diffusion, impaction, interception, and sedimentation. Wet scavenging is treated with  
554   simple scavenging ratios, taking into account in-cloud and sub-cloud processes. For secondary organic aerosol (SOA) a  
555   volatility-basis set approach (Simpson et al., 2012) is used, which is a somewhat simplified version of the mechanisms  
556   discussed in detail by (Bergström et al., 2012a). The EmChem19a scheme also has explicit toluene and benzene with different  
557   SOA yields to the o-xylene surrogate that was used previously.

### 558   **3.3.9   Assimilation system**

559   The EMEP data assimilation system (EMEP-DAS) is based on the 3D-Var implementation for the MATCH model (Kahnert,  
560   2008). The background error covariance matrix is estimated following the NMC method (Parrish and Derber, 1992). Recent  
561   changes involved increased computational efficiency, tuning of model and observation representation uncertainties, and  
562   improved impact of the assimilation in the vertical.

563   The EMEP-DAS delivers analyses of D-1 (driven by the operational IFS forecast of 00UTC of yesterday) assimilating  $\text{O}_3$ ,  
564    $\text{NO}_2$ , CO,  $\text{PM}_{2.5}$ , and  $\text{PM}_{10}$  surface observations.

565



## 566    **3.4    EURAD-IM**

### 567    **3.4.1    Model Overview**

568    The EURAD-IM (European Air pollution Dispersion - Inverse Model) system consists of 5 major parts: the meteorological  
569    driver WRF (Weather Research and Forecasting<sup>4</sup>), the pre-processors EEP and PREP for preparation of anthropogenic  
570    emission data and observations, the EURAD-IM Emission Model EEM, and the chemistry transport model EURAD (Hass et  
571    al., 1995; Memmesheimer et al., 2004). EURAD-IM is a Eulerian meso-scale chemistry transport model involving advection,  
572    diffusion, chemical transformation, wet and dry deposition and sedimentation of tropospheric trace gases and aerosols. It  
573    includes 3d-var and 4d-var chemical data assimilation (Elbern et al., 2007) and is able to run in nesting mode.

### 574    **3.4.2    Model geometry**

575    To cover the CAMS domain from 25°E to 45°W and 30°N to 72°N, two lambert conformal projections subdomains with  
576    respectively 45 km (199x166 grid boxes) and 9 km horizontal resolution (581x481 grid boxes) are used. The model domain  
577    with the finer resolution covering the entire European part of the CAMS domain is nested within the halo domain with the  
578    coarser resolution.

579    Variables are horizontally staggered using an Arakawa C grid. Vertically, the atmosphere is divided by 23 terrain-following  
580    sigma coordinate layers between the surface and the 100 hPa pressure level. About 15 layers are within the first 2 km of the  
581    atmosphere. The thickness of the lowest layer is about 35 m. No vertical downscaling is used to derive surface concentrations  
582    from the first model level.

### 583    **3.4.3    Forcing Meteorology**

584    The meteorological forcing is obtained from 3-hourly IFS forecasts, but unlike the other models, the Weather Research and  
585    Forecast (WRF) model is used to compute meteorological fields on the grid needed to drive the EURAD-IM CTM. This  
586    intermediate processing is essentially for historical reasons as in the past the IFS temporal and spatial resolution required  
587    interpolation for use in the CTM. A direct use of the IFS data to dynamically drive EURAD-IM has been developed and is  
588    currently in the testing to enter the operational production in the near future.

### 589    **3.4.4    Chemical initial and boundary conditions**

590

---

<sup>4</sup> <https://www.mmm.ucar.edu/models/wrf>, last accessed 30/10/2024

591 The CAMS-Global 00:00 UTC forecast for the previous day is extracted from the MARS archive at ECMWF using 36 model  
592 levels with a temporal resolution of 3 hours. The full list of species used from the CAMS-Global model is given in Table 2.  
593 Sea salt concentrations from CAMS-Global are divided by the constant 4.3 for the conversion from wet to dry mass.

#### 594 **3.4.5 Emissions**

595 The common annual anthropogenic emissions CAMS-REG are implemented as explained in Section 2.5.1. The VOC and PM  
596 split, the vertical distribution of area sources, and the emission strength per hour are calculated within the EURAD-IM CTM  
597 with the distribution profiles provided with the CAMS-REG-AP\_v6.1/2019 inventory (Kuenen et al., 2022). The VOC and  
598 PM split depends on source category and country, the vertical distribution only depends on the source category. The CAMS-  
599 TEMPO v4.1 (Guevara et al., 2021) profiles are used for the annual, monthly, weekly and daily distribution of emissions.

600 Biogenic emissions and NO<sub>x</sub> emissions from soil are calculated within the EURAD-IM CTM with MEGAN (Guenther et al.,  
601 2012). Fire emissions are taken into account using hourly data from GFASv1.2 product (Kaiser et al., 2012). Zero fire  
602 emissions are assumed for D+2 and D+3 forecasts.

#### 603 **3.4.6 Solver, advection and mixing**

604 The positive definite advection scheme of (Bott, 1989), implemented in a one-dimensional realisation, is used to solve the  
605 advective transport. An operator splitting technique is employed (Mcrae et al., 1982) to handle the varying numerical  
606 specificities of processes to be solved.

607 An Eddy diffusion approach is used to parameterize the vertical sub-grid-scale turbulent transport. The calculation of vertical  
608 Eddy diffusion coefficients is based on the specific turbulent structure in the individual regimes of the planetary boundary  
609 layer (PBL) according to the PBL height and the Monin-Obukhov length (Holtslag and Nieuwstadt, 1986). A semi-implicit  
610 (Crank-Nicholson) scheme is used to solve the diffusion equation.

611 The sub-grid cloud scheme in EURAD-IM was derived from the cloud model in the EPA Models-3 Community Multiscale  
612 Air Quality (CMAQ) modelling system (Roselle and Binkowski, 1999). Convective cloud effects on both gas phase species  
613 and aerosols are considered.

#### 614 **3.4.7 Deposition**

615 The gas phase dry deposition modelling follows the method proposed by (Zhang et al., 2003). Dry deposition of aerosol species  
616 is treated size dependent, using the resistance model of (Petroff and Zhang, 2010) with consideration of the canopy. Dry  
617 deposition is applied as lower boundary condition of the diffusion equation.

Wet deposition of gases and aerosols is derived from the cloud model in the CMAQ modelling system (Roselle and Binkowski, 1999). The wet deposition of pollen is treated according to (Baklanov and Sørensen, 2001).

Size dependent sedimentation velocities are calculated for aerosol and pollen species. The sedimentation process is parameterized with the vertical advective transport equation and solved using the fourth order positive definite advection scheme of (Bott, 1989).

#### **3.4.8 Chemistry and aerosols**

In the EURAD-IM CTM, the gas phase chemistry is represented by an extension of the Regional Atmospheric Chemistry Mechanism (RACM) (Stockwell et al., 1997) based on the Mainz Isoprene Mechanism (MIM) (Geiger et al., 2003). A 2-step Rosenbrock method is used to solve the set of stiff ordinary differentials equations (Sandu and Sander, 2006). Photolysis frequencies are derived using the FTUV model (fast TUV) according to (Tie et al., 2003). The radiative transfer model therein is based on the Tropospheric Ultraviolet-Visible Model (TUV) developed by (Madronich and Weller, 1990).

The modal aerosol dynamics model MADE (Ackermann et al., 1998) is used to provide information on the aerosol size distribution and chemical composition. To solve for the concentrations of the secondary inorganic aerosol components, a FEOM (fully equivalent operational model) version, using the HDMR (high dimensional model representation) technique (Nieradzick, 2005; Rabitz and Aliş, 1999), of an accurate mole fraction based thermodynamic model (Frieese and Ebel, 2010) is used. The updated SORGAM module (Li et al., 2013) simulates secondary organic aerosol formation.

#### **3.4.9 Assimilation system**

The EURAD-IM assimilation system (Elbern et al., 2007) includes (i) the EURAD-IM CTM and its adjoint, (ii) the formulation of both background error covariance matrices for the initial states and the emission, and their treatment to precondition the minimisation problem, (iii) the observational basis and its related error covariance matrix, and (iv) the minimisation including the transformation for preconditioning. The quasi-Newton limited memory L-BFGS algorithm described in (Liu and Nocedal, 1989; Nocedal, 1980) is applied for the minimisation.

Currently assimilated in the EURAD-IM analysis and interim re-analysis are surface in-situ observations of O<sub>3</sub>, NO<sub>2</sub>, SO<sub>2</sub>, CO, PM<sub>2.5</sub>, PM<sub>10</sub>.

## 644    **3.5    GEM-AQ**

### 645    **3.5.1    Model Overview**

646    GEM-AQ is a numerical weather prediction model where air quality processes (gas phase and aerosols) are implemented on-  
647    line in the host meteorological model, the Global Environmental Multiscale (GEM) model, developed at Environment and  
648    Climate Change Canada (Côté et al., 1998a). The model is used for operational air quality forecasting in Poland. Also, it is  
649    used in a research project to investigate air quality in different environmental conditions (Struzewska and Kaminski, 2008,  
650    2012; Struzewska et al., 2015; Struzewska et al., 2016).

### 651    **3.5.2    Model geometry**

652    The GEM-AQ model can be configured to simulate atmospheric processes over a broad range of scales, from the global scale  
653    down to the meso-gamma scale. An arbitrarily rotated latitude-longitude mesh focuses resolution on any part of the globe. In  
654    the CAMS regional production, the model is run in the limited area mode with a resolution of  $0.1^\circ \times 0.1^\circ$  on a spherical  
655    coordinate system. The coordinates are the following: lower-left ( $17.4^\circ\text{N} / 22.1^\circ\text{W}$ ), upper-right ( $58.6^\circ\text{N} / 86.6^\circ\text{E}$ ). In the  
656    vertical, GEM-AQ uses the generalised sigma vertical coordinate system. It has terrain-following sigma surfaces near the  
657    ground that transform to pressure surfaces higher in the atmosphere. The model top is set at 10 hPa.

### 658    **3.5.3    Forcing Meteorology**

659    The operational IFS model provides meteorological fields for the initial and boundary conditions used by the meteorological  
660    part of the GEM-AQ model. The GEM-AQ model is started using the 12-hour forecast (valid at 00:00 UT of the following  
661    day) as the initial conditions. The IFS data are used as boundary conditions with a nesting interval of 3 hours. The IFS  
662    meteorological fields are computed from spectral coefficients for the target GEM-AQ grid. Meteorological fields, in the GEM-  
663    AQ model domain, are constrained within the nesting zone (absorber), which is defined over 10 grid points on each lateral  
664    boundary of the limited area domain.

665

### 666    **3.5.4    Chemical initial and boundary conditions**

667    Chemical species of the CAMS-Global forecast for the previous day are used with a temporal resolution of 3 hours (Table 2).  
668    For dust aerosols, the three available size bins from the CAMS-Global model are distributed uniformly over the 10  
669    corresponding bins in GEM-AQ. For organic matter aerosol, black carbon and sulphates, the same log-normal based profile  
670    was applied. For organic aerosol and black carbon, hydrophobic and hydrophilic components were summed as “total organic  
671    aerosol” and “total black carbon aerosol” before applying size-bin distribution profiles.

### 672   **3.5.5   Emissions**

673   The common annual anthropogenic emissions CAMS-REG are implemented as explained in Section 2.5.1. Based on this  
674   information, emission fluxes for 15 gaseous species (9 hydrocarbons and 6 inorganics) and 4 aerosol components (primary  
675   organic aerosol, black carbon, sulphates, nitrates) are derived using factors provided by TNO. Total emission fluxes for each  
676   aerosol component are distributed into 12 bins in the GEM-AQ aerosol module.

677   Anthropogenic emissions are distributed within the 7 lowest model layers (up to 1350 m) with injection height profiles for  
678   each of the GNFR sectors re-mapped for the GEM-AQ levels (Bieser et al., 2011). Temporal profiles modulating annual and  
679   diurnal variation of emission fluxes for each GNFR are used.

680   For biogenic emissions, a temperature-dependent, monthly averaged MEGAN-MACC (Sindelarova et al., 2014) dataset for  
681   the year 2010 was used specifically to avoid the short-term variability of reactive biogenic VOCs that would otherwise be  
682   generated in an online approach. In contrast to the online method, this approach provides an anticipated variability range,  
683   particularly by reducing the influence of online factors such as meteorological errors and extreme values.

### 684   **3.5.6   Solver, advection and mixing**

685   The set of non-hydrostatic Eulerian equations (with a switch to revert to the hydrostatic primitive equations) maintains the  
686   model's dynamical validity right down to the meso-gamma scales. The time discretization of the model dynamics is fully  
687   implicit, 2 time-level (Côté et al., 1998b; Côté et al., 1998a). The spatial discretization for the adjustment step employs a  
688   staggered Arakawa C grid that is spatially offset by half a mesh length in the meridional direction. It is second-order accurate,  
689   whereas the interpolations for the semi-Lagrangian advection are of fourth-order accuracy.

690   Deep convective processes are handled by Kain-Fritsch convection parameterisation (Kain and Fritsch, 1990). The vertical  
691   diffusion of momentum, heat and tracers is a fully implicit scheme based on turbulent kinetic energy (TKE) theory.

### 692   **3.5.7   Deposition**

693   The effects of dry deposition are included as a flux boundary condition in the vertical diffusion equation. Dry deposition  
694   velocities are calculated from a 'big leaf' multiple resistance model (Wesely, 1989; Aamaas et al., 2013) with aerodynamic,  
695   quasi-laminar layer, and surface resistances acting in series. The process assumes 15 land-use types and takes snow cover into  
696   account. Wet deposition takes into account cloud scavenging for soluble gas species and aerosols.

### 697   **3.5.8   Chemistry and aerosols**

698   The gas-phase chemistry mechanism currently used in the GEM-AQ model is based on a modification of version 2 of the Acid  
699   Deposition and Oxidants Model (ADOM) (Venkatram et al., 1988), derived from the condensed mechanism of (Lurmann et  
700   al., 1986). The ADOM-II mechanism comprises 47 species, 98 chemical reactions and 16 photolysis reactions. In order to  
701   account for background tropospheric chemistry, 4 species ( $\text{CH}_3\text{OOH}$ ,  $\text{CH}_3\text{OH}$ ,  $\text{CH}_3\text{O}_2$ , and  $\text{CH}_3\text{CO}_3\text{H}$ ) and 22 reactions were  
702   added. All species are solved using a mass-conserving implicit time stepping discretization, with the solution obtained using  
703   Newton's method. Heterogeneous hydrolysis of  $\text{N}_2\text{O}_5$  is calculated using the on-line distribution of aerosol. Although the model  
704   meteorology is calculated up to 10 hPa, the focus of the chemistry is in the troposphere where all species are transported  
705   throughout the domain. To avoid the overhead of stratospheric chemistry, the ozone and  $\text{NO}_y$  fields are replaced above 100  
706   hPa with those from the CAMS-Global model. Additionally, stratospheric columns for absorbing species used in photolysis  
707   calculations (cf., ozone) are taken from the CAMS-Global model. Photolysis rates (J values) are calculated on-line every  
708   chemical time step using the method described in (Landgraf and Crutzen, 1998). In this method, radiative transfer calculations  
709   are done using a delta-two stream approximation for 8 spectral intervals in the UV and visible applying pre-calculated effective  
710   absorption cross sections. This method also allows for scattering by cloud droplets and for clouds to be presented over a  
711   fraction of a grid cell. The host meteorological model provides both cloud cover and water content. The J value package used  
712   was developed for MESSy (Jöckel et al., 2006) and is implemented in GEM-AQ.

713   The current version of GEM-AQ has 5 size-resolved aerosol types, viz. sea salt, sulphate, black carbon, organic carbon and  
714   dust as well as nitrates. The microphysical processes that describe the formation and transformation of aerosols are calculated  
715   by a sectional aerosol module (Gong et al., 2003). The particle mass is distributed into 12 logarithmically spaced bins from  
716   0.005 to 10.24-micron radius. This size distribution leads to an additional 60 advected tracers. The following aerosol processes  
717   are accounted for in the aerosol module: nucleation, condensation, coagulation, sedimentation and dry deposition, in-cloud  
718   oxidation of  $\text{SO}_2$ , in-cloud scavenging, and below-cloud scavenging by rain and snow.

### 719   **3.5.9   Assimilation system**

720   Data assimilation in the GEM-AQ modelling system is done with Optimal Interpolation method (Robichaud and Ménard,  
721   2014) and is applied to the forecast. Error statistics are computed with the Hollingsworth - Lönnberg (HL) method  
722   (Hollingsworth and Lönnberg, 1986). It estimates the correlation length and the ratio of observation to model error variances  
723   by a least-square fit of a correlation model against the sample of the spatial autocorrelation of observation-minus-model  
724   residuals.

725   Currently, data assimilation is done at each forecast hour for  $\text{O}_3$ ,  $\text{NO}_2$ ,  $\text{SO}_2$ , CO,  $\text{PM}_{10}$  and  $\text{PM}_{2.5}$ , using surface observations.

726

## 727   **3.6    LOTOS-EUROS**

### 728   **3.6.1    Model Overview**

729   The LOTOS-EUROS model is a 3D chemistry transport model aimed to simulate air pollution in the lower troposphere. The  
730   model has been used in a large number of studies for the assessment of particulate air pollution and trace gases (e.g. O<sub>3</sub>, NO<sub>2</sub>)  
731   (Hendriks et al., 2016; Schaap et al., 2013; Thürkow et al., 2021; Timmermans et al., 2022). A detailed description of the  
732   model is given in (Manders et al., 2017). At present the version used in the production is v2.2.009.

### 733   **3.6.2    Model geometry**

734   The domain of LOTOS-EUROS is the CAMS regional domain from 25°W to 45°E and 30°N to 72°N. The projection is regular  
735   longitude-latitude, at 0.1°x0.1° grid spacing. In the vertical and for the forecasts there are currently 12 model layers and 2 more  
736   reservoir layers at the top, defined by coarsening in a mass conservative way the first 77 model levels of the IFS. For output  
737   purposes, the concentrations at measuring height (usually 2.5 m) are diagnosed by assuming that the flux is constant with  
738   height and equal to the deposition velocity times the concentration at height  $z$  (taken as average over the grid cell). This applies  
739   for several of the gaseous species, namely O<sub>3</sub>, NO, NO<sub>2</sub>, HNO<sub>3</sub>, N<sub>2</sub>O<sub>5</sub>, H<sub>2</sub>O<sub>2</sub>, CO, SO<sub>2</sub> and NH<sub>3</sub>. For aerosols, the same  
740   approach is utilized, only sedimentation velocity is used instead of deposition velocity.

### 741   **3.6.3    Forcing Meteorology**

742   The forcing meteorology is retrieved from the 00:00 and 12:00 UTC runs of the IFS model at hourly (surface fields) or 3-  
743   hourly temporal resolution (model layer fields). The meteorological data is retrieved on a regular horizontal resolution of about  
744   9 km and for all layers covered by the model's vertical extent. The meteorological variables included are 3-hourly 3D fields  
745   for wind direction, wind speed, temperature, humidity and density, augmented by hourly 2D gridded fields of mixing layer  
746   height, surface wind and temperature, precipitation rates, heat fluxes, cloud cover and surface variables snow depth, sea ice  
747   cover and volumetric soil water.

### 748   **3.6.4    Chemical initial and boundary conditions**

749   The lateral and top boundary conditions for trace gases and aerosols are obtained from the CAMS-Global daily forecasts (see  
750   Table 2). LOTOS-EUROS uses a bulk approach for the aerosol size distribution differentiating between a fine and a coarse  
751   fraction, but for dust and sea salt there are 5 distinct size classes: ff: 0.1-1 µm, f:1-2.5 µm, ccc: 2.5-4 µm, cc: 4-7 µm, c:7-10  
752   µm. When the chemical boundary conditions from CAMS-Global are missing (which is very rare, typically less than once a  
753   year, and can, e.g., be due to delays in the file transfer or other serious technical issues at ECMWF), the model uses  
754   climatological boundary concentrations derived from CAMS-Global data. The forecasts are initialised with the LOTOS-  
755   EUROS forecast of the previous day.

### 756 3.6.5 Emissions

757 The common annual anthropogenic emissions CAMS-REG are implemented as explained in Section 2.5.1. Injection height  
758 distribution from the EuroDelta study is implemented, which is per SNAP (or more recently, GNFR) category. Time profiles  
759 used are defined per country and GNFR emission category type.

760 Biogenic NMVOC emissions are calculated online using actual meteorological data and a detailed landuse and tree species  
761 database including emission factors from (Köble and Seufert, 2001). The isoprene emissions follow the mathematical  
762 description of the temperature and light dependence of the isoprene emissions, proposed by (Guenther et al., 1993). Sea salt  
763 emissions are parameterised following (Martensson et al., 2003; Monahan, 1986) from the wind speed at 10-meter height.

764 The fire emissions are taken from the near real-time GFAS fire emissions database. For the forecast, we assume persistence,  
765 so that the latest downloaded emission for the specific hour is used. When the hourly emission is more than 3 days old, it is  
766 set to zero.

767 Mineral dust emissions within the modelling domain are calculated online based on the sand blasting approach by (Marticorena  
768 and Bergametti, 1995) with soil moisture inhibition as described by (Fécan et al., 1998). Finally, a parameterization using land  
769 cover and temperature is used for handling soil NO<sub>x</sub> emissions, based on (Yienger and Levy, 1995).

### 770 3.6.6 Solver, advection and mixing

771 The transport consists of advection in 3 dimensions, horizontal and vertical diffusion, and entrainment/detrainment. The  
772 advection is driven by meteorological fields ( $u, v$ ), which are input every 3 hours. The vertical wind speed  $w$  is calculated by  
773 the model as a result of the divergence of the horizontal wind fields. A linear advection scheme is used to ensure tracer mass  
774 conservation, which also allows more efficient parallelization and reduced model complexity. This scheme uses piece-wise  
775 linear functions to define sub-grid concentrations, which is sometimes referred to as MUSCL ("Monotonic Upwind-centered  
776 Scheme for Conservation Laws") following (Van Leer, 1984).

777 Vertical diffusion is described using the standard  $K_z$  theory. Vertical exchange is calculated employing the new integral scheme  
778 by (Yamartino et al., 2007). For the forecasting set-up with 12 layers, atmospheric stability values and functions, including  $K_z$   
779 values, are derived based on the surface heat fluxes from ECMWF meteorology and similarity profiles following the IFS  
780 approach (Ecmwf, 2021) to adapt for land-use specific conditions. For the 5-layer version in the assimilation, a correction is  
781 made for the vertical diffusion to correct for the height difference between surface and mixing layer.



### 782   **3.6.7   Deposition**

783   The dry deposition in LOTOS-EUROS is parameterised following the resistance approach. The laminar layer resistance and  
784   the surface resistances for acidifying components are described following the EDACS system (Van Zanten et al., 2010), the  
785   deposition velocities for particles are based on (Zhang et al., 2001). Wet deposition is divided between in-cloud and below-  
786   cloud scavenging. The in-cloud scavenging module is based on the approach described in (Seinfeld and Pandis, 1998) and  
787   (Banzhaf et al., 2012).

### 788   **3.6.8   Chemistry and aerosols**

789   LOTOS-EUROS uses the TNO CBM-IV scheme, which is a modified version of the original CBM-IV (Gery et al., 1989).  
790   N<sub>2</sub>O<sub>5</sub> hydrolysis is described explicitly based on the available (wet) aerosol surface area (using  $\gamma = 0.05$ ) (Schaap et al., 2004).  
791   Aqueous phase and heterogeneous formation of sulphate is described by a simple first order reaction constant (Barbu et al.,  
792   2009; Schaap et al., 2004). Inorganic aerosol chemistry is represented using ISORROPIA II (Fountoukis and Nenes, 2007)  
793   and secondary organic aerosols formation based on a VBS scheme (Bergström et al., 2012a; Zare et al., 2014) will be included  
794   in the operational forecast version in the future.

### 795   **3.6.9   Assimilation system**

796   The LOTOS-EUROS model is equipped with a data assimilation package with the ensemble Kalman filter technique (Curier  
797   et al., 2012). The ensemble is created by specification of uncertainties for emissions (NO<sub>x</sub>, VOC, NH<sub>3</sub> and aerosol), ozone  
798   deposition velocity, and ozone top boundary conditions. Currently, data assimilation is performed for O<sub>3</sub>, NO<sub>2</sub>, PM<sub>10</sub> and PM<sub>2.5</sub>  
799   surface observations, OMI NO<sub>2</sub> is also assimilated.

800

## 801    **3.7    MATCH**

### 802    **3.7.1    Model Overview**

803    The Multi-scale Atmospheric Transport and Chemistry model (MATCH) (Robertson et al., 1999) is an off-line chemical  
804    transport model (CTM) with a flexible design, accommodating different weather data forcing on different resolutions and  
805    projections, and a range of alternative schemes for deposition and chemistry.

### 806    **3.7.2    Model geometry**

807    The model's geometry is taken from the input weather data. To reduce computational costs, the vertical resolution is reduced  
808    compared to the ECMWF operational model by merging pairs of IFS vertical layers, while retaining the use of hybrid vertical  
809    coordinates. The horizontal resolution in the MATCH simulation matches that of the meteorological forcing, which is currently  
810    provided on a 0.1° latitude–longitude grid. The lowest 78 layers of the ECMWF model are lumped in 39 levels, which then  
811    are used for the air quality simulations. The model top is at about 8000 m height. The model domain covers the area between  
812    28.8° W to 45.8° E and 29.2° N to 72.0° N. The grid is an Arakawa C-grid with staggered wind components.

### 813    **3.7.3    Forcing Meteorology**

814    The forcing meteorology for MATCH forecasts is retrieved from the 12:00 UTC run of the IFS modelling system on a  
815    0.1°×0.1° spatial grid and with a temporal resolution of three hour. For the analyses, the 00:00 UTC analysis of the IFS is used  
816    at 0.2°×0.2° resolution. The reason for applying a coarser resolution in the analysis is twofold: 1) the delivery time is rather  
817    short from when the in-situ observations are available, 2) the analysis increments are on a larger scale. The meteorological  
818    variables included are 3D fields of the horizontal wind components (U, V), temperature, specific humidity, cloud cover, cloud  
819    water content, cloud ice water content, and surface fields of surface pressure, logarithm of surface pressure, surface  
820    temperature, sea surface temperature, snow depth, albedo, roughness height, total cloud cover, precipitation, and volumetric  
821    soil water at the surface.

### 822    **3.7.4    Chemical initial and boundary conditions**

823    The lateral boundary conditions for trace gases and aerosols are obtained from the CAMS-Global forecasts at 3-hourly  
824    resolution for the following species: O<sub>3</sub>, CO, HCHO, NO, NO<sub>2</sub>, SO<sub>2</sub>, HNO<sub>3</sub>, PAN, CH<sub>4</sub>, C<sub>3</sub>H<sub>8</sub>, o-xylene, sulphate and C<sub>2</sub>H<sub>6</sub>  
825    (see Table 2). In the event that the chemical boundary conditions from CAMS-Global would be missing (which has never  
826    happened in practice but could in theory happen due to corruption or other technical issues), the model uses seasonal  
827    climatological boundary concentrations instead.

### 828 3.7.5 Emissions

829 The common annual anthropogenic emissions CAMS-REG are implemented as explained in Section 2.5.1. Temporal  
830 disaggregation is based on the GENEMIS tables (Ebel et al., 1997), using a GNFR to SNAP matrix. The vertical distribution  
831 of the emissions depends on the sector. Near-surface emission sources (SNAP 2,6,7,8,10) are distributed in the lowest 90 m;  
832 for other sectors the emissions are allocated over varying model levels up to a maximum of about 1100 m height. According  
833 to the sector, the anthropogenic VOC emissions are split into the MATCH chemical mechanism surrogate species: C<sub>2</sub>H<sub>6</sub>,  
834 NC<sub>4</sub>H<sub>10</sub>, C<sub>2</sub>H<sub>4</sub>, C<sub>3</sub>H<sub>6</sub>, OXYLENE, BENZENE, TOLUENE, CH<sub>3</sub>OH, C<sub>2</sub>H<sub>5</sub>OH, HCHO, CH<sub>3</sub>CHO, CH<sub>3</sub>COC<sub>2</sub>H<sub>5</sub>; the particulate  
835 matter components elemental carbon, organic matter, anthropogenic dust (other than soil and road dust) are allocated to two  
836 bins (PM<sub>2.5</sub> and PM-coarse), as well as the road dust estimated according to (Schaap et al., 2009) and (Omstedt et al., 2005),  
837 and the teluric dust calculated according to (Zender et al., 2003).

838 Biogenic emissions of isoprene, monoterpenes and sesquiterpenes are calculated following (Simpson et al., 2012; Simpson et  
839 al., 1995; Bergström et al., 2012a), taking into account temperature at 2 m, radiation fluxes and the vegetation cover.

840 The dimethyl sulphide - DMS – emissions from the Ocean and Baltic Sea are also considered; whereas the particulate matters  
841 from sea salt are calculated according to the parameterisation proposed by (Sofiev et al., 2011).

842 The GFAS biomass burning emissions are taken into the model mapping the following species into the MATCH chemical  
843 mechanism: NO<sub>x</sub>, SO<sub>2</sub>, CO, CH<sub>4</sub>, C<sub>2</sub>H<sub>4</sub>, C<sub>2</sub>H<sub>6</sub>, C<sub>3</sub>H<sub>6</sub>, C<sub>4</sub>H<sub>10</sub>, C<sub>8</sub>H<sub>10</sub>, benzene, toluene, CH<sub>3</sub>OH, C<sub>2</sub>H<sub>5</sub>OH, formaldehyde,  
844 acetaldehyde, OC, BC, PM<sub>2.5</sub>, and PM<sub>10</sub>. The vertical injection is made by a parabolic curve with central height taken from the  
845 GFAS INJH parameter. In case the injection height is missing for a GFAS emission cell this is assigned from some neighbour  
846 height present. The diurnal emission profile is based on the D-1 GFAS hourly data filled up with GFAS data for D-2 for the  
847 not yet available hours in D-1. This diurnal hourly profile is repeated throughout the forecast.

### 848 3.7.6 Solver, advection and mixing

849 Mass conservative transport schemes are used for advection and turbulent transport. The advection is formulated as a Bott-like  
850 scheme (Robertson et al., 1999). A second order transport scheme is used in the horizontal as well as the vertical. The vertical  
851 diffusion is described by an implicit mass conservative first order scheme, where the exchange coefficients for neutral and  
852 stable conditions are parameterized following (Holtslag and Nieuwstadt, 1986). In the convective case the turbulent Courant  
853 number is directly determined from the turnover time in the boundary layer.

854 Part of the dynamical core is the initialisation and adjustment of the horizontal wind components. This is a very important step  
855 to ensure mass conservative transport. The initialisation is based on a procedure proposed by (Heimann and Keeling, 1989),

856 where the horizontal winds are adjusted by means of the difference between the input surface pressure tendency, and the  
857 calculated pressure tendency assumed to be an error in the divergent part of the wind field.

858 Boundary layer parameterisation is based on surface heat and water vapour fluxes as described by (Van Ulden and Holtslag,  
859 1985) for land surfaces, and (Burridge, 1977) for sea surfaces. The boundary layer height is calculated from formulations  
860 proposed by (Zilitinkevich and Mironov, 1996) for the neutral and stable case, and from (Holtslag et al., 1995) for the  
861 convective case. These parameterisations drive the formulations for dry deposition and vertical diffusion.

### 862 **3.7.7 Deposition**

863 Dry deposition of gases and aerosols is modelled using a resistance approach (based on the scheme in (Simpson et al., 2012)),  
864 which includes stomatal and non-stomatal pathways for vegetated surfaces. In the current operational system, the model applies  
865 this scheme across various physiographic tiles derived from the CLC/SEI inventory<sup>5</sup> (Simpson et al., 2012). MATCH uses 3D-  
866 precipitation (estimated in the model, based on the surface precipitation and 3D cloud water information from the IFS forecast)  
867 and separates wet scavenging into in-cloud and sub-cloud scavenging. For most gaseous components the scavenging is  
868 assumed to be proportional to the precipitation intensity (with higher scavenging ratios in-cloud than sub-cloud). For the  
869 particulate components in-cloud scavenging is also treated using simple scavenging ratios while the sub-cloud scavenging is  
870 treated using a scheme based on (Berge, 1993) with size dependent collection efficiencies (as in (Simpson et al., 2012)).

### 871 **3.7.8 Chemistry and aerosols**

872 The photochemistry scheme is based on the EMEP MSC-W chemistry scheme (Simpson et al., 2012), with a modified scheme  
873 for isoprene, based on the so-called Carter-1 mechanism (Carter, 1996; Langner et al., 1998). The standard MATCH setup  
874 used in CAMS treats particles as bulk aerosol in two size classes, fine ( $PM_{2.5}$ ) and coarse ( $PM_{2.5-10}$ ) particles. Particle formation  
875 from gases include secondary inorganic aerosol (ammonium sulphate and nitrate) and secondary organic aerosol. Ammonium  
876 nitrate equilibrium is calculated according to (Mozurkewich, 1993). Coarse nitrate formation from gas-phase  $HNO_3$  is also  
877 included (Strand and Hov, 1994). Secondary organic aerosol formation from oxidation of volatile organic compounds is treated  
878 using a volatility basis set scheme based on (Hodzic et al., 2016). Exception is made for the isoprene oxidation for which the  
879 chain of reactions is following the Carter-1 chemical mechanism, which has proven to give the comparable results with fewer  
880 reactions (Carter, 1996; Langner et al., 1998).

---

<sup>5</sup> [www.sei.org/projects/sei-european-land-cover-map](http://www.sei.org/projects/sei-european-land-cover-map) (last accessed 30/10/2024)

### 881   **3.7.9   Assimilation system**

882   The model for data assimilation is an integrated part of the MATCH modelling system. The data assimilation scheme as such  
883   is a variational spectral scheme (Kahnert, 2008), implying that the background covariance matrices are modelled in spectral  
884   space. The limitation is that covariance structures are described as isotropic and homogeneous. The advantage is that the  
885   background error matrix becomes block diagonal, and there are no scale separations as the covariance between spectral  
886   components are explicitly handled. The block diagonal elements are the covariance between wave components at model layers  
887   and chemical compounds.

888   Modelling the background error covariance matrices is the central part in data assimilation. This is conducted by means of the  
889   so-called NMC approach (Parrish and Derber, 1992). The CTM (MATCH) is run for a 3-month period for photochemistry and  
890   aerosols with analysed and forecasted ECMWF weather data. The differences are assumed to mimic the background errors,  
891   and the statistics in spectral space are generated for different combinations of the model compounds: O<sub>3</sub>, NO<sub>2</sub>, NO, SO<sub>2</sub>, CO,  
892   PM<sub>2.5</sub>, PM<sub>10</sub>.

893   The scheme is fully intermittent in hour-by-hour steps and the above-listed components are assimilated from in-situ  
894   measurements. The analysed components are propagated by chemistry and transport into unobserved components as  
895   NMVOCs, PAN and NH<sub>3</sub>.

896

## 897    **3.8    MINNI**

### 898    **3.8.1    Model Overview**

899    MINNI (Italian Integrated Assessment Modelling System for supporting the International Negotiation Process on Air Pollution  
900    and assessing Air Quality Policies at national/local level; (D'elia et al., 2021; Mircea et al., 2014) has been developed to support  
901    the Italian Ministry for Environment and Territory and Sea. The core of the modelling system is the 3-dimensional offline  
902    Eulerian CTM FARM (Flexible Air quality Regional Model, (Silibello et al., 2008) that accounts for the transport, chemistry  
903    and removal of atmospheric pollutants.

### 904    **3.8.2    Model geometry**

905    For the CAMS regional forecast, the model is configured with a regular latitude-longitude grid of  $0.15^\circ \times 0.10^\circ$  resolution.  
906    The domain spans from  $-25^\circ$  to  $45.05^\circ$  degree East and from  $30^\circ$  to  $72^\circ$  degree North. The model uses z-level terrain following  
907    mesh with the first central grid point at 20 m AGL (above ground level) and the last one at 6290 m AGL. No vertical  
908    downscaling is applied to extrapolate concentrations from 20 meters above the ground to the surface.

### 909    **3.8.3    Forcing Meteorology**

910    The forcing meteorology is retrieved from the 12:00 UTC run of the IFS modelling system on a  $0.1^\circ \times 0.1^\circ$  spatial grid and with  
911    a temporal resolution of one hour. The meteorological variables included are 3D fields such as temperature, relative humidity,  
912    pressure and wind velocity and 2D fields such as boundary layer height, roughness length, albedo, sea surface temperature,  
913    total cloud cover and precipitation.

### 914    **3.8.4    Chemical initial and boundary conditions**

915    The lateral and top boundary conditions for trace gases and aerosols are obtained from the CAMS-Global daily forecasts with  
916    a 3-hr temporal resolution (see Table 2). The initial condition is taken from the previous forecast of the MINNI model.

### 917    **3.8.5    Emissions**

918    The common annual anthropogenic emissions CAMS-REG are implemented as explained in Section 2.5.1. Point emissions  
919    are summed up to gridded emissions for each GNFR sector, since no information was available about the characterization of  
920    the point sources in terms of injection height. Conservative mass horizontal interpolation has been applied to map the emissions  
921    on the actual model domain. Vertical splitting has been applied for each GNFR sector adapting the vertical injection profiles  
922    provided by TNO to the actual model levels. Temporal emission profiles for each GNFR sector, as they were provided by  
923    TNO, have been applied considering local hour (i.e. the time zones shift has been taken into account).

925 PM<sub>2.5</sub> has been speciated following the TNO table as a function of country and sector and AERO3 (Binkowski and Shankar,  
 926 1995; Binkowski, 1999) species size fractions below 2.5µm. The coarse component (PM<sub>10</sub>-PM<sub>2.5</sub>) was associated to non-  
 927 speciated coarse mode since MINNI dispersion model considers all the secondary aerosol fraction as PM<sub>2.5</sub>. This method leaves  
 928 the detailed chemical speciation out but ensures mass conservation.

929 The NMVOC speciation originated from the TNO table as a function of country and sector obtaining the v01-v25 species. The  
 930 mapping among the v01-v25 species to SAPRC99 species has been done in agreement with the choices made and tested in the  
 931 frame of EURODELTA III intercomparison exercise (Colette et al., 2017).

932 Biogenic emissions are computed with the MEGAN model v.2.04 (Guenther et al., 2006), and NO<sub>x</sub> emissions from soil  
 933 following (Williams et al., 1992) approach.

934 Erosion and resuspension of the dust are calculated by means of method proposed by (Vautard et al., 2005). Road dust  
 935 emissions are parameterized following (Zender et al., 2003).

936 Fire emissions are taken into account using hourly data from the GFAS database considering emissions from D-1 for AN (D-  
 937 1) and FC (D+0 and D+1, zero for the remaining days).

### 938 **3.8.6 Solver, advection and mixing**

939 FARM is a 3-dimensional Eulerian model with first order turbulence closure. Physical and chemical processes influencing the  
 940 concentration fields within the modelling domain are described by a system of partial differential equations (PDE). The  
 941 numerical integration of the above system of PDEs is performed by a method that splits the multi-dimensional problem into  
 942 time dependent one-dimensional problems, which are then solved sequentially over the time step.

943 Partial differential equations involved in horizontal and vertical advection-diffusion operators are solved in FARM using the  
 944 schemes employed in CALGRID model (Yamartino et al., 1992). In particular, horizontal advection-diffusion operators are  
 945 solved using a finite elements method based on Blackman cubic polynomials. The coefficients of a cell-centered cubic  
 946 polynomial are constrained to maintain high-accuracy and low-diffusion characteristics and to avoid undesirable negative  
 947 concentrations. In addition, a filter is used for filling undesired short wavelength minima. The numerical integration of the  
 948 vertical diffusion equation is performed in a hybrid way employing a hybrid semi-implicit Crank-Nicholson / fully implicit  
 949 scheme (Yamartino et al., 1992).

950 The calculation of horizontal diffusion coefficients is based on Stress tensor formulation of (Smagorinsky, 1963) also including  
951 a dependence on the local stability class and wind speed. For the calculation of vertical diffusion coefficients, the (Lange,  
952 1989) approach to boundary layer scaling regimes is used. Mixing due to deep convection is not explicitly taken into account.

953 Two different schemes to compute the PBL scaling parameters are used. In the daytime, the (Maul et al., 1980) version of  
954 (Carson, 1973)encroachment method is used. During night-time, the minimum value between (Nieuwstadt, 1981) and  
955 (Venkatram, 1980) is used.

### 956 **3.8.7 Deposition**

957 The dry deposition velocities are modelled following a resistance analogy approach, as an inverse sum of a series of 3  
958 resistances: the aerodynamic resistance, the quasi-laminar layer resistance and the surface resistance. Aerodynamic resistance  
959 is dependent on surface characteristics and atmospheric stability conditions (described through friction velocity and Monin-  
960 Obukhov length). Quasi-laminar layer resistance is parameterised using (Hicks et al., 1987). Surface resistance is approximated  
961 as a set of parallel resistance associated with leaf stomata, leaf cuticles, lower canopy and surface soil, litter and water (Wesely,  
962 1989). Deposition to water surfaces is based on (Slinn et al., 1978).

963 The deposition velocity of particulate species also depends on particle size distribution and density because of gravitational  
964 settling. Sedimentation velocity acts in parallel to the other resistances. Hygroscopic growth is considered over water for  
965 particles less than 2  $\mu\text{m}$ . For particles ranging from 0.1 to 1  $\mu\text{m}$  deposition velocity is computed as the inverse of the resistance  
966 computed from canopy height, friction velocity and Monin-Obukhov length.

967 The parameterization of wet deposition follows the (Simpson et al., 2012) approach, including in-cloud and below-cloud  
968 scavenging of gas and particles.

### 969 **3.8.8 Chemistry and aerosols**

970 The gas-phase chemical mechanism used for CAMS forecast is SAPRC-99 with the inclusion of Polycyclic aromatic  
971 hydrocarbons (PAHs) and Mercury chemistry; moreover, a simplified aqueous phase mechanism is included for  $\text{SO}_2$  oxidation  
972 and chemical processes involving Mercury in both gas and aqueous phases.

973 A simple approach is used to estimate photolysis rates based on look-up tables to calculate the rate constants for photolysis  
974 reactions (Nenes et al., 1998). Photolysis rates are computed and adjusted according to local solar zenith angle using an  
975 empirical formula based on (Peterson, 1976) data.



976 The aerosols module is AERO3 (Binkowski and Shankar, 1995; Binkowski, 1999). In AERO3 the representation of the particle  
977 size is three-modal (Aitken, accumulation and coarse), following lognormal distributions. The aerosol species included are  
978 sulphate, nitrate, ammonium, anthropogenic primary and secondary organic aerosol, biogenic secondary organic aerosol,  
979 elemental carbon, sea-salt and dust. The aerosol dynamics takes into account nucleation, condensation and coagulation  
980 processes. The gas/particle mass transfer is implemented by means of ISORROPIA v1.7 (Nenes et al., 1998) and SORGAM  
981 (Schell et al., 2001a) for secondary inorganic and organic aerosol, respectively.

### 982 **3.8.9 Assimilation system**

983 The assimilation scheme used is optimal interpolation: the correlation function is factorized in vertical and horizontal  
984 components. The horizontal component has pollutant dependent fixed correlation length with a terrain-following exponential  
985 decay. The vertical component is modelled with a Cressman function dependent on the boundary layer height. The system  
986 assimilates NO<sub>2</sub>, O<sub>3</sub>, SO<sub>2</sub>, CO, PM<sub>10</sub> and PM<sub>2.5</sub>. In case of aerosol components, the correction applied to each of them is  
987 proportional to their content in PM. At present, only data from surface stations are assimilated. More details are available in  
988 (Adani and Uboldi, 2023).

989

## 990     **3.9     MOCAGE**

### 991     **3.9.1     Model Overview**

992     The MOCAGE 3D multi-scale Chemistry and Transport Model has been designed for both research and operational  
993     applications in the field of environmental modelling. Since 2000, MOCAGE has been allowing to cover a wide range of topical  
994     issues ranging from chemical weather forecasting, tracking and backtracking of accidental point source releases, trans-  
995     boundary pollution assessment, assimilation of remote sensing measurements of atmospheric composition, to studies of the  
996     impact of anthropogenic emissions of pollutants on climate change (Guth et al., 2018; Cussac et al., 2020).

### 997     **3.9.2     Model geometry**

998     For the CAMS Regional Service, MOCAGE operates on a regular latitude-longitude grid at 0.1 resolution covering the 28° to  
999     72° North and 26°W to 46°E domain, for both forecast and assimilation. The products delivered for the CAMS service are  
1000     issued from the regional domain only. In the vertical, 47 hybrid levels go from the surface up to 5 hPa, with approximately 8  
1001     levels in the Planetary Boundary Layer (i.e. below 2km), 16 in the free troposphere and 24 in the stratosphere. The thickness  
1002     of the lowest layer is about 40 m. There is no downscaling applied to surface concentration.

### 1003     **3.9.3     Forcing Meteorology**

1004     The forcing meteorology is retrieved from the IFS model vertical layers covering the MOCAGE vertical extent on a 0.1°x0.1°  
1005     horizontal grid resolution with a temporal resolution of one hour for the 3 first forecast days and 3 hours for the last forecast  
1006     day. The forecast released at 12UTC of the previous days is used. The meteorological parameters used for the dynamics  
1007     calculation in MOCAGE are: horizontal and vertical winds, temperature, humidity, cloud fraction, surface pressure, albedo,  
1008     precipitations and incoming radiative flux. The variables relevant for the deposition module are soil humidity and temperature,  
1009     wind speed and direction, specific humidity, pressure at ground level, and sensible heat flux.

### 1010     **3.9.4     Chemical initial and boundary conditions**

1011     Chemical initial values in the regional domain are provided by MOCAGE 24h forecast from the day before. The boundary  
1012     conditions are taken from global CAMS operational suite for the species (chemical and aerosols) that are distributed (see Table  
1013     2). For aerosols, the 2 or 3 bins from CAMS-Global are summed to get total concentration and then distributed onto the 6  
1014     MOCAGE bins considering Mean CAMS-Global bin size as emission modes. A factor 4.3 is applied to convert Sea Salt from  
1015     wet to dry fractions. Aerm03 (of diameter larger than 10µm) is only marginally distributed within MOCAGE PM<sub>10</sub> sea salt  
1016     because of the matching between bins and log-normal modes. For the species not included in Table 2, the concentrations from  
1017     the MOCAGE global domain are used, which helps to introduce smoothly, on the horizontal as well as on the vertical, these  
1018     chemical boundary conditions into the CAMS regional domain.

1019     **3.9.5     Emissions**

1020     The common annual anthropogenic emissions CAMS-REG are implemented as explained in Section 3.2. Temporal  
1021     disaggregation is based on the GENEMIS tables (Ebel et al., 1997), using a GNFR to SNAP matrix. Chemical disaggregation  
1022     for PM species and VOCs is based on sector and country-dependent split factors proposed by TNO.

1023     Isoprene biogenic emissions are computed online using MEGAN model (Guenther et al., 2012), while other biogenic emissions  
1024     are computed from CAMS global biogenic emission inventory (version 3.1). NO<sub>x</sub> soil emissions are taken from the CAMS-  
1025     GLOB-SOILv2.2 emission inventory.

1026     Concerning biomass burning sources, GFAS emissions are emitted according to an ‘umbrella’ profile, with a maximum  
1027     injecting height climatologically determined. GFAS “near real time” observation-based fire emissions are made available with  
1028     a 8-hr delay. So that when the forecast system is initiated, most GFAS emission cover Day-2 of the forecast to be produced.  
1029     As a consequence, the 2-day persistence is interpreted in a way that fire emissions are only applied for D+0.

1030     **3.9.6     Solver, advection and mixing**

1031     The chemical solver used is a semi-implicit solver as presented in (Cariolle and Teyssedre, 2007).

1032     Concerning physical and chemical parameterisations, an operator splitting approach is used. Parameterisations are called  
1033     alternatively in forward and reverse order, with the objective to reduce systematic errors.

1034     Meteorological forcings are read every 3 hours from IFS input data, and are linearly interpolated to yield hourly values, which  
1035     is the time-step for advection; smaller time-steps are used for physical processes and chemistry, but the meteorological  
1036     variables are kept constant over each hour. MOCAGE is based upon a semi-lagrangian advection scheme (Williamson and  
1037     Rasch, 1989), using a cubic polynomial interpolation in all 3 directions.

1038     For sub-gridscale transport processes, vertical diffusion is treated following (Louis, 1979) and transport by convection is from  
1039     (Bechtold et al., 2001). Scavenging within convective clouds is following (Mari et al., 2000), allowing to compute wet removal  
1040     processes directly within the convective transport parameterisation.

1041     **3.9.7     Deposition**

1042     Wet deposition in stratiform clouds and below clouds follows (Giorgi and Chameides, 1986). A description of MOCAGE  
1043     surface exchanges module is presented in (Michou et al., 2005). The dry deposition parameterisation relies on a fairly classical  
1044     surface resistance approach (Wesely, 1989), but with a refined treatment of the stomatal resistance, similar to the one used in

1045 Meteo-France numerical weather prediction models (Noilhan and Planton, 1989). Sedimentation of aerosol follows (Nho-Kim  
1046 et al., 2004).

### 1047 **3.9.8 Chemistry and aerosols**

1048 The MOCAGE configuration for CAMS comprises 118 species and over 300 reactions and photolysis. It is a merge of reactions  
1049 of the RACM scheme (Stockwell et al., 1997) with the reactions relevant to the stratospheric chemistry of REPROBUS  
1050 (Lefevre et al., 1994). Aqueous chemistry for the formation of sulphate is represented, following (Ménégoz et al., 2009).  
1051 Detailed heterogeneous chemistry on Polar Stratospheric Clouds (types I, II) is accounted for, as described in (Lefevre et al.,  
1052 1994). Other heterogeneous chemistry processes are currently not included.

1053 Photolysis is taken into account using a multi-entry look-up table computed off-line with the TUV software version 4.6  
1054 (Madronich, 1987). Photolysis depends on month (including monthly aerosol climatologies), solar zenith angle, ozone column  
1055 above each cell (as the model extends to the mid-stratosphere, it is actually the ozone profile computed by MOCAGE which  
1056 is used at every time step), altitude and surface albedo in the UV. They are computed for clear-sky conditions and the impact  
1057 of cloudiness on photolysis rates is applied afterwards.

1058 The aerosol module of MOCAGE includes the primary species dusts, black carbon, sea salts, organic carbon, and the secondary  
1059 inorganic species sulphate, nitrate and ammonium. The formation and the multi-phasic equilibrium of inorganic secondary  
1060 aerosols are modelled by the ISORROPIA-II module. Details on MOCAGE aerosol simulation evaluation can be found in  
1061 (Martet et al., 2009) for dusts, in (Nho-Kim et al., 2005) for black carbon, and in (Sič et al., 2015) for the latest version of  
1062 MOCAGE primary aerosol module. The implementation and the evaluation of secondary inorganic aerosols in MOCAGE are  
1063 described by (Guth et al., 2016). Further improvements of the representation of aerosols in MOCAGE are expected in the  
1064 future with on-going work regarding organic secondary aerosols.

### 1065 **3.9.9 Assimilation system**

1066 MOCAGE operations for CAMS use the assimilation system based upon MOCAGE and PALM (Lahoz et al., 2007). As a first  
1067 approximation, background error standard deviations are prescribed as proportional to background amounts. In order to spread  
1068 assimilation increments spatially, background error correlations are modelled using a generalized diffusion operator (Weaver  
1069 and Courtier, 2001). Several assimilation strategies are available in PALM but for CAMS MOCAGE uses a 3D-VAR  
1070 technique, with an assimilation window that is 1h every hour.

1071 For surface analyses (NRT, IRA and VRA), MOCAGE assimilates O<sub>3</sub>, NO<sub>2</sub>, CO, PM<sub>10</sub> and PM<sub>2.5</sub> in-situ surface observations.  
1072 The species are assimilated independently every hour without any cross-species covariances, and then the increments per

1073 species are added to the analysis that serves as initial condition for computing the background of the next hour of the  
1074 assimilation process, in this reanalysis mode.

1075 An hourly assimilation cycle is also used to update the atmospheric state of aerosols, with the assimilation of French lidars  
1076 (mini-MPL) and some ceilometers from the European network E-profile in the regional domain of MOCAGE. The quantity  
1077 modified during the assimilation process is the 3D field of total mass of all aerosol types and all sizes all together. The split  
1078 per aerosol type and particle size is not modified during the assimilation. This hourly assimilation cycle is the backbone and  
1079 every day at 00 UTC, the +96h forecast is initialised from this assimilation cycle.  
1080

### 1081   **3.10   MONARCH**

#### 1082   **3.10.1   Model Overview**

1083   The MONARCH model is a fully online multiscale chemical weather prediction system for regional and global-scale  
1084   applications (Badia and Jorba, 2015; Badia et al., 2017; Jorba et al., 2012; Klose et al., 2021; Pérez et al., 2011). The system  
1085   is based on the meteorological Nonhydrostatic Multiscale Model on the B-grid (NMMB; (Janjic and Gall, 2012)), developed  
1086   and widely verified at the National Center for Environmental Prediction (NCEP). The model couples online the NMMB with  
1087   the gas-phase and aerosol continuity equations to solve the atmospheric chemistry processes in detail. The model is designed  
1088   to account for the feedbacks among gases, aerosol particles and meteorology. Currently, it can consider the direct radiative  
1089   effect of aerosols while ignoring cloud–aerosol interactions.

#### 1090   **3.10.2   Model geometry**

1091   The hybrid pressure-sigma coordinate is used in the vertical direction and the Arakawa B-grid is applied in the horizontal  
1092   direction. The regional model is formulated on a rotated longitude–latitude grid, with the Equator of the rotated system running  
1093   through the middle of the integration domain, resulting in more uniform grid distances. In the operational regional CAMS  
1094   forecasts, the model is configured for a regional domain covering Europe and part of northern Africa with a regular horizontal  
1095   grid spacing on the rotated projection of 0.15° (lower-left corner at 16.37°N 22.14°W, upper-right corner at 58.56°N 88.18°E)  
1096   and the top of the domain is set at 50hPa using 24 vertical layers. Surface concentrations of gases and aerosols are derived  
1097   directly from the first model level; no particular vertical downscaling is implemented. The depth of the first vertical layer of  
1098   the model is around 45 m and about 7 layers are set below 2 km.

#### 1099   **3.10.3   Forcing Meteorology**

1100   The forcing meteorology is retrieved from the IFS model on a 0.125°x0.125° horizontal grid resolution (the native resolution  
1101   is remapped as close as possible to the MONARCH grid to optimise transfer time) with a temporal resolution of 6 hours and  
1102   dynamically interpolated to the final chemistry grid and time steps using the meteorological component of MONARCH. The  
1103   IFS forecast released at 12:00UTC of the previous days is used. The meteorological variables obtained from IFS are: Skin  
1104   temperature, Soil temperature, Soil moisture, Snow depth, Sea-ice mask, Sea-level pressure, U component of the wind, V  
1105   component of the wind, Temperature, Geopotential height, Relative humidity or specific humidity, Cloud water content.

#### 1106   **3.10.4   Chemical initial and boundary conditions**

1107   The variables used from chemical species available in the CAMS-Global forecast model are detailed in Table 2. Note that CH<sub>4</sub>  
1108   is not used from CAMS-Global because the MONARCH chemical mechanism considers a constant CH<sub>4</sub> concentration of 1.85

1109 ppmv. A remapping has been applied to couple the modal distribution of the CAMS-Global aerosols with the aerosols  
1110 distribution of the MONARCH model (see Table 2). The forecasts are initialised by the model results of the previous day.

### 1111 **3.10.5 Emissions**

1112 The common annual anthropogenic emissions CAMS-REG are implemented as explained in Section 2.5.1. The High-Elective  
1113 Resolution Modelling Emission System version 3 (HERMESv3; (Guevara et al., 2019)) is used to pre-process the  
1114 anthropogenic, ocean and biomass burning emissions for the MONARCH model. HERMESv3 is an open source, parallel and  
1115 stand-alone multiscale atmospheric emission modelling framework that processes gaseous and aerosol emissions for use in  
1116 atmospheric chemistry models.

1117 CAMS\_REG-AP NMVOC and PM<sub>2.5</sub> emissions are speciated using the sector and country-dependent split factors proposed  
1118 by TNO. In terms of NO<sub>x</sub>, a fraction of 90% NO and 10% NO<sub>2</sub> is considered for all sectors except for road transport, in which  
1119 the following fractions are applied: (i) 95% NO, 4.2% NO<sub>2</sub> and 0.8 HONO for gasoline road transport and (ii) 70% NO, 28.3%  
1120 NO<sub>2</sub> and 1.7% HONO for diesel road transport (Rappenglück et al., 2013). The vertical distribution of anthropogenic emissions  
1121 is performed following the sector-dependent profiles proposed by TNO. The temporal distribution follows the gridded CAMS-  
1122 REG-TEMPO v4.1 profiles (Guevara et al., 2021).

1123 The biogenic emissions for NMVOC and NO are computed on-line within the MONARCH model using the Model of  
1124 Emissions of Gases and Aerosols from Nature version 2.04 (MEGANv2.04; (Guenther et al., 2006)), while monthly oceanic  
1125 emissions of DMS are obtained from the CAMS-GLOB-OCEA v3.1 dataset (Granier et al., 2019; Lana et al., 2011).

1126 Mineral dust emissions can be calculated online using one of the schemes described in (Klose et al., 2021). For sea salt aerosol  
1127 emissions, multiple source functions are available (Spada et al., 2013).

1128 Finally, biomass burning emissions (forest, grassland and agricultural waste fires) of organic carbon, black carbon, SO<sub>2</sub>, and  
1129 DMS are taken from the GFASv1.4 dataset. This product reports hourly emissions at a horizontal gridded resolution of 0.1° x  
1130 0.1°. The vertical allocation of GFAS emissions is done using the maximum fire plume injection height and distributing  
1131 uniformly all the emissions across the layers below this height. The persistence of the fires in forecast mode is set to 2 days,  
1132 afterwards biomass burning emissions are set to zero.

### 1133 **3.10.6 Solver, advection and mixing**

1134 Different chemical processes were implemented following a modular operator splitting approach to solve the advection,  
1135 diffusion, emission, dry and wet deposition, and chemistry processes. In order to maintain consistency with the meteorological  
1136 solver, the chemical species are advected and mixed at the corresponding time step of the meteorological tracers following the

1137 principles described in (Janjic and Gall, 2012) and references therein. The advection scheme is Eulerian, positive definite and  
1138 monotone, maintaining a consistent mass conservation of the chemical species within the domain of study. Lateral diffusion  
1139 is formulated following the Smagorinsky non-linear approach, while vertical diffusion is based on the Mellor–Yamada–Janjic  
1140 level 2.5 turbulence closure scheme.

1141 The convective mixing, however, is treated differently for aerosols and gases. The scheme implemented for aerosols is  
1142 described in detail in (Pérez et al., 2011) and follows a relaxation approach similar to the Betts-Miller-Janjic convective  
1143 parameterization of the NMMB. On the other hand, the convective mixing of gases is solved following the sub-grid cloud  
1144 scheme of (Foley et al., 2010) as described in (Badia et al., 2017).

### 1145 **3.10.7 Deposition**

1146 The deposition processes implemented in the MONARCH model are dry deposition, in-cloud grid-scale, and in-cloud subgrid-  
1147 scale scavenging for gases and aerosols, and below cloud scavenging for aerosols only.

1148 For gases, the dry deposition scheme follows the classical deposition velocity analogy, enabling the calculation of deposition  
1149 fluxes from airborne concentrations. The canopy resistance is simulated following (Wesely, 1989). The cloud-chemistry  
1150 processes are included in the system considering both the sub-grid and grid-scale scheme described in (Foley et al., 2010). The  
1151 processes included are the scavenging, vertical mixing and wet-deposition. Only in-cloud scavenging is considered in the  
1152 current implementation (Badia et al., 2017).

1153 Regarding aerosols, the parameterization of the aerosol dry deposition is based on (Zhang et al., 2001) which includes  
1154 simplified empirical parameterizations for the deposition processes of Brownian diffusion, impaction, interception and  
1155 gravitational settling. Wet scavenging of aerosols by precipitation is computed separately for convective and grid-scale  
1156 (stratiform) precipitation. The model includes parameterizations for in-cloud scavenging, and for below cloud scavenging.  
1157 Detailed description of the schemes can be found in (Pérez et al., 2011).

### 1158 **3.10.8 Chemistry and aerosols**

1159 A gas-phase module combined with a hybrid sectional-bulk mass-based aerosol module is implemented in the MONARCH  
1160 model. The gas-phase chemical mechanism used is the Carbon Bond 2005 chemical mechanism (CB05; (Yarwood. G. et al.,  
1161 2005)) extended with Chlorine chemistry (Sarwar et al., 2012). The rate constants were updated based on evaluations from  
1162 (Atkinson et al., 2004; Sander et al., 2006). The photolysis scheme used is the Fast-J scheme (Wild et al., 2000). It is coupled  
1163 with physics of each model layer (e.g., aerosols, clouds, absorbers as ozone) and it considers grid-scale clouds from the  
1164 atmospheric driver.



1165 The aerosol module in MONARCH model solves the life cycle of sea salt, dust, organic matter (both primary and secondary),  
1166 black carbon, sulphate, and nitrate aerosols. While a sectional approach is used for dust and sea salt, a bulk description of the  
1167 other aerosol species is adopted. A simplified gas–aqueous–aerosol mechanism accounts for sulphur chemistry (Spada, 2015).  
1168 The production of secondary nitrate–ammonium aerosol is solved using the thermodynamic equilibrium model EQSAM  
1169 (Metzger et al., 2002). The coarse nitrate production is computed with an uptake reaction of  $\text{HNO}_3$  on dust and sea salt coarse  
1170 particles. The formation of SOA is considered using a simple non-volatile scheme accounting for the contribution of  
1171 anthropogenic, biomass burning, and biogenic formation (Pai et al., 2020). Hygroscopic growth is considered for all aerosol  
1172 components except mineral dust.

### 1173 **3.10.9 Assimilation system**

1174 The MONARCH assimilation system (MONARCH-DA) is based on a Local Ensemble Transform Kalman Filter (LETKF)  
1175 scheme (Di Tomaso et al., 2022; Di Tomaso et al., 2017; Escribano et al., 2022; Hunt et al., 2007; Miyoshi and Yamane, 2007;  
1176 Schutgens et al., 2010) coupled to the model through I/O routines. MONARCH ensemble is created by perturbing  
1177 anthropogenic, biomass burning, soil and ocean emissions that are pre-processed by HERMESv3 or that are modelled by  
1178 MONARCH via a physically-based scheme for dust aerosol. For analysis production in CAMS, MONARCH ensemble is run  
1179 at a horizontal resolution of  $0.2^\circ$  latitude  $\times$   $0.2^\circ$  longitude in a rotated grid and initialised by the ensemble forecast of the  
1180 previous day.

1181 Hourly surface observations from in-situ measurements are currently assimilated operationally for  $\text{O}_3$ ,  $\text{NO}_2$ ,  $\text{SO}_2$ ,  $\text{CO}$ ,  $\text{PM}_{10}$ ,  
1182  $\text{PM}_{2.5}$ . For near-real time operational analysis production, previous-day observations are combined with a MONARCH 24-  
1183 hour ensemble forecast initialised at 12 UTC of the previous day.

1184

## 1185    **3.11   SILAM**

### 1186    **3.11.1   Model Overview**

1187    The System for Integrated modelLling of Atmospheric coMposition SILAM (silam.fmi.fi) is a global-to-sub-km chemistry  
1188    transport model developed for a wide range of atmospheric composition and air quality assessment tasks (Sofiev et al., 2015b),  
1189    emergency decision support applications (Sofiev et al., 2008), and data assimilation and source inversion problems (Vira and  
1190    Sofiev, 2015; Sofiev et al., 2013). The model incorporates Eulerian and Lagrangian dispersion frameworks (the Eulerian  
1191    transport routine is used for CAMS) and a set of chemical and physical transformation modules for the troposphere and the  
1192    stratosphere (Carslaw et al., 1995; Damski et al., 2007; Yarwood. G. et al., 2005; Sofiev, 2000; Sofiev et al., 2010). Apart from  
1193    the transport and physico-chemical cores described below, SILAM includes a set of supplementary tools including a  
1194    meteorological pre-processor, input-output converters, reprojection and interpolation routines, etc. In the operational forecasts,  
1195    these enabled direct forcing of the model by the ECMWF IFS meteorological fields.

1196    SILAM has been extensively evaluated in a variety of regional and global air quality projects (Brasseur et al., 2019; Huijnen  
1197    et al., 2010; Kouznetsov et al., 2020; Petersen et al., 2019; Sofiev et al., 2015b; Xian et al., 2019) and health impact assessment  
1198    studies (Korhonen et al., 2008; Kukkonen et al., 2020; Lehtomäki et al., 2018).

### 1199    **3.11.2   Model geometry**

1200    The centre points of the model grid cover 25.05°W to 44.95°E and 30.05°N to 71.95°N on a regular latitude longitude grid of  
1201    0.1°resolution. Following (Sofiev, 2002), SILAM uses a multi-vertical approach with the meteorology-resolving grid  
1202    corresponding to the tropospheric part of the IFS vertical: hybrid levels from 69 to 137. The chemical transformations and  
1203    vertical fluxes are computed based on 10 thick staggered layers, with the thickness increasing from 25 m for the lowest layer  
1204    to 1000-2000 m in the free troposphere. The layer tops are located at 25, 75, 175, 375, 775, 1500, 2700, 4700, 6700 and 8700m  
1205    above the surface. Within the thick layers, the sub-grid information is used to evaluate the weighted averages of the high-  
1206    resolution meteorological parameters and effective diffusion coefficients after (Sofiev, 2002).

### 1207    **3.11.3   Forcing Meteorology**

1208    Meteorological forcing is the ECMWF IFS operational forecasts taken from the 12:00UTC forecast of the previous day  
1209    extracted at a resolution of 0.1° and temporal frequency of one hour for the first 72 hours and three hours for the last day of  
1210    the forecast. The list of meteorological parameters extracted is: U and V components of 10m wind [m/s], 2m temperature [K],  
1211    dew point temperature 2m [K] accumulated large scale rain [kg/m<sup>2</sup>], accumulated convective rain [kg/m<sup>2</sup>], surface roughness  
1212    [m], total cloud cover [fract], convective available potential energy [J/kg], U and V -wind components at model levels [m/s],

1213 temperature at model levels [K], cloud water at model levels [kg/kg], cloud ice at model levels [kg/kg], specific humidity at  
 1214 model levels [kg/kg], cloud cover at model levels[fract], logarithm of surface pressure.

1215 **3.11.4 Chemical initial and boundary conditions**

1216 Boundary conditions are taken from the CAMS-Global (see Table 2). The full fields are imported every 3 hours; in-between,  
 1217 the linear interpolation is applied. The forecasts are initialised with the SILAM forecast of the previous day.

1218 **3.11.5 Emissions**

1219 The common annual anthropogenic emissions CAMS-REG are implemented as explained in Section 3.2. The PM<sub>2.5</sub> emissions  
 1220 are split into EC, OC and mineral components, and OC is mapped to the volatility bins according to (Shrivastava et al., 2008).  
 1221 Emissions of biogenic VOCs, wind-blown dust, and sea salt are computed online in dedicated SILAM modules (Poupkou et  
 1222 al., 2010; Sofiev et al., 2011; Soares et al., 2016; Sofieva et al., 2022). GFAS hourly emissions from wild-land fires are  
 1223 replicated from D-2 to D+1 for forecast and shut down after; in the analysis mode it is used as is.

1224 Emissions of 6 pollen species are computed online following the heat-sum approach for trees (Sofiev et al., 2015b),  
 1225 climatological season for grasses and mugwort species, and multi-criteria hybrid model for ragweed (Prank et al., 2013).

1226 **3.11.6 Solver, advection and mixing**

1227 The SILAM Eulerian transport core (Sofiev et al., 2015a) is based on the coupled developments: refined advection scheme of  
 1228 (Galperin and Sofiev, 1994) and vertical diffusion and dry deposition algorithm of (Sofiev, 2002) and (Kouznetsov and Sofiev,  
 1229 2012). The methods are compatible, in a sense that both use the same set of variables to determine the sub-grid distribution of  
 1230 tracer mass. The approach, in particular, allows computing correct vertical exchange using high-resolution input data but low-  
 1231 resolution chemistry and diffusion grids. The later feature is used in the vertical setup with thick layers.

1232 Diffusion is parameterised following the first-order K-theory based closure. Horizontal diffusion is embedded into the  
 1233 advection routine, which itself has zero numerical viscosity, thus allowing full control over the diffusion fluxes. The vertical  
 1234 diffusivity parameterisation follows the approach suggested by (Groisman and Genikhovich, 1997) and (Sofiev et al., 2010).  
 1235 The procedure diagnoses all the similarity theory parameters using the profiles of the basic meteorological quantities: wind,  
 1236 temperature and humidity. Output includes the value of eddy diffusivity for scalars at some reference height (taken to be 1m).

1237 The model uses process-wise splitting and 1-D advection implementation flipping the order of processes every other time step.

1238 **3.11.7 Deposition**

1239 Dry deposition parameterisation for gases generally follows the resistive analogy of (Wesely, 1989). Deposition velocities for  
1240 aerosols are evaluated using the original (Kouznetsov and Sofiev, 2012) algorithm. Wet deposition parameterisation is based  
1241 on the scavenging coefficient after (Sofiev, 2000) for gas species and follows the generalised formulations of (Kouznetsov and  
1242 Sofiev, 2012) for aerosols.

1243 **3.11.8 Chemistry and aerosols**

1244 The main gas-phase chemical mechanism is CB05 with additions for SO<sub>x</sub> from (Sofiev, 2000) and organics from VBS  
1245 (Volatility-Basis Set, (Shrivastava et al., 2008)). The heterogeneous scheme is an updated version of the DMAT model scheme  
1246 (Sofiev, 2000). The formation pathways of secondary inorganic aerosols follow the VBS approach extended with the feedback  
1247 to the main gas-phase chemical module. The aerosol size distribution is represented via sectional approach, with species-  
1248 specific bin selections. Each bin is characterised with its lower and upper borders, as well as the mass-mean diameter, which  
1249 is precomputed / predefined for each bin and species from its size spectrum. Primary anthropogenic aerosols are emitted into  
1250 bins with mass-mean diameter of 0.5 µm (fine aerosol, dry size) and 6 µm (coarse aerosols, dry size). Secondary inorganic  
1251 aerosols were put into 0.2 and 0.7 µm bins, plus a separate 3 µm bin for coarse nitrates formed on the sea salt surface. The  
1252 dust size spectrum is described with 4 bins from 0.3 µm up to 20 µm. Finally, the seasalt spectrum is represented with 5 bins,  
1253 from 0.05 µm up to 20 µm of mass-mean nominal diameter. Throughout computations, the particles are transported in  
1254 accordance with their mass-mean diameter corrected with regard to actual humidity and the particle solubility. External mixing  
1255 is assumed.

1256 **3.11.9 Assimilation system**

1257 The embedded data assimilation is based on the 3d- and 4d-dimensional variational approach, as well as with the EnKF (Vira  
1258 and Sofiev, 2012, 2015). Tangent-linear (if needed) and adjoint formulations exist for the transport module, the transformation  
1259 schemes and for the deposition modules. The assimilation procedure has been tested for both initialising the concentration  
1260 fields and for refinement of the emission (Sofiev, 2019). The observation operators exist for in-situ observations and for the  
1261 vertically integrated columns observed by the nadir-looking satellites. For the near-real time operational analyses in CAMS,  
1262 the previous-day observations are used in a 3D-VAR data assimilation suite. That routine assimilates in-situ observations of  
1263 NO<sub>2</sub>, O<sub>3</sub> and PM<sub>2.5</sub>, PM<sub>10</sub>, SO<sub>2</sub> and CO.

1264

## 1265     **4     Post-processing**

### 1266     **4.1     ENSEMBLE model**

1267     All eleven individual operational model deliver their results to the CRPU (Météo-France for NRT/FC and NRT/AN, and  
1268     INERIS for IRA and VRA, using the product definition introduced in Section 2.2). An ENSEMBLE model is subsequently  
1269     computed as a median of all available operational models. As explicated in Section 3, there are slight differences in the  
1270     individual model geometry even if they are as close as possible to the common grid. Five models are operated their forecasts  
1271     directly on the target grid (CHIMERE, DEHM, EMEP, LOTOS-EUROS, and SILAM), one uses area-weighted interpolation  
1272     of overlapping polygon (EURAD-IM), and the other models use a bilinear interpolation to deliver model output on the common  
1273     grid. The ENSEMBLE is computed across all models at each horizontal and vertical grid point of the common grid. Each of  
1274     the model deliver the full list of required species.

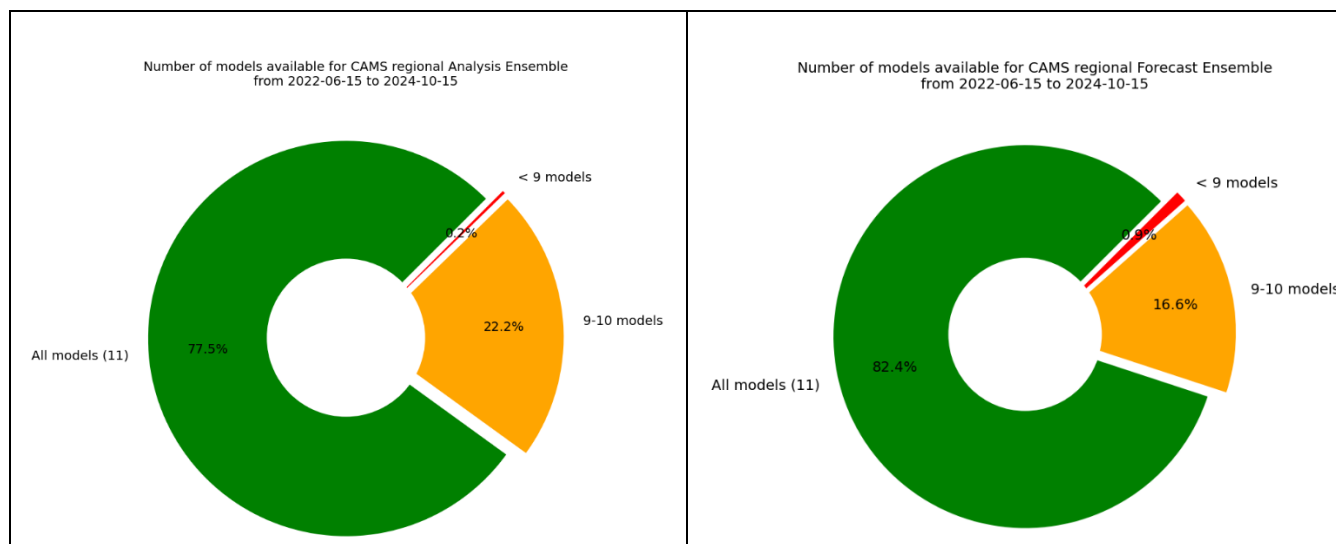
1275     Relying on 11 different models offers a very comprehensive view on the various possible representations of key atmospheric  
1276     processes relevant to air quality (see the wide range of modelling design detailed in Section 3) and thus a characterisation of  
1277     the intrinsic modelling uncertainty. The flipside of this diversity is a relatively higher risk of one model not being able to  
1278     deliver in a timely basis. A median ENSEMBLE is computed everyday no matter how many models are successfully delivered  
1279     for that given day. A Key Performance Indicator is documented to track the number of models which have delivered on time  
1280     to be included in the ENSEMBLE for either the analyses or the forecasts (Figure 2). The fact that timeliness of forecast delivery  
1281     is higher than for analyses might seem counterintuitive as forecast are expected earlier, but this is due to the fact that most  
1282     analyses are produced later due to the late availability of assimilated observations, and not necessarily used at present as initial  
1283     conditions of the forecast.

1284     Using the median to compute such an ensemble is a very robust approach to cope with potential missing members, and it has  
1285     been shown to outperform individual models for average performances (Galmarini et al., 2004). It is however a very  
1286     conservative approach and developments are ongoing, in particular to improve the skills of the system to capture air quality  
1287     exceedance detections by making use of machine learning algorithm coupled to the raw CAMS regional forecasts. Firstly,  
1288     optimised forecasts at observation sites are produced operationally for 4 pollutants (PM10, PM2.5, NO2 and O3) at thousands  
1289     of AQ e-reporting stations throughout Europe on a daily basis and for the 96hr forecast period. This product is referred to as  
1290     CAMS-MOS (Model Output Statistics)<sup>6</sup>. The underlying algorithm is a random forest using as predictor air pollutant  
1291     concentration in the ENSEMBLE CTM as well as meteorological variables (temperature at 2m, relative humidity, wind speed  
1292     and boundary layer height)(Bertrand et al., 2022). It is trained on a daily basis using the past 3 days of observations. As such,

---

<sup>6</sup><https://confluence.ecmwf.int/display/CKB/CAMS+Regional%3A+European+Air+Quality+Forecast+Optimised+at+Observation+Sites+data+documentation> (accessed 24 April 2025)

1293 CAMS-MOS is a statistical model of the meteorological dependant ENSEMBLE error, which proved very effective in  
 1294 improving the forecast skills in detecting exceedances of air quality information thresholds. Second, an weighted ensemble  
 1295 forecast at the same resolution as the CTMs (10x10km2) has been developed. It consists of an optimum weighting of the 11  
 1296 models calibrated on the past 7 days, but in this case the weights are constant and uniform and not dependent on meteorological  
 1297 predictors. CAMS-MOS is already available in the ADS as an operational product. But the weighted ensemble is still  
 1298 experimental. With the rapid development of machine learning and artificial intelligence, such experimental products will be  
 1299 further developed in the future.



1300 *Figure 2: Distribution of the number of operational models having delivered on time to be included in the ENSEMBLE computation for the*  
 1301 *period 15/06/2022-15/10/2024: left NRT/AN (analysis) and right: NRT/FC (forecasts).*

## 1302 4.2 Evaluation and Quality Control (EQC)

1303 Evaluation and quality control is an essential part of CAMS in order to ensure the reliability and transparency of the products.  
 1304 For all the chemical species where a dense enough monitoring network allows a recurrent and statistically significant  
 1305 evaluation, synthetic performance reports are produced and made available on the CAMS website<sup>7</sup>. These evaluations focus  
 1306 primarily on the surface in-situ air quality regulatory monitoring networks for O<sub>3</sub>, NO<sub>2</sub>, PM<sub>10</sub>, and PM<sub>2.5</sub>. For the assimilated  
 1307 products, the evaluation is performed on about one third of the stations, deliberately left out of the assimilation workflow  
 1308 (Section 2.3). The forecasts are evaluated using all available surface stations whose spatial representativity ranges from rural  
 1309 to urban background air quality. The skill scores are updated on a daily frequency and available publicly through an interactive  
 1310 interface on the CAMS EQC pages for the ENSEMBLE and individual models. Quarterly summaries are produced in publicly

<sup>7</sup> <https://atmosphere.copernicus.eu/regional-services>, last accessed 30/10/2024

1311 available reports. They also include an evaluation of the models in the troposphere against above-surface measurements  
1312 (aircraft and space borne remote sensing and profiling). For the Interim and Validated reanalyses, the evaluation reports are  
1313 produced on an annual basis.

1314 The present article is essentially a description of the system rather than a detailed analysis of its performance. Nevertheless,  
1315 we present here several evaluation diagnostics for illustration purposes. Therefore, the performances of individual models  
1316 contributing to the ENSEMBLE are anonymised as it would be too complex to enter here in the details of the performances of  
1317 each model, which relate to intrinsic parametrisations. Such analysis is left for a dedicated future publication, but the interested  
1318 user can also consult the interactive viewers and reference public reports on the Evaluation and Quality Control website to  
1319 analyse the performances of individual models.

1320 In Figure 3 we show the root mean square error for surface ozone and PM<sub>10</sub> taken as the median over each quarter since the  
1321 beginning of the CAMS production at the end of 2014 and over hundreds of European air quality monitoring stations. The  
1322 figure is divided in two parts as urban background stations were only included in the evaluation as of fall 2018 (note also that  
1323 the vertical scales differ). It appears clearly that while the spread of the models was still substantial in the first part of the  
1324 period, the system has reached a level of maturity since 2017 with more homogeneous performances between the various  
1325 models and very few outliers. The ENSEMBLE model appears to give better scores overall. It can be surpassed in terms of  
1326 RMSE in some occasions but not always by the same model, therefore still illustrating the added value of the multi-model  
1327 ensemble approach. The range of performances is today about 12-18µg/m<sup>3</sup> for the RMSE (root mean square error) of daily  
1328 maxima ozone, so that the Key Performance Indicator of 18µg/m<sup>3</sup> is not always met depending on the models and the season.  
1329 For PM<sub>10</sub>, the RMSE is between 5 to 8µg/m<sup>3</sup> so that the same KPI of 18µg/m<sup>3</sup> is usually met. Without entering in a more  
1330 detailed analysis, it is visible that the scores are still gradually improving over the 2018-2023 period. Over the recent years,  
1331 the median ENSEMBLE seems to produce more systematically better performances and becomes more difficult to beat.

1332

1333

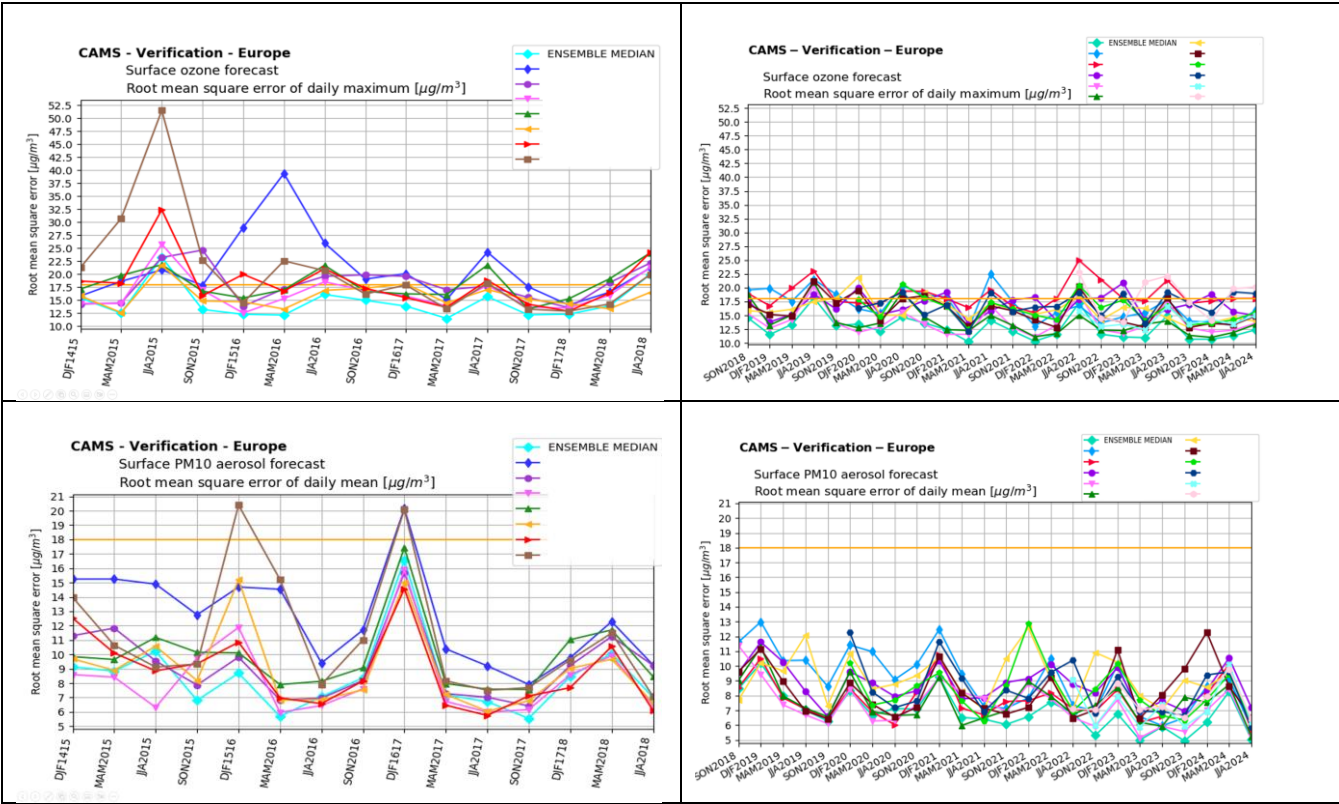
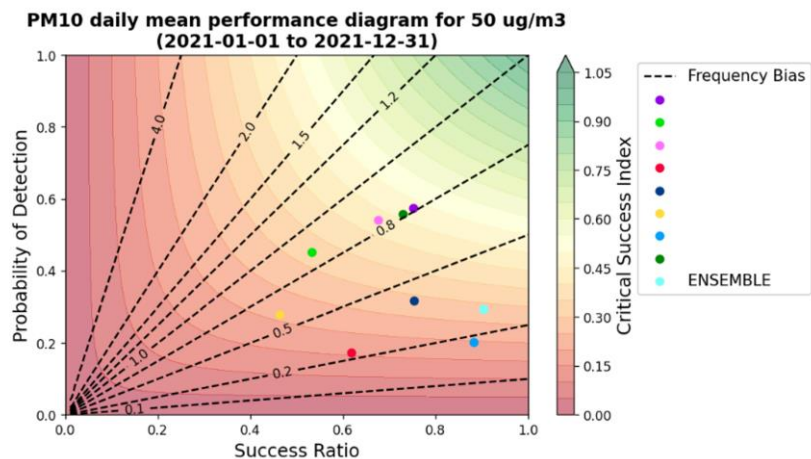


Figure 3: Evolution of the skill scores of the CAMS Regional Air Quality Forecasts (individual models and ENSEMBLE median) between 2014 and 2024 (divided in two parts: before and after 2018 as urban background stations were not included in the evaluation over the first period, and fewer models were available) Each point is the quarterly median of the RMSE ( $\mu\text{g}/\text{m}^3$ ) computed at regulatory air quality monitoring stations for top: daily maximum ozone and bottom: daily mean  $\text{PM}_{10}$ . The straight yellow line corresponds to the Key Performance Indicator for RMSE of  $18\mu\text{g}/\text{m}^3$ .

In the European Air Quality regulation, detrimental air quality situations are identified in terms of various exceedance levels depending on the air pollutants. For  $\text{PM}_{10}$ , the daily mean concentrations should not exceed  $50\mu\text{g}/\text{m}^3$  more than 35 days (EC, 2008). The performance of the CAMS Regional reanalyses in capturing that threshold can be assessed through the performance diagram presented in Figure 4. On the x-axis the success ratio is the number of hits divided by the number of hits and false alarms. On the y-axis, the probability of detection is the number of hits divided by the number of hits and misses. The dashed lines provide the frequency bias defined as the ratio of the total number of predicted exceedances to the total number of observed exceedances. For this example, for the year 2021, the ENSEMBLE median has the best success ratio, but some individual models outperform in terms of probability of detection. It is not possible to point one single model which would outperform systematically the ENSEMBLE (the best performing model will vary depending on the targeted pollutant, threshold, geographic area, etc.). Therefore the reference product remains the median ENSEMBLE which provides the best



1349 scores for conservative annual average metrics, but interested users can refer to the annual evaluation report to select alternative  
 1350 depending on their specific needs.



1351  
 1352 *Figure 4: Performance of the CAMS Regional ENSEMBLE and individual models reanalyses in capturing air quality threshold detection*  
 1353 *for daily mean PM<sub>10</sub> above 50µg/m<sup>3</sup> in 2021.*

1354 An illustration of the evaluation above the surface is provided in Figure 5. The tropospheric column of NO<sub>2</sub> in the CAMS  
 1355 regional ENSEMBLE forecast is compared to the observations from the TROPOMI instrument on board the Sentinel 5p  
 1356 satellite. The higher spatial resolution (approximately 5km) available since the launch of the instrument allows reaching out  
 1357 to urban level NO<sub>2</sub> concentrations therefore providing an excellent opportunity for the evaluation of spatial patterns of air  
 1358 pollution. Beyond surface and total columns, it is also essential to assess the performances of the vertical structure as illustrated  
 1359 for the comparison with ozone soundings in Belgium (Uccle). Here both the regional forecast and analyses are compared to  
 1360 assess the impact of surface assimilation of air quality measurement on the vertical profiles. The CAMS global model forecast  
 1361 is also included along with the CAMS regional ensemble range for the forecast and the analysis. A more detailed analysis of  
 1362 the comparison with satellite data can be found in (Douros et al., 2022).

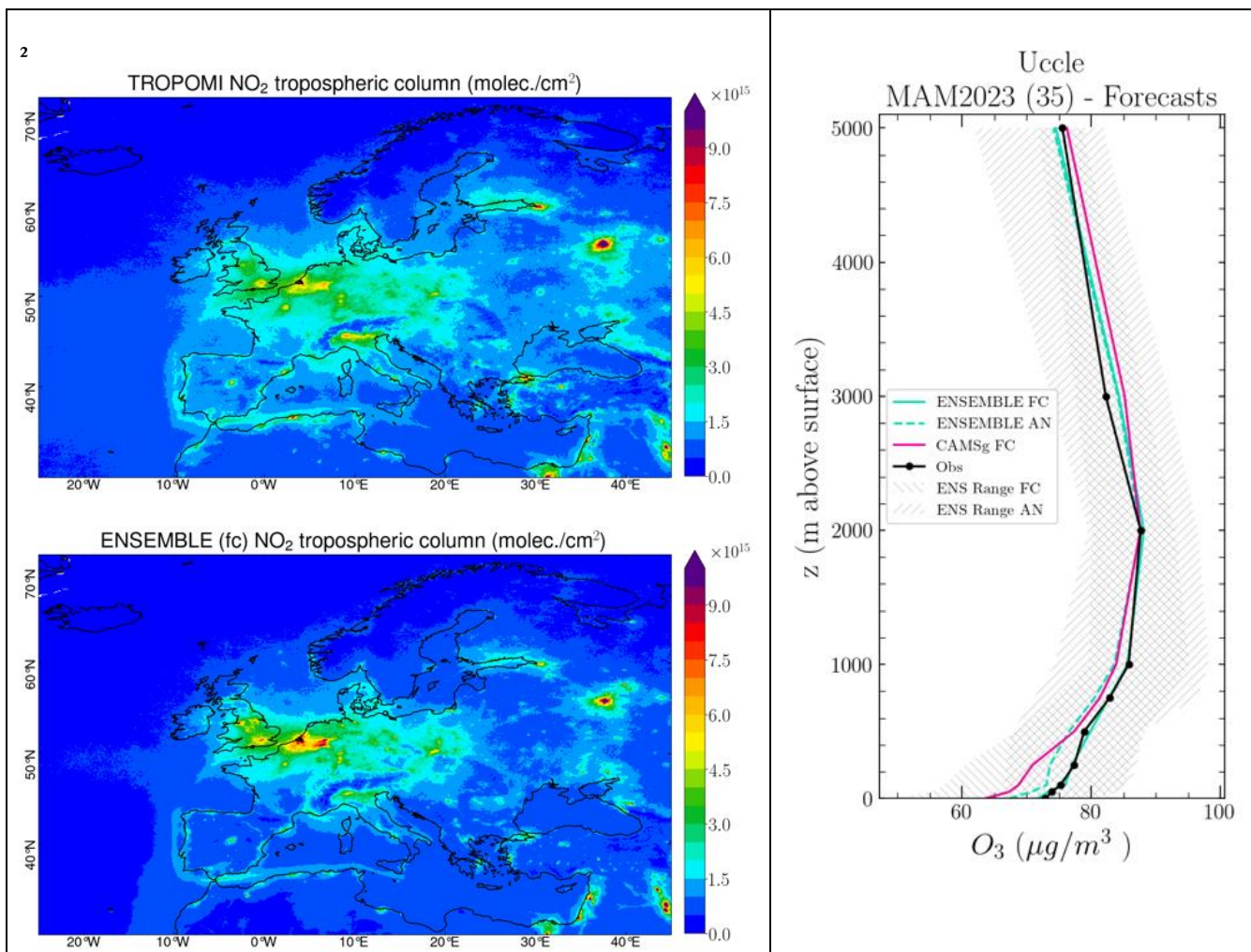


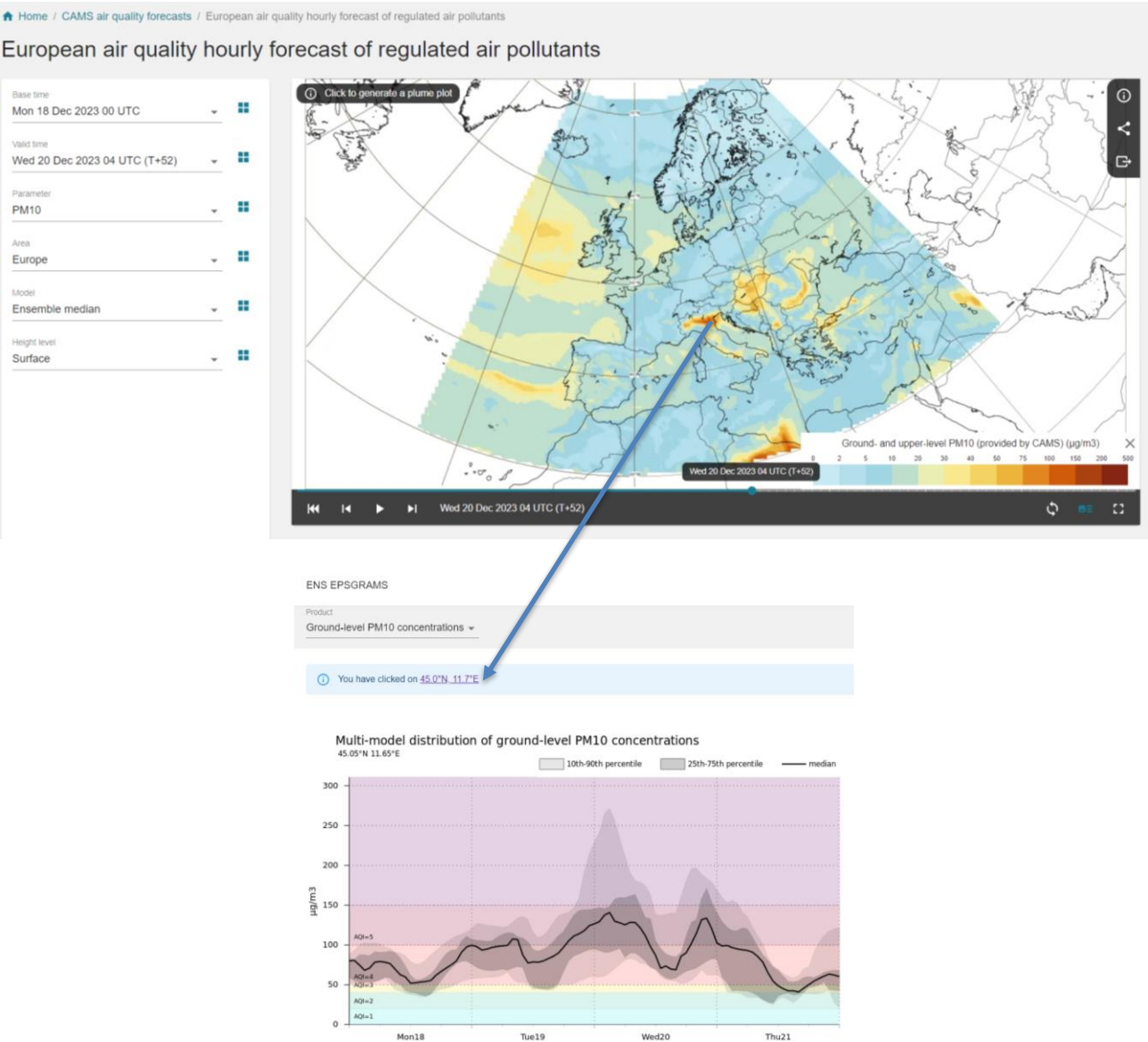
Figure 5: Left: Evaluation over MAM-2023 of the CAMS Regional ensemble forecasts against TROPOMI satellite NO<sub>2</sub> tropospheric columns (10<sup>15</sup> molecules/cm<sup>2</sup>). The CAMS NO<sub>2</sub> profiles have been multiplied with the TROPOMI kernels to remove the dependency on the retrieval a-priori profile shape. Right: Regional and global CAMS forecast and regional analyses of ozone compared to vertical profiles measured with ozone sondes over Uccle, Brussels, Belgium for MAM-2023 (μg/m<sup>3</sup>). source: CAMS2\_83 Evaluation and Quality Control Service, <https://atmosphere.copernicus.eu/regional-services>

### 4.3 Dissemination and further use of the CAMS Regional Products

The results of the CAMS regional production system are made available publicly on the website <https://atmosphere.copernicus.eu/european-air-quality-forecast-plots> where maps and time series of the various air pollutant and pollen species can be displayed. The results of the median ENSEMBLE as well as each individual model are available for both forecast and analysis products with a three years retention time. Daily means, daily maxima, and hourly fields are available. The list of vertical levels available for interactive plotting on the website is: surface, 100m, 1000m, 3000m and

1374 5000m (note that more vertical levels are available on the ADS). The model spread can also be assessed by selecting any grid  
1375 point in the map to display the time series of the 4 day forecast including modelled dispersion which provides an information  
1376 on the uncertainty in the ensemble forecast (Figure 6).

1377



1378 Figure 6: Screenshot of the CAMS Regional Production website displaying air quality forecasts over Europe (atmosphere.copernicus.eu6)

1379 The Copernicus Atmosphere Data Store (ADS) constitutes an important dissemination pathway for the CAMS Regional  
1380 production system. All the numerical data can be freely retrieved through the website [ads.atmosphere.copernicus.eu](https://ads.atmosphere.copernicus.eu) where  
1381 automated requests can be built to download entire fields or custom extractions in either grib or netcdf formats.

1382 The typical use of CAMS Regional forecast product is for national and local air quality management agencies to understand  
1383 the day-to-day air quality situation and anticipate major air pollution events. This can be done either by a qualitative analysis  
1384 of quicklooks available on the CAMS website or external companies that have developed alternative visualisation tools.

1385 The numerical data obtained on the ADS can also be used as background information for national or local scale air quality  
1386 modelling applications. Such uses range from the nesting of a Chemistry Transport Model as three-dimensional and hourly  
1387 concentrations of several chemical species are available in the CAMS Regional Forecast. They can also be used to feed  
1388 gaussian city-scale surface air quality models. There are also reported uses of the CAMS Regional Forecast to inform machine-  
1389 learning air quality statistical prediction tools (Bertrand et al., 2022; Petetin et al., 2022).

1390 The use of CAMS Regional reanalyses is rather to inform longer term air quality applications. They can be used as background  
1391 information for land-use regression models used in air quality policy products or exposure assessment for health impact studies  
1392 (Horálek et al., 2022). They are also the primary source of information for the Interim Assessment Report produced annually  
1393 by the CAMS Policy Service and serves as background information for European Member States in the Regulatory Air Quality  
1394 reporting obligations (Hamer et al., 2023).

## 1395 **5 Conclusion & Perspectives**

1396 The regional production of the Copernicus Atmosphere Monitoring Service is today a well-established reference for air quality  
1397 forecast and analysis in Europe and beyond. It is constituted of a unique ensemble of eleven European Chemistry-Transport  
1398 models operated in ten countries under the management of a Centralised Regional Production Unit. The system follows strict  
1399 requirements in order to produce consistent air quality products through the ensemble of individual CTM. Those requirements  
1400 include in particular forcing fields such as meteorology, chemical hemispheric boundary conditions, and surface fluxes of  
1401 anthropogenic and wildfire emissions. But the added value of the use of an ensemble of models also lies in the diversity of the  
1402 modelling strategy. As of today, the ensemble offers a very wide array of choices in terms of model design and structure, as  
1403 well as regarding the formulation of underlying physical and chemical processes or forcing and coupling at the interfaces (land,  
1404 sea, biosphere, ...).

1405 In the present paper, we provide a comprehensive scientific documentation of the technical characteristics for the common  
1406 forcing requirements as well as the diversity in modelling design brought about by the individual contributing modelling

1407 groups. We also explained how the billions of data produced on a daily basis are aggregated centrally, evaluated and  
1408 disseminated for a wide range of air quality applications. The CAMS Service has been operational since the end of 2014 and  
1409 has reached today a high level of performance and stability. Since 2017 the spread of model performances has converged and  
1410 it continues to improve gradually over the years.

1411 As an operational service, the Regional Production of CAMS follows closely the research developments in the field of air  
1412 quality modelling. A substantial part of the model development is undertaken independently by the modelling teams through  
1413 various research projects and PhD work at national level. The international benchmarking activities (such as the AQMEII or  
1414 Eurodelta initiatives, (Galmarini et al., 2017; Colette et al., 2017)) are also an important source of information to identify  
1415 model development priorities. More recently, the European Union has launched a series of research projects devoted to the  
1416 Evolution of Copernicus in the Horizon Europe Programme<sup>8</sup>.

1417 In order to ensure a continuous improvement, the system follows a regular development cycle. The individual models are  
1418 improved in time so that they remain in the state of the art of chemistry transport modelling. When the progress becomes  
1419 mature enough, system upgrades are scheduled on a bi-annual basis to allow individual modelling groups to bring their  
1420 development into the operational model version. These bi-annual upgrades are also the opportunity to carry coordinated  
1421 changes, such as the regular update of anthropogenic emission fluxes. Through these upgrades, the portfolio of products is also  
1422 continuously expanding. For instance, in addition to the 19 chemical species already being delivered, the current plan at the  
1423 time of submission of the present article (i.e. for the year 2024) is to include new PM species such as ammonium nitrate and a  
1424 tracer of shipping emissions.

1425 A large part of the research effort in relation to the Regional Production is related to Chemistry-Transport deterministic  
1426 modelling. But there are also interesting prospects in the coupling between machine learning and physical and chemical  
1427 modelling. The Regional Service already produces operationally optimised forecasts at station level on the basis of Model  
1428 Output Statistics which relies on Machine Learning to offer unprecedented performance in particular for air quality threshold  
1429 detection (Bertrand et al., 2022). Novel methodologies to compute the ENSEMBLE model from the eleven individual  
1430 production and move away from the conservative median approach are also under consideration.

1431 Besides the modelling developments, the uptake of innovative observations is also instrumental in the long-term perspective  
1432 of CAMS. The production of deposition fluxes is a good illustration of the need to make the best of available observations.  
1433 While CTMs are producing by nature deposition fluxes, they are not systematically quality checked and therefore the output  
1434 products are limited at present to ambient air concentrations. A mid-term development is therefore ongoing to benchmark wet

---

<sup>8</sup> <https://atmosphere.copernicus.eu/copernicus-research-whats-horizon>

1435 and dry deposition fluxes to ensure their robustness. To achieve this, CAMS relies on the network of deposition data collected  
1436 in the EMEP network of rural supersites in Europe. But there are also promising prospects in the uptake of near-real-time  
1437 advanced observations of atmospheric composition at the supersites of the ACTRIS European Research Infrastructure, in  
1438 particular with regards to particulate matter chemical composition and source apportionment. Lastly, in the outlook of the  
1439 future perspectives there are also high expectations regarding the uptake of geostationary satellite retrievals with the  
1440 perspective of the launch of the Sentinel 4 satellite which will bring unprecedented high-frequency atmospheric composition  
1441 information over Europe.

## 1442 **6 Data Availability**

1443 Copernicus is funded under the Copernicus Regulation and operated by ECMWF under the ECMWF Agreement. Access to  
1444 all Copernicus (previously known as GMES or Global Monitoring for Environment and Security) Information and Data is  
1445 regulated under Regulation (EU) No 1159/2013 of the European Parliament and of the Council of 12 July 2013 on the European  
1446 Earth monitoring programme, under the ECMWF Agreement and under the European Commission's Terms and Conditions.  
1447 Access to all Copernicus information is regulated under Regulation (EU) No 1159/2013 and under the ECMWF Agreement.

1448 The Copernicus Licence is free of charge, worldwide, non-exclusive, royalty free and perpetual. Access to Copernicus Products  
1449 is given for any purpose in so far as it is lawful, whereas use may include, but is not limited to: reproduction; distribution;  
1450 communication to the public; adaptation, modification and combination with other data and information; or any combination  
1451 of the foregoing.

1452 The full terms of the Copernicus Licence are available at: [https://ads.atmosphere.copernicus.eu/api/v2/terms/static/licence-to-](https://ads.atmosphere.copernicus.eu/api/v2/terms/static/licence-to-use-copernicus-products.pdf)  
1453 [use-copernicus-products.pdf](https://ads.atmosphere.copernicus.eu/api/v2/terms/static/licence-to-use-copernicus-products.pdf)

## 1454 **7 Code Availability**

1455 Following the Copernicus Programme Data Policy, the Regional Production data and information are available on a full, open,  
1456 and free-of-charge basis, subject to limitations concerning registration, dissemination formats, and access restrictions. The  
1457 Copernicus Atmosphere Data Store is located at: <https://ads.atmosphere.copernicus.eu/>.

1458 The CHIMERE model is available to registered users through the dedicated website at  
1459 <https://www.lmd.polytechnique.fr/chimere/>, the actual version used in CAMS is available at  
1460 <https://zenodo.org/records/14724119>.

1461 The DEHM model used in CAMS is available at <https://zenodo.org/records/14628278>.

1462 The EMEP model is available at <https://github.com/metno/emep-ctm> under the GPLv3 licence. The model version for CAMS  
1463 is updated once or twice a year in the frame of the regular updates in the CAMS regional service. The current version is  
1464 <https://zenodo.org/records/14507729>.

1465 The EURAD-IM version 5.11.1 source code used in CAMS is <https://doi.org/10.5281/zenodo.15198902>.

1466 The GEM model is a free software that can be redistributed and/or modified under the terms of the GNU Lesser General Public  
1467 License published by the Free Software Foundation. It is available on a repository administered by Environment and Climate  
1468 Change Canada at <https://github.com/ECCC-ASTD-MRD/gem/>. GEM-AQ includes an additional source code tree accessed  
1469 via an interface routine in GEM. The GEM-AQ code used in CAMS is available at <https://zenodo.org/records/14720848>.

1470

1471 The LOTOS-EUROS model is available to registered users from the website [https://airqualitymodeling.tno.nl/lotos-](https://airqualitymodeling.tno.nl/lotos-euros/open-source-version/)  
1472 [euros/open-source-version/](https://airqualitymodeling.tno.nl/lotos-euros/open-source-version/) the version used in CAMS is available at <https://zenodo.org/records/14711996>.

1473 The MATCH model as used in CAMS is available at <https://zenodo.org/records/14719885>.

1474 The FARM code embedded in the MINNI System as used in CAMS is available at <https://zenodo.org/records/14650298>  
1475

1476 The MOCAGE source code used in CAMS is available at <https://doi.org/10.5281/zenodo.14625973>.

1477 The MONARCH model is available at <https://earth.bsc.es/gitlab/es/monarch> under the GPLv3 licence. The version used in  
1478 CAMS is <https://zenodo.org/records/5215467>.

1479 The SILAM code is available at <https://github.com/fmidev/silam-model> under the GPLv3 licence. The model is updated  
1480 several times a year, including two CAMS-related updates. The version used in CAMS is <https://zenodo.org/records/14608973>.

1481



1482  
1483  
1484  
  
1485  
  
1486  
1487  
  
1488  
1489  
1490  
  
1491  
  
1492  
  
1493  
  
1494  
  
1495  
  
  
  
1496  
  
1497  
1498  
1499  
  
1500  
1501  
  
1502  
1503  
  
1504  
1505  
1506  
1507  
1508

**8 Author Contribution**

AC designed and drafted the overall manuscript and coordinated all contributions.

GC, FB, EB, VG, FM, AR, VP, CM, OF, AJ, VHP and LR contributed to drafting the centralised production specifics and general review of the draft.

MA, JA, AB, RB, DB, JB, GB, AC, JHC, FC, IDE, MDI, GD, EDT, JD, JE, HF, YF, JF, EF, LF, MG, CG, GG, MG, AG, JG, RH, MK, JWK, RKo, RKr, ACL, JL, VL, FM, AM, MM, AN, MO, CPGP, JP, AP, BR, LR, AS, MS, PS, DS, MS, AS, JS, CT, RT, TT, ST, ST, AUn, AU<sub>p</sub>, AV, PvV, LV, ZY contributed to draft the specificities of individual model description.

HE contributed to draft the text on model evaluation

JK, Hd<sub>v</sub>G: contributed to draft the text on emissions.

MR, OF, VP, AR, EB, provided plots and figures

**9 Competing Interest**

The authors declare that they have no conflict of interest.

**10 Acknowledgements**

The activities described in this paper have been funded by the Copernicus Atmosphere Monitoring Service. ECMWF implements the Copernicus Atmosphere Monitoring Service and the Copernicus Climate Change Service with funding from the European Union on behalf of the European Commission.

INERIS acknowledged the support of the French Ministry in Charge of Ecology for continuous support in developing the CHIMERE model and related air quality forecasting activities.

FMI acknowledges the support of Academy of Finland projects PS4A (grant 318194) and ALL-Impress (grant 329215) for the pollen module developments.

The computing resources and the related technical support for MINNI forecast are provided by CRESCO/ENEAGRID High Performance Computing infrastructure and its staff. CRESCO/ENEAGRID High Performance Computing infrastructure is funded by ENEA, the Italian National Agency for New Technologies, Energy and Sustainable Economic Development and by Italian and European research programmes (see <http://www.cresco.enea.it/english>).



		CHIMERE	DEHM	EMEP	EURAD-IM	GEM-AQ	LOTOS-EUROS	MATCH	MINNI	MOCAGE	MONARCH	SILAM
Discretisation	Horizontal resolution	0.1° x 0.1° regular lat-lon	0.1° x 0.1° regular lat-lon	0.1° x 0.1° regular lat-lon	9x9 km Lambert conformal	0.1° x 0.1° lat-lon spherical grid	0.1° x 0.1° regular lat-lon	0.1° x 0.1° regular lat-lon	0.15° x 0.1° regular lat-lon	0.1° x 0.1° regular lat-lon	0.15° x 0.15° rotated regular lat-lon	0.1° x 0.1° regular lat-lon
	number of vertical levels	9	29	20	23	28	12	26	14	47	24	10
	top altitude	500hPa	100hPa	100hPa	100hPa	10hPa	200hPa	8000m	7040m	5hPa	50hPa	8700m
	depth of lowermost layer	20m	20m	50m	35m	20m	20m	45m	40m	40m	40m	25m
	number of lower layers	7 below 2km	12 below 1km	10 in PBL	15 below 2km	14 below 5km	7 below 1km	10 below 850hPa	8 below 1km	8 below 2km	7 below 2km	5 below 1km
Initial & boundary conditions & meteorology	Meteorological driver	D-1 00:00 UTC IFS, 3hrly	D-1 12:00 UTC IFS, 3hrly	D-1 12:00 UTC IFS, 3hrly	D-1 12:00 UTC IFS for FC, IFS analysis for AN, 3hrly for FC, 6hrly for AN, downscaled with WRF	D-1 12:00 UTC IFS, 3hrly	D-1 00:00/12:00 UTC IFS, 3hrly	D-1 12:00 UTC IFS, 3hrly	D-1 12:00 UTC IFS, 1hrly	D-1 12:00 UTC IFS for FC, 1hrly (from +00h to +72h), 3hrly (from +72h to +96h) ; D00:00 UTC IFS for AN, 1hrly	D-1 12:00 UTC IFS, 6hrly, downscaled with NMMB	D-1 12:00 UTC IFS, 1hrly (from +00h to +72h), 3hrly (from +72h to +96h)

		CHIMERE	DEHM	EMEP	EURAD-IM	GEM-AQ	LOTOS-EUROS	MATCH	MINNI	MOCAGE	MONARCH	SILAM
	Boundary values	CAMS-Global	CAMS-Global	CAMS-Global	CAMS-Global	CAMS-Global	CAMS-Global	CAMS-Global	CAMS-Global	CAMS-Global + MOCAGE global for additional species	CAMS-Global	CAMS-Global & SILAM
	Initial values	Previous forecast	Previous forecast	Previous analysis	Previous forecast	Previous forecast	Previous forecast	Previous forecast	Previous forecast	Previous forecast	Previous forecast	Previous forecast
Emissions anthropogenic	Inventory	CAMS-REG v6.1 REF2 2022	CAMS-REG v6.1 REF2 2022	CAMS-REG v6.1 REF2 2022	CAMS-REG v6.1 REF2 2022	CAMS-REG v6.1 REF2 2022	CAMS-REG v6.1 REF2 2022	CAMS-REG v6.1 REF2 2022	CAMS-REG v6.1 REF2 2022	CAMS-REG v6.1 REF2 2022	CAMS-REG v6.1 REF2 2022	CAMS-REG v6.1 REF2 2022
	Temporal disaggregation	TNO	CAMS-REG-TEMPO_v4.1	CAMS-REG-TEMPO_v4.1	CAMS-REG-TEMPO_v4.1	CAMS-REG-TEMPO_v4.1	CAMS-REG-TEMPO_v4.1	GENEMIS	CAMS-REG-TEMPO_v3.2	GENEMIS	CAMS-REG-TEMPO_v4.1	TNO
Emissions: natural & biogenic	in-domain soil and road dust emissions	(Marticorena and Bergametti, 1995)	none	(Marticorena and Bergametti, 1995; Marticorena et al., 1997; Dabdub and Seinfeld, 1994; Gomes et al., 2003; Fécan et al., 1998) Road dust emissions currently switched off.	Based on DREAM model	(Marticorena and Bergametti, 1995)	(Marticorena and Bergametti, 1995) and soil moisture inhibition as in (Fécan et al., 1998)	Road dust from (Schaap et al., 2009) and (Omstedt et al., 2005) and mineral dust based on the DEAD model of (Zender et al., 2003) (mainly attributed to the Mediterranean area).	Erosion and resuspension from (Vautard et al., 2005), soil suitable for mobilization parameterized following (Zender et al., 2003)	(Ginoux et al., 2001) and ECOCLI MAP database	Mineral dust scheme based on (Klose et al., 2021) and (Pérez et al., 2011)	SILAM dust source, SILAM sea salt source, Silam BIO-VOC source

		CHIMERE	DEHM	EMEP	EURAD-IM	GEM-AQ	LOTOS-EUROS	MATCH	MINNI	MOCAGE	MONARCH	SILAM
	<b>in-domain sea-salt emissions</b>	(Martensson et al., 2003) (Monahan, 1986)	(Martensson et al., 2003) (Monahan, 1986)	(Martensson et al., 2003) (Monahan, 1986; Tsyro et al., 2011)	(Sofiev et al., 2011)	(Gong et al., 2003)	(Martensson et al., 2003) {Monahan, 1986 #822	(Sofiev et al., 2011)	(Zhang et al., 2005)	(Sič et al., 2015)	(Jaeglé et al., 2011)	(Sofiev et al., 2011)
	<b>Birch, Grass, Olive, Ragweed,</b>	yes	yes	yes	yes	yes	yes	yes	yes	yes	yes	yes
	<b>Biogenic emissions</b>	MEGAN V2.10 (Guenther et al., 2012)	MEGAN v2.04 (Guenther et al., 2006)	(Simpson et al., 2012)	MEGAN V2.10 (Guenther et al., 2012)	MEGAN-MACC climatology	(Guenther et al., 1993) with detailed tree types for Europe	(Simpson et al., 2012)	MEGAN v2.04 (Guenther et al., 2006)	CAMS-GLOB-BIOv3.1 (Sinderalova et al., 2022) isoprene from MEGAN v2.04 (Guenther et al., 2006)	MEGAN v2.04 (Guenther et al., 2006)	Dynamic biogenic, (Poupkou et al., 2010)
	<b>Soil NOx</b>	MEGAN V2.10 (Guenther et al., 2012)	GEIA (Yienger and Levy, 1995)	CAMS-GLOB-SOIL v2.4 (Simpson et al., 2023)	MEGAN V2.10 (Guenther et al., 2012)	none	(Yienger and Levy, 1995)	none	(Williams et al., 1992)	CAMS-GLOB-SOILv2.2 (Simpson et al., 2021)	MEGAN v2.04 (Guenther et al., 2006)	none
	<b>Wildfires emissions</b>	Hourly emissions from D-2 cycled for AN (D-1) and FC (D+0 and D+1, zero for the remaining days)	last available 24h cycle over D-2 and D-1 cycled for AN (D-1) and FC (D+0 and D+1, zero for the remaining days)	Hourly emissions from D-2 cycled for AN (D-1) and FC (D+0 and D+1, zero for the remaining days)	last available 24h cycle over D-2 and D-1 cycled for AN (D-1) and FC (D+0 and D+1, zero for the remaining days)	last available 24h cycle over D-2 and D-1 cycled for AN (D-1) and FC (D+0 and D+1, zero for the remaining days)	Hourly emissions from D-2 cycled for AN (D-1) and FC (D+0 and D+1, zero for the remaining days)	Hourly emissions from D-1 for AN (D-1) and last available 24h from D-2 and D-1 cycled for FC (D+0 to D+4)	Hourly emissions from D-1 for AN (D-1) and FC (D+0 and D+1, zero for the remaining days)	Hourly emissions from D-2 cycled for AN (D-1) and FC (D+0 and D+1, zero for the remaining days)	Hourly emissions from D-2 cycled for AN (D-1) and FC (D+0 and D+1, zero for the remaining days)	Hourly emissions from D-2 cycled for AN (D-1) and FC (D+0 and D+1, zero for the remaining days)

		CHIMERE	DEHM	EMEP	EURAD-IM	GEM-AQ	LOTOS-EUROS	MATCH	MINNI	MOCAGE	MONARCH	SILAM
Chemistry/Physics	Gas phase chemistry	MELCHIOR2 (Derognat et al., 2003), 44 gaseous species and 120 reactions	Modified (Strand and Hov, 1994), 74 species and 158 reactions	EmChem 19a, (Bergström et al., 2022) 127 species and 198 reactions (Simpson et al., 2020a)	RACM-MM (Geiger et al., 2003)	Modified ADOM IIB mechanism, 51 species and 120 reactions	Modified CBM-IV (Schaap et al., 2004)	EmChem 09 (Simpson et al., 2012) and (Langner et al., 1998)	SAPRC 99 (Carter, 2000)	RACM (tropospheric) and REPROB US (stratospheric)	CB05 (Yarwood, G. et al., 2005)	CBM-IV
	Heterogeneous chemistry	Conversion of NO2 into HNO3 and N2O5 and Conversion of HO2 into H2O2	Oxidation of NO2 by O3 on aerosols	Aerosol-uptake of HNO3, HO2 and to NO3 and O3 and hydrolysis of N2O5 (Stadler et al., 2018)	Hydrolysis of N2O5	Hydrolysis of N2O5	Hydrolysis of N2O5	Hydrolysis of N2O5, aerosol uptake of HNO3 and CH3O2H	none	only relevant for polar stratospheric clouds	Hydrolysis of N2O5 and aerosol uptake of HNO3 on dust and sea salt	Sofiev (2000)
	Aerosol size distribution	10 bins from 10 nm to 40 µm	2 size fractions: PM2.5 and coarse fraction of PM10	2 size fractions: PM2.5 and coarse fraction of PM10	3 log-normal modes: 2 fine + 1 coarse	12 bins from 10nm to 20.5µm	5 size bins for dust and sea-salt, 2 size bins for other aerosols	2 size fractions: PM2.5 and coarse fraction of PM10	3 log-normal model: Aitken, accumulation and coarse	6 bins	8 bins for dust and sea salt. Fine mode for BC, OM, SO4 and NH4. Coarse and fine mode for NO3	2 bins, except for dust (4 bins from 10nm to 30µm) and sea salt (5 bins from 10nm to 30µm)

		CHIMERE	DEHM	EMEP	EURAD-IM	GEM-AQ	LOTOS-EUROS	MATCH	MINNI	MOCAGE	MONARCH	SILAM
	Inorganic aerosols	(Couvidat et al., 2018): Thermodynamic equilibrium for particles under 1 µm and a dynamic approach for particles above 1 µm. Thermodynamic for the H <sup>+</sup> -NH <sub>4</sub> <sup>+</sup> -SO <sub>4</sub> <sup>2-</sup> -Na <sup>+</sup> -Cl <sup>-</sup> -H <sub>2</sub> O system is based on ISORROPIA 2.1.	(Frohn, 2004)	MARS (Binkowski and Shankar, 1995), thermodynamic equilibrium for the SO <sub>4</sub> -HNO <sub>3</sub> -NO <sub>3</sub> -NH <sub>3</sub> -NH <sub>4</sub> -H <sub>2</sub> O system	thermodynamic equilibrium for the H <sup>+</sup> -NH <sub>4</sub> <sup>+</sup> -SO <sub>4</sub> <sup>2-</sup> -NO <sub>3</sub> <sup>-</sup> -H <sub>2</sub> O system (Frieese and Ebel, 2010)	(Gong et al., 2003)	ISORROPIA-2 (Fountoukis and Nenes, 2007)	(Mozurkewich, 1993)	ISORROPIA v1.7 (Nenes et al., 1998)	ISORROPIA-2 (Guth et al., 2016)	EQSAM (Metzger et al., 2002)	(Sofiev, 2000)
	Secondary organic aerosols	(Bessagnet et al., 2009)	VBS approach (NPAS scheme of (Bergström et al., 2012a))	VBS approach (NPAS scheme, (Bergström et al., 2012a; Simpson et al., 2012))	updated SORGAM module (Li et al., 2013)	(Jiang, 2003)	not included	VBS schemes for ASOA and BSOA (Bergström et al., 2012a) (Hodzic et al., 2016)	SORGAM (Schell et al., 2001b)	(Castro et al., 1999)	non-volatile scheme for anthropogenic, biogenic and pyrogenic precursors (Pai et al., 2020)	VBS
	Aqueous phase chemistry	SO <sub>2</sub> oxidation by O <sub>3</sub> and H <sub>2</sub> O <sub>2</sub>	SO <sub>2</sub> oxidation by O <sub>3</sub> and H <sub>2</sub> O <sub>2</sub> (Jonson et al., 2000)	SO <sub>2</sub> oxidation by ozone and H <sub>2</sub> O <sub>2</sub> and metal ion-catalyzed O <sub>2</sub> (Jonson et al., 2000)	10 gas/aqueous phase equilibria, 5 irreversible S(IV) → S(VI) transformations	SO <sub>2</sub> oxidation	SO <sub>2</sub> oxidation	SO <sub>2</sub> oxidation	SO <sub>2</sub> oxidation (Seinfeld and Pandis, 1998)	SO <sub>2</sub> oxidation	SO <sub>2</sub> oxidation by ozone and H <sub>2</sub> O <sub>2</sub>	SO <sub>2</sub> oxidation, nitrate formation (Sofiev, 2000), heterogeneous nitrate formation on sea salt particles

		CHIMERE	DEHM	EMEP	EURAD-IM	GEM-AQ	LOTOS-EUROS	MATCH	MINNI	MOCAGE	MONARCH	SILAM
	Dry deposition: gases	resistance approach (Wesely, 1989)	resistance approach (Simpson et al., 2003; Emberson et al., 2000a)	resistance approach, including non-stomatal deposition of NH3 (Simpson et al., 2012)	resistance approach (Zhang et al., 2003)	resistance approach	resistance approach (Erisman et al., 1994)	resistance approach (Simpson et al., 2012)	resistance approach (Michou et al., 2005) (Wesely, 1989)	resistance approach (Michou et al., 2005)	resistance approach (Wesely, 1989)	resistance approach (Wesely, 1989)
	Dry deposition: aerosols	gravitational settling	gravitational settling (Simpson et al., 2003; Emberson et al., 2000a)	(Simpson et al., 2012; Venkatram and Pleim, 1999)	resistance approach (Petroff and Zhang, 2010)	gravitational settling	(Zhang et al., 2001)	resistance approach (Simpson et al., 2012)	gravitational settling (Binkowski and Shankar, 1995)	(Sič et al., 2015)	(Zhang et al., 2001; Pérez et al., 2011)	(Kouznetsov and Sofiev, 2012)
	Wet deposition	In-cloud scavenging for all gas/aerosols is taken into account. Below cloud by rain and snow falls is taken into account for soluble gas (HNO3, H2O2) and particles	(Simpson et al., 2003)	In-cloud and sub-cloud scavenging ratios for gases; in-cloud scavenging ratios and sub-cloud scavenging efficiencies for aerosols. (Berge, 1993; Simpson et al., 2012)	CMAQ (Salameh et al., 2007)	Below cloud scavenging for soluble gas species and aerosols	(Banzhaf et al., 2012)	gases: species dependent in-cloud and sub-cloud scavenging ratios; particles: in-cloud scavenging ratio, sub-cloud scavenging (Berge, 1993) and (Simpson et al., 2012)	(Simpson et al., 2003)	Convective: (Maret et al., 2000) Stratiform: (Giorgi and Chameides, 1986), (Slinn et al., 1978; Slinn, 1983)	(Foley et al., 2010; Pérez et al., 2011)	SILAM
Assimilation	Assimilation method	Kriging-based analysis	3D-Var	Intermittent 3d-var	Intermittent 3d-var	Optimal Interpolation	ENKF	Intermittent 3d-var	Optimal Interpolation	3D VAR	LETKF (Di Tomaso et al., 2017)	Intermittent 3d-var

		CHIMERE	DEHM	EMEP	EURAD-IM	GEM-AQ	LOTOS-EUROS	MATCH	MINNI	MOCAGE	MONARCH	SILAM
	Assimilated surface pollutants	NO2, O3, PM2.5, PM10, CO, SO2	NO2, O3, CO, SO2, PM2.5, PM10	NO2, O3, SO2, CO, PM2.5, PM10	NO2, O3, CO, SO2, PM2.5, PM10	NO2, O3, PM2.5, PM10, CO, SO2	NO2, O3, PM2.5, PM10	NO2, O3, CO, SO2, PM2.5, PM10	NO2, O3, CO, SO2, PM2.5, PM10	NO2, O3, PM2.5, PM10	NO2, O3, CO, SO2, PM2.5, PM10	NO2, O3, CO, SO2, PM2.5, PM10
	assimilated satellite	none	none	NO2 (OMI) until 2021, currently disabled	currently none	none	NO2 (OMI) until 2021	none	none	ground-based lidars from French network, ceilometers from e-profile, SO2 Tropomi	none	none
	Assimilation of concentrations	Yes	Yes	Yes	Yes	Yes	None	Yes	Yes	Yes	Yes	Yes
	Assimilation of emissions	None	None	None	None	None	Yes	None	None	None	None	None
	Assimilation of deposition	None	None	None	None	None	Yes	None	None	None	None	None
	Assimilation of other processes	None	None	None	None	None	Ozone top boundary	None	None	None	None	None

		CHIMERE	DEHM	EMEP	EURAD-IM	GEM-AQ	LOTOS-EUROS	MATCH	MINNI	MOCAGE	MONARCH	SILAM
	Frequency of assimilation	Hourly	Hourly	Hourly	Hourly	Hourly	Hourly	Hourly	Hourly	Hourly	Hourly	Hourly

1511



1512  
1513

Table 2: Overview of the matching between chemical species used as boundary conditions from the CAMS-Global model and the eleven regional models of the CAMS Regional production

CAMS-Global	CHIME RE	DEHM	EMEP	EURAD	GEM-AQ	LOTOS EUROS	MATCH	MINNI	MOCAGE	MONARCH	SILAM
aermr01 (wet) (sea salt 0.03-0.5 $\mu\text{m}$ radius)	sea salt bins 3 to 5	SS_25= aermr01/4.3+ 0.5*aermr02/4.3	SS_25= aermr01/4.3+ 0.5*aermr02/4.3	not used	not used	SS bins 1=aermr01/4.3 (where SS_25 = SS bin 1 and 2)	SS_25=aermr01/4.3+0.4*aermr02/4.3	SS bin [1-2.5 $\mu\text{m}$ ] = aermr01/4.3+0.40*aermr02/4.3	SS bins 1-6 = aermr01/4.3	SS bin 1=0.34*aermr01/4.3 + 0.02*aermr02/4.3	SS bin 0.5 $\mu\text{m}$ = aermr01/4.3
aermr02 (wet) (sea salt 0.5-5 $\mu\text{m}$ radius)	sea salt bins 6 to 8	SS_co= 0.5*aermr02/4.3	SS_co=0.5*aermr02/4.3	not used	not used	SS bins 2=0.1*aermr02/4.3 SS bins 3=0.2*aermr02/4.3 SS bins 4=0.4*aermr02/4.3 SS bins 5=0.3*aermr02/4.3	SS_co=0.6*aermr02/4.3	SS bin [2.5-10 $\mu\text{m}$ ] = 0.60*aermr02/4.3	SS bins 1-6 = aermr02/4.3	SS bin 3=0.13*aermr02/4.3 SS bin 4=0.18*aermr02/4.3 SS bin 5=0.35*aermr02/4.3 SS bin 6=0.32*aermr02/4.3 + 0.06*aermr03/4.3	SS bin 3 $\mu\text{m}$ = aermr02/4.3
aermr03 (wet) (sea salt 5-20 $\mu\text{m}$ radius)	sea salt bin 9	not used	not used	not used	not used	not used	not used	not used	SS bins 1-6 = aermr03/4.3	SS bin 7=0.40*aermr03/4.3 SS bin 8=0.54*aermr03/4.3	SS bin 9 $\mu\text{m}$ = 0.5*aermr02/4.3 SS bin 20 $\mu\text{m}$ = 0.5*aermr02/4.3
aermr04 (dust 0.03-0.55 $\mu\text{m}$ radius)	dust bins 4 to 6	DUST_25=aermr04+ aermr05	DUST_25= aermr04+ aermr05	DUST_a cc=0.05 total CAMS-Global dust, DUST_c oa=0.95 total CAMS-Global dust	dust bins 3-7	dust bin 1 = 0.2*aermr04+ 0.2*aermr05 dust bin 2 = 0.8*aermr04+ 0.8*aermr05	dust_25= aermr04+ aermr05+ 0.11*aermr06	dust bin [1-2.5 $\mu\text{m}$ ] = aermr04+ aermr05+ aermr06*0.11	Dust bins 1-6	DUST bin 1 = 0.03 * aermr04 DUST bin 2 = 0.14 * aermr04	Dust 0.3 $\mu\text{m}$ = 0.4*aermr04 Dust 1.5 $\mu\text{m}$ = 0.6*aermr04

aermr05 (dust 0.55-0.9 μm radius)	dust bin 7	not used	DUST_2 5= aermr04+ aermr05	DUST_a cc=0.05 total CAMSGlobal dust, DUST_c oa=0.95 total CAMSGlobal dust	dust bins 8		dust_25= aermr04+ aermr05+ 0.11*aer mr06	used above in dust bin [1- 2.5um]	Dust bins 1-6	DUST bin 3 = 0.82 * aermr04 + 0.11 * aermr05	Dust 6μm = aermr05
aermr06 (dust 0.9- 20 μm radius)	dust bins 7 to 10	DUST_c o = 0,4*aerm r06	DUST_c o =0,4*aer mr06	DUST_a cc=0.05 total CAMSGlobal dust, DUST_c oa=0.95 total CAMSGlobal dust	dust bins 9-12	dust bin 3 = 0.08*aer mr06 dust bin 4 = 0.16*aer mr06 dust bin 5 = 0.16*aer mr06	dust_co= 0.44*aer mr06	dust bin [2.5- 10μm] = aermr06* 0,44	Dust bins 1-6	DUST bin 4 = 0.89 * aermr05 + 0.01 * aermr06 DUST bin 5 = 0.11 * aermr06 DUST bin 6 = 0.23 * aermr06 DUST bin 7 = 0.50 * aermr06 DUST bin 8 = 0.14 * aermr06	Dust 6μm = 0.4*aerm r06 Dust 20μm = 0.6*aerm r06
aermr07 hydrophil ic OM	PPM bins 3 to 6	not used	not used	80% accumula tion mode, 20% Aitken mode	OC bins 1-12	POM_25	EC_25=0 .7*aermr 07; EC_co=0 .15*aerm r07	AORPA bin 0- 1μm = 0,00050* aermr07+ 0,00050* aermr08 AORPA bin 1- 2.5μm = 0,44955* aermr07+ 0,44955* aermr08 AORA bin 0- 1μm = 0,00050* aermr07 + 0,00050* aermr08 AORA	OC bins 1-6	hydrophil ic POM	Non- volatile bin of organic aerosol

								bin 1-2.5µm = 0,49950*aermr07 + 0,49950*aermr08			
aermr08 hydrophobic OM	PPM bins 3 to 6	not used	not used	80% accumulation mode, 20% Aitken mode	OC bins 1-12	POM_25	EC_25=0.7*aermr08; EC_co=0.15*aermr08	AORB bin 0-1µm = 0,00010*aermr07 + 0,00010*aermr08 AORB bin 1-2.5µm = 0,09990*aermr07 + 0,09990*aermr08	OC bins 1-6	hydrophobic POM	Non-volatile bin of organic aerosol
aermr09 hydrophilic BC	PPM bins 3 to 6	BCfresh	not used	70% accumulation mode, 30% Aitken mode	BC bins 1-12	EC_25	OC_25=0.7*aermr09 OC_co=0.15*aermr09	AEC bin 0-1µm = 0,0011*aermr09+0,001*aermr10	BC bins 1-6	hydrophilic BC	EC
aermr10 hydrophobic BC	PPM bins 3 to 6	BCaged	not used	70% accumulation mode, 30% Aitken mode	BC bins 1-12	EC_25	OC_25=0.7*aermr10 OC_co=0.15*aermr10	AEC bin 1-2.5µm = 0,999*aermr09+0,999*aermr10	BC bins 1-6	hydrophobic BC	EC
aermr11 Sulphate Aerosol	SO4 bins 3 to 6	SO4	SO4	90% accumulation mode, 10% Aitken mode	SO4 bins 1-12	SO4_25	SO4	SO4 bin 0-1µm = 0,001*aermr11 SO4 bin 1-2,5µm = 0,999*aermr11	MOCAG E-global	SO4	SO4 split equally on 2 modes
aermr16 Nitrate fine mode	not used	not used	NO3_F (0-2.5 µm)	90% accumulation mode, 10%	not used	NO3_25	NO3_f	NO3 bin 0-1µm = 0,001*aermr16 NO3 bin	MOCAG E-global	not used	not used

				Aitken mode				1-2,5µm = 0,999*ae rmr16 + 0,55*aer mr17			
aermr17 Nitrate coarse mode	not used	not used	NO3_C (2.5-10 µm)	not used	not used	NO3_co	NITRAT E(coarse)	Coarse unspecifi ed =0.45*ae rmr17	MOCAG E-global	not used	not used
aermr18 Ammoni um	not used	not used	NH4_F (0-2.5 µm)	90% accumula tion mode, 10% Aitken mode	not used	NH4_25	NH4_f	NH4 bin 0-1µm = 0,001*ae rmr18 NH4 bin 1-2,5µm = 0,999*ae rmr18	MOCAG E-global	not used	not used
aerm19 Biogenic SOA	OM	OM	not used	not used	BSOA	not used	SOA	BSOA	BSOA	not used	BSOA
aerm20 Anthropo genic SOA	OM	OM	not used	not used	ASOA	not used	SOA	ASOA	ASOA	not used	ASOA
CHOCH O (Glyoxal)	CHOCH O	not used	CHOCH O	CHOCH O	CHOCH O	not used	CHOCH O	CHOCH O	CHOCH O	not used	CHOCH O
C2H6 (ethane)	C2H6	C2H6	C2H6	C2H6	C2H6	not used	C2H6	ALK1	MOCAG E-global	C2H6	2xPAR5
C5H8 (isoprene )	C5H8	C5H8	C5H8	C5H8	C5H8	C5H8	C5H8	C5H8	MOCAG E-global	C5H8	C5H8
CH4_c (methane )	CH4	not used	CH4	not used	CH4	CH4	CH4	CH4	MOCAG E-global	not used	not used

CO (carbon monoxide)	CO	CO	CO	CO	CO	CO	CO	CO	CO	CO	CO
GO3 (ozone)	O3	O3	O3	O3	O3	O3	O3	O3	O3	O3	O3
H2O2 (hydrogen peroxide)	not used	not used	not used	H2O2	H2O2	not used	seasonal climatological conc used	not used	MOCAG E-global	H2O2	not used
HCHO (formaldehyde)	HCHO	HCHO	HCHO	HCHO	HCHO	HCHO	HCHO	HCHO	MOCAG E-global	HCHO	HCHO
HNO3 (nitric acid)	HNO3	HNO3	HNO3	HNO3	HNO3	HNO3	HNO3	HNO3	MOCAG E-global	HNO3	HNO3
NO (nitrogen monoxide)	not used	NO	NO	NO	NO	NO	NO	NO	MOCAG E-global	NO	NO
NO2 (nitrogen dioxide)	NO2	NO2	NO2	NO2	NO2	NO2	NO2	NO2	MOCAG E-global	NO2	NO2
PAN (Peroxyacetyl nitrate)	PAN	PAN	PAN	PAN	PAN	PAN	PAN	PAN	MOCAG E-global	PAN	PAN
SO2 (Sulphur dioxide)	SO2	SO2	SO2	SO2	SO2	SO2	SO2	SO2	SO2	SO2	SO2

1514

1515

1516

1517 **References**

1518

1519 Aamaas, B., Peters, G. P., and Fuglestad, J. S.: Simple emission metrics for climate impacts, *Earth Syst. Dynam.*, 4, 145-  
1520 170, 2013.

1521 Ackermann, I. J., Hass, H., Memmesheimer, M., Ebel, A., Binkowski, F. S., and Shankar, U.: Modal aerosol dynamics  
1522 model for Europe: development and first applications, *Atmospheric Environment*, 32, 2981-2999,  
1523 [http://dx.doi.org/10.1016/S1352-2310\(98\)00006-5](http://dx.doi.org/10.1016/S1352-2310(98)00006-5), 1998.

1524 Adani, M. and Uboldi, F.: Data assimilation experiments over Europe with the Chemical Transport Model FARM,  
1525 *Atmospheric Environment*, 306, 119806, 2023.

1526 Alfaro, S. C. and Gomes, L.: Modeling mineral aerosol production by wind erosion: Emission intensities and aerosol size  
1527 distributions in source areas, *Journal of Geophysical Research: Atmospheres*, 106, 18075-18084, 2001.

1528 Andersson-Sköld, Y. and Simpson, D.: Comparison of the chemical schemes of the EMEP MSC-W and IVL photochemical  
1529 trajectory models, *Atmospheric Environment*, 33, 1111-1129, 1999.

1530 Atkinson, R., Baulch, D. L., Cox, R. A., Crowley, J. N., Hampson, R. F., Hynes, R. G., Jenkin, M. E., Rossi, M. J., and Troe,  
1531 J.: Evaluated kinetic and photochemical data for atmospheric chemistry: Volume I - gas phase reactions of Ox, HOx, NOx  
1532 and SOx species, *Atmos. Chem. Phys.*, 4, 1461-1738, 10.5194/acp-4-1461-2004, 2004.

1533 Badia, A. and Jorba, O.: Gas-phase evaluation of the online NMMB/BSC-CTM model over Europe for 2010 in the  
1534 framework of the AQMEII-Phase2 project, *Atmospheric Environment*, 115, 657-669, 2015.

1535 Badia, A., Jorba, O., Voulgarakis, A., Dabdub, D., Pérez García-Pando, C., Hilboll, A., Gonçalves, M., and Janjic, Z.:  
1536 Description and evaluation of the Multiscale Online Nonhydrostatic Atmosphere Chemistry model (NMMB-MONARCH)  
1537 version 1.0: gas-phase chemistry at global scale, *Geoscientific Model Development*, 10, 609-638, 2017.

1538 Baklanov, A. and Sørensen, J.: Parameterisation of radionuclide deposition in atmospheric long-range transport modelling,  
1539 *Physics and Chemistry of the Earth, Part B: Hydrology, Oceans and Atmosphere*, 26, 787-799, 2001.

1540 Banzhaf, S., Schaap, M., Kerschbaumer, A., Reimer, E., Stern, R., van der Swaluw, E., and Buitjes, P. J. H.:  
1541 Implementation and evaluation of pH-dependent cloud chemistry and wet deposition in the chemical transport model REM-  
1542 Calgrid, *Atmos. Environ.*, 49, 2012.

1543 Barbu, A., Segers, A., Schaap, M., Heemink, A., and Buitjes, P.: A multi-component data assimilation experiment directed  
1544 to sulphur dioxide and sulphate over Europe, *Atmospheric Environment*, 43, 1622-1631, 2009.

1545 Bechtold, P., Bazile, E., Guichard, F., Mascart, P., and Richard, E.: A mass-flux convection scheme for regional and global  
1546 models, *Quarterly Journal of the Royal Meteorological Society*, 127, 869-886, 2001.

1547 Berge, E.: Coupling of wet scavenging of sulphur to clouds in a numerical weather prediction model, *Tellus B: Chemical and*  
1548 *Physical Meteorology*, 45, 1-22, 1993.

1549 Bergström, R., Hayman, G. D., Jenkin, M. E., and Simpson, D.: Update and comparison of atmospheric chemistry  
1550 mechanisms for the EMEP MSC-W model system — EmChem19a, EmChem19X, CRIV2R5Em, CB6r2Em, and  
1551 MCMv3.3Em, The Norwegian Meteorological Institute, Oslo, Norway, 2022.

1552 Bergström, R., Denier Van Der Gon, H., Prévôt, A. S., Yttri, K. E., and Simpson, D.: Modelling of organic aerosols over  
1553 Europe (2002–2007) using a volatility basis set (VBS) framework: application of different assumptions regarding the  
1554 formation of secondary organic aerosol, *Atmospheric Chemistry and Physics*, 12, 8499-8527, 2012a.

1555 Bergström, R., Denier van der Gon, H. A. C., Prévôt, A. S. H., Yttri, K. E., and Simpson, D.: Modelling of organic aerosols  
1556 over Europe (2002–2007) using a volatility basis set (VBS) framework: application of different assumptions regarding the  
1557 formation of secondary organic aerosol, *Atmos. Chem. Phys.*, 12, 8499-8527, doi:10.5194/acp-12-8499-2012, 2012b.

1558 Bertrand, J. M., Meleux, F., Ung, A., Descombes, G., and Colette, A.: Technical note: Improving the European air quality  
1559 forecast of Copernicus Atmosphere Monitoring Service using machine learning techniques, *Atmos. Chem. Phys. Discuss.*,  
1560 2022, 1-28, 10.5194/acp-2022-767, 2022.

1561 Bessagnet, B., Brignon, J.-M., Le Gall, A.-C., Meleux, F., Schucht, S., and Rouil, L.: Politiques combinées de gestion de la  
1562 qualité de l'air et du changement climatique (partie 1): enjeux, synergies et antagonismes, INERIS, Verneuil en Halatte,  
1563 2009.

1564 Bessagnet, B., Hodzic, A., Vautard, R., Beekmann, M., Cheinet, S., Honore, C., Liousse, C., and Rouil, L.: Aerosol  
1565 modeling with CHIMERE - preliminary evaluation at the continental scale, *Atmospheric Environment*, 38, 2803-2817,  
1566 10.1016/j.atmosenv.2004.02.034, 2004.

1567 Bessagnet, B., Menut, L., Colette, A., Couvidat, F., Dan, M., Mailler, S., Létinois, L., Pont, V., and Rouil, L.: An Evaluation  
1568 of the CHIMERE Chemistry Transport Model to Simulate Dust Outbreaks across the Northern Hemisphere in March 2014,  
1569 *Atmosphere*, 8, 251, 2017.

1570 Bessagnet, B., Menut, L., Curci, G., Hodzic, A., Guillaume, B., Liousse, C., Moukhtar, S., Pun, B., Seigneur, C., and Schulz,  
1571 M.: Regional modeling of carbonaceous aerosols over Europe—focus on secondary organic aerosols, *Journal of*  
1572 *Atmospheric Chemistry*, 61, 175-202, 2008.

1573 Bieser, J., Aulinger, A., Matthias, V., Quante, M., and Van Der Gon, H. D.: Vertical emission profiles for Europe based on  
1574 plume rise calculations, *Environmental Pollution*, 159, 2935-2946, 2011.

1575 Binkowski, F. and Shankar, U.: The Regional Particulate Matter Model .1. Model description and preliminary results, *J.*  
1576 *Geophys. Res.*, 100, 26191–26209, 1995.

1577 Binkowski, F. S.: The aerosol portion of Models-3 CMAQ. In *Science Algorithms of the EPA Models-3 Community*  
1578 *Multiscale Air Quality (CMAQ) Modeling System. Part II: Chapters 9-18*, National Exposure Research Laboratory, U.S.  
1579 Environmental Protection Agency, Research Triangle Park, NC, 1999.

1580 Bott, A.: A Positive Definite Advection Scheme Obtained by Nonlinear Renormalization of the Advective Fluxes, *Mon.*  
1581 *Wea. Rev.*, 117, 1006-1015, 1989.

1582 Brandt, J., Silver, J. D., Frohn, L. M., Geels, C., Gross, A., Hansen, A. B., Hansen, K. M., Hedegaard, G. B., Skjoth, C. A.,  
1583 Villadsen, H., Zare, A., and Christensen, J. H.: An integrated model study for Europe and North America using the Danish  
1584 Eulerian Hemispheric Model with focus on intercontinental transport of air pollution, *Atmospheric Environment*, 33, 156-  
1585 176, 2012.

1586 Brasseur, G. P., Xie, Y., Petersen, A. K., Bouarar, I., Flemming, J., Gauss, M., Jiang, F., Kouznetsov, R., Kranenburg, R.,  
1587 and Mijling, B.: Ensemble forecasts of air quality in eastern China—Part 1: Model description and implementation of the  
1588 MarcoPolo—Panda prediction system, version 1, *Geoscientific Model Development*, 12, 33-67, 2019.

1589 Burridge, D.: THE METEOROLOGICAL OFFICE OPERATIONAL 10-LEVEL NUMERICAL WEATHER  
1590 PREDICTION MODEL (DECEMBER 1975), 1977.

1591 Cariolle, D. and Teyssedre, H.: A revised linear ozone photochemistry parameterization for use in transport and general  
1592 circulation models: multi-annual simulations, *Atmospheric chemistry and physics*, 7, 2183-2196, 2007.

1593 Carslaw, K. S., Luo, B., and Peter, T.: An analytic expression for the composition of aqueous HNO<sub>3</sub>-H<sub>2</sub>SO<sub>4</sub> stratospheric  
1594 aerosols including gas phase removal of HNO<sub>3</sub>, *Geophysical Research Letters*, 22, 1877-1880, 1995.

1595 Carson, D.: The development of a dry inversion-capped convectively unstable boundary layer, *Quarterly Journal of the*  
1596 *Royal Meteorological Society*, 99, 450-467, 1973.

1597 Carter, W. P. L.: Condensed atmospheric photooxidation mechanisms for isoprene, *Atmospheric Environment*, 30, 4275-  
1598 4290, [http://dx.doi.org/10.1016/1352-2310\(96\)00088-X](http://dx.doi.org/10.1016/1352-2310(96)00088-X), 1996.

1599 Carter, W. P. L.: Documentation of the SAPRC-99 Chemical Mechanism for VOC Reactivity Assessment, 2000.

1600 Castro, L., Pio, C., Harrison, R. M., and Smith, D.: Carbonaceous aerosol in urban and rural European atmospheres:  
1601 estimation of secondary organic carbon concentrations, *Atmospheric Environment*, 33, 2771-2781, 1999.

1602 Chang, T.: Rain and snow scavenging of HNO<sub>3</sub> vapor in the atmosphere, *Atmospheric Environment* (1967), 18, 191-197,  
1603 1984.

1604 Christensen, J., Brandt, J., Frohn, L., and Skov, H.: Modelling of mercury in the Arctic with the Danish Eulerian  
1605 Hemispheric Model, *Atmospheric Chemistry and Physics*, 4, 2251-2257, 2004.

1606 Christensen, J. H.: The Danish Eulerian hemispheric model—A three-dimensional air pollution model used for the Arctic,  
1607 *Atmospheric Environment*, 31, 4169-4191, 1997.

1608 Colella, P. and Woodward, P. R.: The piecewise parabolic method (PPM) for gas-dynamical simulations, *Journal of*  
1609 *computational physics*, 54, 174-201, 1984.

1610 Colette, A., Bessagnet, B., Meleux, F., Terrenoire, E., and Rouïl, L.: Frontiers in air quality modelling, *Geosci. Model Dev.*,  
1611 7, 203-210, 2014.

1612 Colette, A., Bessagnet, B., Vautard, R., Szopa, S., Rao, S., Schucht, S., Klimont, Z., Menut, L., Clain, G., Meleux, F., Curci,  
1613 G., and Rouïl, L.: European atmosphere in 2050, a regional air quality and climate perspective under CMIP5 scenarios,  
1614 *Atmos. Chem. Phys.*, 13, 7451-7471, 2013.



1615 Colette, A., Andersson, C., Baklanov, A., Bessagnet, B., Brandt, J., Christensen, J. H., Doherty, R., Engardt, M., Geels, C.,  
1616 Giannakopoulos, C., Hedegaard, G. H., Katragkou, E., Langner, J., Lei, H., Manders, A., Melas, D., Meleux, F., Rouïl, L.,  
1617 Sofiev, M., Soares, J., Stevenson, D. S., Tombrou-Tzella, M., Varotsos, K. V., and Young, P.: Is the ozone climate penalty  
1618 robust in Europe?, *Environmental Research Letters*, 10, 084015, 2015.

1619 Colette, A., Andersson, C., Manders, A., Mar, K., Mircea, M., Pay, M. T., Raffort, V., Tsyro, S., Cuvelier, C., Adani, M.,  
1620 Bessagnet, B., Bergström, R., Briganti, G., Butler, T., Cappelletti, A., Couvidat, F., D'Isidoro, M., Doumbia, T., Fagerli, H.,  
1621 Granier, C., Heyes, C., Klimont, Z., Ojha, N., Otero, N., Schaap, M., Sindelarova, K., Stegehuis, A. I., Roustan, Y., Vautard,  
1622 R., van Meijgaard, E., Vivanco, M. G., and Wind, P.: EURODELTA-Trends, a multi-model experiment of air quality  
1623 hindcast in Europe over 1990–2010, *Geosci. Model Dev.*, 10, 3255–3276, 10.5194/gmd-10-3255-2017, 2017.

1624 Côté, J., Gravel, S., Méthot, A., Patoine, A., Roch, M., and Staniforth, A.: The operational CMC–MRB global environmental  
1625 multiscale (GEM) model. Part I: Design considerations and formulation, *Monthly Weather Review*, 126, 1373–1395, 1998a.

1626 Côté, J., Desmarais, J.-G., Gravel, S., Méthot, A., Patoine, A., Roch, M., and Staniforth, A.: The operational CMC–MRB  
1627 global environmental multiscale (GEM) model. Part II: Results, *Monthly Weather Review*, 126, 1397–1418, 1998b.

1628 Couvidat, F., Bessagnet, B., Garcia-Vivanco, M., Real, E., Menut, L., and Colette, A.: Development of an inorganic and  
1629 organic aerosol model (CHIMERE 2017 $\beta$  v1.0): seasonal and spatial evaluation over Europe, *Geosci. Model Dev.*, 11, 165–  
1630 194, 10.5194/gmd-11-165-2018, 2018.

1631 Curier, R., Timmermans, R., Calabretta-Jongen, S., Eskes, H., Segers, A., Swart, D., and Schaap, M.: Improving ozone  
1632 forecasts over Europe by synergistic use of the LOTOS-EUROS chemical transport model and in-situ measurements,  
1633 *Atmospheric environment*, 60, 217–226, 2012.

1634 Cussac, M., Marécal, V., Thouret, V., Josse, B., and Sauvage, B.: The impact of biomass burning on upper tropospheric  
1635 carbon monoxide: a study using MOCAGE global model and IAGOS airborne data, *Atmospheric Chemistry and Physics*,  
1636 20, 9393–9417, 2020.

1637 D'Elia, I., Briganti, G., Vitali, L., Piersanti, A., Righini, G., D'Isidoro, M., Cappelletti, A., Mircea, M., Adani, M., and  
1638 Zanini, G.: Measured and modelled air quality trends in Italy over the period 2003–2010, *Atmospheric Chemistry and*  
1639 *Physics*, 21, 10825–10849, 2021.

1640 Dabdub, D. and Seinfeld, J. H.: Numerical advective schemes used in air quality models—sequential and parallel  
1641 implementation, *Atmospheric Environment*, 28, 3369–3385, 1994.

1642 Damski, J., Thölix, L., Backman, L., Taalas, P., and Kulmala, M.: FinRose--middle atmospheric chemistry transport model,  
1643 *Boreal environment research*, 12, 2007.

1644 Denier van der Gon, H. A. C., Bergström, R., Fountoukis, C., Johansson, C., Pandis, S. N., Simpson, D., and Visschedijk, A.  
1645 J. H.: Particulate emissions from residential wood combustion in Europe – revised estimates and an evaluation, *Atmos.*  
1646 *Chem. Phys.*, 15, 6503–6519, 10.5194/acp-15-6503-2015, 2015.

1647 Derognat, C., Beekmann, M., Baeumle, M., Martin, D., and Schmidt, H.: Effect of biogenic volatile organic compound  
1648 emissions on tropospheric chemistry during the Atmospheric Pollution Over the Paris Area (ESQUIF) campaign in the Ile-  
1649 de-France region, *Journal of Geophysical Research: Atmospheres*, 108, 2003.

1650 Di Tomaso, E., Schutgens, N. A. J., Jorba, O., and Pérez García-Pando, C.: Assimilation of MODIS Dark Target and Deep  
1651 Blue observations in the dust aerosol component of NMMB-MONARCH version 1.0, Geoscientific Model Development, 10,  
1652 1107-1129, 2017.

1653 Di Tomaso, E., Escribano, J., Basart, S., Ginoux, P., Macchia, F., Barnaba, F., Benincasa, F., Bretonnière, P. A., Buñuel, A.,  
1654 Castrillo, M., Cuevas, E., Formenti, P., Gonçalves, M., Jorba, O., Klose, M., Mona, L., Montané Pinto, G., Mytilinaios, M.,  
1655 Obiso, V., Olid, M., Schutgens, N., Votsis, A., Werner, E., and Pérez García-Pando, C.: The MONARCH high-resolution  
1656 reanalysis of desert dust aerosol over Northern Africa, the Middle East and Europe (2007–2016), Earth Syst. Sci. Data, 14,  
1657 2785-2816, 10.5194/essd-14-2785-2022, 2022.

1658 Douros, J., Eskes, H., van Geffen, J., Boersma, K. F., Compennolle, S., Pinardi, G., Blechschmidt, A. M., Peuch, V. H.,  
1659 Colette, A., and Veeckind, P.: Comparing Sentinel-5P TROPOMI NO<sub>2</sub> column observations with the CAMS-regional air  
1660 quality ensemble, EGU sphere, 2022, 1-40, 10.5194/egusphere-2022-365, 2022.

1661 Ebel, A., Friedrich, R., and Rodhe, H.: GENEMIS: Assessment, improvement, and temporal and spatial disaggregation of  
1662 European emission data, in: Tropospheric modelling and emission estimation, Springer, 181-214, 1997.

1663 EC: Directive 2008/50/EC of the European Parliament and of the Council of 21 May 2008 on ambient air quality and cleaner  
1664 air for Europe, European Commission, Brussels, 2008.

1665 ECMWF: IFS Documentation CY47R3 - Part IV Physical processes, Reading, doi: 10.21957/eyrpir4vj, 2021.

1666 Elbern, H., Strunk, A., Schmidt, H., and Talagrand, O.: Emission rate and chemical state estimation by 4-dimensional  
1667 variational inversion, Atmospheric Chemistry and Physics, 7, 3749-3769, 2007.

1668 Emberson, L., Ashmore, M., Cambridge, H., Simpson, D., and Tuovinen, J.-P.: Modelling stomatal ozone flux across  
1669 Europe, Environmental Pollution, 109, 403-413, 2000a.

1670 Emberson, L. D., Ashmore, M. R., Simpson, D., Tuovinen, J.-P., and Cambridge, H. M.: Towards a model of ozone  
1671 deposition and stomatal uptake over Europe, Norwegian Meteorological Institute, Oslo, Norway, 57, 2000b.

1672 EMEP: Transboundary particulate matter, photo-oxydants, acidifying and eutrophying components, EMEP, Oslo, Norway,  
1673 2023.

1674 Erisman, J. W., Van Pul, A., and Wyers, P.: Parametrization of surface resistance for the quantification of atmospheric  
1675 deposition of acidifying pollutants and ozone, Atmospheric Environment, 28, 2595-2607, [http://dx.doi.org/10.1016/1352-  
1676 2310\(94\)90433-2](http://dx.doi.org/10.1016/1352-2310(94)90433-2), 1994.

1677 Escribano, J., Di Tomaso, E., Jorba, O., Klose, M., Gonçalves Ageitos, M., Macchia, F., Amiridis, V., Baars, H., Marinou,  
1678 E., Proestakis, E., Urbanneck, C., Althausen, D., Bühl, J., Mamouri, R. E., and Pérez García-Pando, C.: Assimilating  
1679 spaceborne lidar dust extinction can improve dust forecasts, Atmos. Chem. Phys., 22, 535-560, 10.5194/acp-22-535-2022,  
1680 2022.

1681 Fécan, F., Marticorena, B., and Bergametti, G.: Parametrization of the increase of the aeolian erosion threshold wind friction  
1682 velocity due to soil moisture for arid and semi-arid areas, Annales Geophysicae, 149-157,

1683 Flemming, J., Huijnen, V., Arteta, J., Bechtold, P., Beljaars, A., Blechschmidt, A. M., Diamantakis, M., Engelen, R. J.,  
1684 Gaudel, A., Inness, A., Jones, L., Josse, B., Katragkou, E., Marecal, V., Peuch, V. H., Richter, A., Schultz, M. G., Stein, O.,

1685 and Tsikerdekis, A.: Tropospheric chemistry in the Integrated Forecasting System of ECMWF, *Geosci. Model Dev.*, 8, 975-  
1686 1003, 10.5194/gmd-8-975-2015, 2015.

1687 Foley, K., Roselle, S., Appel, K., Bhawe, P., Pleim, J., Otte, T., Mathur, R., Sarwar, G., Young, J., and Gilliam, R.:  
1688 Incremental testing of the Community Multiscale Air Quality (CMAQ) modeling system version 4.7, *Geoscientific Model*  
1689 *Development*, 3, 205-226, 2010.

1690 Forester, C.: Higher order monotonic convective difference schemes, *Journal of Computational Physics*, 23, 1-22, 1977.

1691 Fountoukis, C. and Nenes, A.: ISORROPIA II: a computationally efficient thermodynamic equilibrium model for K+–  
1692 Ca<sup>2+</sup>–Mg<sup>2+</sup>–NH<sub>4</sub><sup>+</sup>–Na<sup>+</sup>–SO<sub>4</sub><sup>2-</sup>–NO<sub>3</sub><sup>-</sup>–Cl<sup>-</sup>–H<sub>2</sub>O aerosols, *Atmos. Chem. Phys.*, 7, 4639-4659, doi:10.5194/acp-7-4639-  
1693 2007, 2007.

1694 Friese, E. and Ebel, A.: Temperature dependent thermodynamic model of the system H<sup>+</sup>–NH<sub>4</sub><sup>+</sup>–Na<sup>+</sup>–SO<sub>4</sub><sup>2-</sup>–NO<sub>3</sub><sup>-</sup>–  
1695 Cl<sup>-</sup>–H<sub>2</sub>O, *The Journal of Physical Chemistry A*, 114, 11595-11631, 2010.

1696 Frohn, L.: A study of long-term high-resolution air pollution modelling, Ministry of the Environment, National  
1697 Environmental Research Institute, Roskilde, Denmark, 2004.

1698 Galmarini, S., Kioutsioukis, I., and Solazzo, E.: E pluribus unum\*: ensemble air quality predictions, *Atmos. Chem. Phys.*,  
1699 13, 7153-7182, 10.5194/acp-13-7153-2013, 2013.

1700 Galmarini, S., Bianconi, R., Addis, R., Andronopoulos, S., Astrup, P., Bartzis, J., Bellasio, R., Buckley, R., Champion, H.,  
1701 and Chino, M.: Ensemble dispersion forecasting—Part II: Application and evaluation, *Atmospheric Environment*, 38, 4619-  
1702 4632, 2004.

1703 Galmarini, S., Koffi, B., Solazzo, E., Keating, T., Hogrefe, C., Schulz, M., Benedictow, A., Griesfeller, J. J., Janssens-  
1704 Maenhout, G., Carmichael, G., Fu, J., and Dentener, F.: Technical note: Coordination and harmonization of the multi-scale,  
1705 multi-model activities HTAP2, AQMEII3, and MICS-Asia3: simulations, emission inventories, boundary conditions, and  
1706 model output formats, *Atmos. Chem. Phys.*, 17, 1543-1555, 10.5194/acp-17-1543-2017, 2017.

1707 Galperin, M. and Sofiev, M.: Errors in the validation of models for long-range transport and critical loads stipulated by  
1708 stochastic properties of pollution fields., *EMEP Chemical Coordinating Centre, Lillestrom, Passau*, 162–179, 1994.

1709 Geels, C., Winther, M., Andersson, C., Jalkanen, J.-P., Brandt, J., Frohn, L. M., Im, U., Leung, W., and Christensen, J. H.:  
1710 Projections of shipping emissions and the related impact on air pollution and human health in the Nordic region,  
1711 *Atmospheric Chemistry and Physics*, 21, 12495-12519, 2021.

1712 Geiger, H., Barnes, I., Bejan, I., Benter, T., and Spittler, M.: The tropospheric degradation of isoprene: an updated module  
1713 for the regional atmospheric chemistry mechanism, *Atmospheric Environment*, 37, 1503-1519, 2003.

1714 Gery, M. W., Whitten, G. Z., Killus, J. P., and Dodge, M. C.: A photochemical kinetics mechanism for urban and regional  
1715 scale computer modeling, *Journal of Geophysical Research: Atmospheres*, 94, 12925-12956, 1989.

1716 Ginoux, P., Chin, M., Tegen, I., Prospero, J. M., Holben, B., Dubovik, O., and Lin, S. J.: Sources and distributions of dust  
1717 aerosols simulated with the GOCART model, *Journal of Geophysical Research: Atmospheres*, 106, 20255-20273, 2001.

1718 Giorgi, F. and Chameides, W. L.: Rainout lifetimes of highly soluble aerosols and gases as inferred from simulations with a  
1719 general circulation model, *Journal of Geophysical Research: Atmospheres*, 91, 14367-14376, 1986.

1720 Gomes, L., Rajot, J., Alfaro, S., and Gaudichet, A.: Validation of a dust production model from measurements performed in  
1721 semi-arid agricultural areas of Spain and Niger, *Catena*, 52, 257-271, 2003.

1722 Gong, S., Barrie, L., Blanchet, J. P., Von Salzen, K., Lohmann, U., Lesins, G., Spacek, L., Zhang, L., Girard, E., and Lin, H.:  
1723 Canadian Aerosol Module: A size-segregated simulation of atmospheric aerosol processes for climate and air quality models  
1724 1. Module development, *Journal of Geophysical Research: Atmospheres*, 108, AAC 3-1-AAC 3-16, 2003.

1725 Granier, C., Darras, S., van der Gon, H. D., Doubalova, J., Elguindi, N., Galle, B., Gauss, M., Guevara, M., Jalkanen, J. P.,  
1726 and Kuenen, J.: The Copernicus Atmosphere Monitoring Service global and regional emissions (April 2019 version),  
1727 Copernicus Atmosphere Monitoring Service, 10.24380/d0bn-kx16, 2019.

1728 Groisman, P. Y. and Genikhovich, E. L.: Assessing surface-atmosphere interactions using former Soviet Union standard  
1729 meteorological network data. Part I: Method, *Journal of climate*, 10, 2154-2183, 1997.

1730 Guenther, A., Zimmerman, P., Harley, P., Monson, R., and Fall, R.: Isoprene and monoterpene rate variability: model  
1731 evaluations and sensitivity analyses, *J. Geophys. Res.*, 98, 12609-12617, 1993.

1732 Guenther, A., Karl, T., Harley, P., Wiedinmyer, C., Palmer, P. I., and Geron, C.: Estimates of global terrestrial isoprene  
1733 emissions using MEGAN (Model of Emissions of Gases and Aerosols from Nature), *Atmos. Chem. Phys.*, 6, 3181-3210,  
1734 2006.

1735 Guenther, A., Jiang, X., Heald, C. L., Sakulyanontvittaya, T., Duhl, T. a., Emmons, L., and Wang, X.: The Model of  
1736 Emissions of Gases and Aerosols from Nature version 2.1 (MEGAN2. 1): an extended and updated framework for modeling  
1737 biogenic emissions, *Geoscientific Model Development*, 5, 1471-1492, 2012.

1738 Guevara, M., Tena, C., Porquet, M., Jorba, O., and Pérez García-Pando, C.: HERMESv3, a stand-alone multi-scale  
1739 atmospheric emission modelling framework-Part 1: global and regional module, *Geoscientific Model Development*, 12,  
1740 1885-1907, 2019.

1741 Guevara, M., Jorba, O., Tena, C., Denier van der Gon, H., Kuenen, J., Elguindi, N., Darras, S., Granier, C., and Pérez  
1742 García-Pando, C.: Copernicus Atmosphere Monitoring Service TEMPORal profiles (CAMs-TEMPO): global and European  
1743 emission temporal profile maps for atmospheric chemistry modelling, *Earth Syst. Sci. Data*, 13, 367-404, 10.5194/essd-13-  
1744 367-2021, 2021.

1745 Guth, J., Josse, B., Marécal, V., Joly, M., and Hamer, P.: First implementation of secondary inorganic aerosols in the  
1746 MOCAGE version 2.15.0 chemistry transport model, *Geosci. Model Dev.*, 9, 137-160, 10.5194/gmd-9-137-2016, 2016.

1747 Guth, J., Marécal, V., Josse, B., Arteta, J., and Hamer, P.: Primary aerosol and secondary inorganic aerosol budget over the  
1748 Mediterranean Basin during 2012 and 2013, *Atmospheric Chemistry and Physics*, 18, 4911-4934, 2018.

1749 Hamer, P., Fjaeraa, A.-M., Soares, J., Meleux, F., Colette, A., Ung, A., Raux, B., and Tarrason, L.: Copernicus Atmosphere  
1750 Monitoring Service Interim Annual Assessment Report on European Air Quality in 2022, ECMWF, Bonn,  
1751 [https://policy.atmosphere.copernicus.eu/reports/CAMS271\\_2021SCx\\_D1.1.1\\_202306\\_2022\\_Interim\\_Assessment\\_Report\\_v](https://policy.atmosphere.copernicus.eu/reports/CAMS271_2021SCx_D1.1.1_202306_2022_Interim_Assessment_Report_v1.pdf)  
1752 [1.pdf](https://policy.atmosphere.copernicus.eu/reports/CAMS271_2021SCx_D1.1.1_202306_2022_Interim_Assessment_Report_v1.pdf), 2023.

1753 Hansen, K. M., Christensen, J. H., Brandt, J., Frohn, L. M., Geels, C., Skjøth, C. A., and Li, Y. F.: Modeling short-term  
1754 variability of  $\alpha$ -hexachlorocyclohexane in Northern Hemispheric air, *Journal of Geophysical Research: Atmospheres*, 113,  
1755 2008.

1756 Hass, H., Jakobs, H., and Memmesheimer, M.: Analysis of a regional model (EURAD) near surface gas concentration  
1757 predictions using observations from networks, *Meteorology and Atmospheric Physics*, 57, 173-200, 1995.

1758 Heidam, N. Z., Christensen, J., Wählin, P., and Skov, H.: Arctic atmospheric contaminants in NE Greenland: levels,  
1759 variations, origins, transport, transformations and trends 1990–2001, *Science of the Total Environment*, 331, 5-28, 2004.

1760 Heimann, M. and Keeling, C. D.: A three-dimensional model of atmospheric CO<sub>2</sub> transport based on observed winds: 2.  
1761 Model description and simulated tracer experiments, *Max-Planck-Institut für Meteorologie* 1989.

1762 Hendriks, C., Forsell, N., Kiesewetter, G., Schaap, M., and Schöpp, W.: Ozone concentrations and damage for realistic  
1763 future European climate and air quality scenarios, *Atmospheric Environment*, 144, 208-219, 2016.

1764 Hertel, O., Christensen, J., Runge, E. H., Asman, W. A., Berkowicz, R., Hovmand, M. F., and Hov, Ø.: Development and  
1765 testing of a new variable scale air pollution model—ACDEP, *Atmospheric Environment*, 29, 1267-1290, 1995.

1766 Hicks, B., Baldocchi, D., Meyers, T., Hosker, R., and Matt, D.: A preliminary multiple resistance routine for deriving dry  
1767 deposition velocities from measured quantities, *Water, Air, and Soil Pollution*, 36, 311-330, 1987.

1768 Hodzic, A., Kasibhatla, P. S., Jo, D. S., Cappa, C. D., Jimenez, J. L., Madronich, S., and Park, R. J.: Rethinking the global  
1769 secondary organic aerosol (SOA) budget: stronger production, faster removal, shorter lifetime, *Atmospheric Chemistry and  
1770 Physics*, 16, 7917-7941, 2016.

1771 Hollingsworth, A.: Toward a monitoring and forecasting system for atmospheric composition: The GEMS Project, *Bull.  
1772 Amer. Meteor. Soc.*, 89, 1147-1164, <https://doi.org/10.1175/2008BAMS2355.1>, 2008.

1773 Hollingsworth, A. and Lönnberg, P.: The statistical structure of short-range forecast errors as determined from radiosonde  
1774 data. Part I: The wind field, *Tellus A*, 38, 111-136, 1986.

1775 Holtslag, A., Van Meijgaard, E., and De Rooy, W.: A comparison of boundary layer diffusion schemes in unstable  
1776 conditions over land, *Boundary-Layer Meteorology*, 76, 69-95, 1995.

1777 Holtslag, A. A. and Nieuwstadt, F. T.: Scaling the atmospheric boundary layer, *Boundary-Layer Meteorology*, 36, 201-209,  
1778 1986.

1779 Horálek, J., Schreiberová, M., Vlasáková, L., Hamer, P., Schneider, P., and Marková, J.: Interim European air quality maps  
1780 for 2020. PM<sub>10</sub>, NO<sub>2</sub> and ozone spatial estimates based on non-validated UTD data., NILU, Oslo,  
1781 [https://www.eionet.europa.eu/etcs/etc-atni/products/etc-atni-report-19-2021-interim-european-air-quality-maps-for-2020-  
1782 pm10-no2-and-ozone-spatial-estimates-based-on-non-validated-utd-data](https://www.eionet.europa.eu/etcs/etc-atni/products/etc-atni-report-19-2021-interim-european-air-quality-maps-for-2020-pm10-no2-and-ozone-spatial-estimates-based-on-non-validated-utd-data), 2022.

1783 Huang, G., Brook, R., Crippa, M., Janssens-Maenhout, G., Schieberle, C., Dore, C., Guizzardi, D., Muntean, M., Schaaf, E.,  
1784 and Friedrich, R.: Speciation of anthropogenic emissions of non-methane volatile organic compounds: a global gridded data  
1785 set for 1970–2012, *Atmospheric Chemistry and Physics*, 17, 7683-7701, 2017.

1786 Huijnen, V., Eskes, H., Poupkou, A., Elbern, H., Boersma, K., Foret, G., Sofiev, M., Valdebenito, A., Flemming, J., and  
1787 Stein, O.: Comparison of OMI NO<sub>2</sub> tropospheric columns with an ensemble of global and European regional air quality  
1788 models, *Atmospheric Chemistry and Physics*, 10, 3273-3296, 2010.

1789 Hunt, B. R., Kostelich, E. J., and Szunyogh, I.: Efficient data assimilation for spatiotemporal chaos: A local ensemble  
1790 transform Kalman filter, *Physica D: Nonlinear Phenomena*, 230, 112-126, <https://doi.org/10.1016/j.physd.2006.11.008>,  
1791 2007.

1792 Jaeglé, L., Quinn, P. K., Bates, T. S., Alexander, B., and Lin, J.-T.: Global distribution of sea salt aerosols: new constraints  
1793 from in situ and remote sensing observations, *Atmospheric Chemistry and Physics*, 11, 3137, 2011.

1794 Janjic, Z. and Gall, L.: Scientific documentation of the NCEP nonhydrostatic multiscale model on the B grid (NMMB). Part  
1795 1 Dynamics, NCAR/TN-489+STR, 2012.

1796 Jöckel, P., Tost, H., Pozzer, A., Brühl, C., Buchholz, J., Ganzeveld, L., Hoor, P., Kerkweg, A., Lawrence, M., and Sander,  
1797 R.: The atmospheric chemistry general circulation model ECHAM5/MESSy1: consistent simulation of ozone from the  
1798 surface to the mesosphere, *Atmospheric Chemistry and Physics*, 6, 5067-5104, 2006.

1799 Joly, M. and Peuch, V.-H.: Objective classification of air quality monitoring sites over Europe, *Atmospheric Environment*,  
1800 47, 111-123, 2012.

1801 Jonson, J., Kylling, A., Berntsen, T., Isaksen, I., Zerefos, C., and Kourtidis, K.: Chemical effects of UV fluctuations inferred  
1802 from total ozone and tropospheric aerosol variations, *Journal of Geophysical Research: Atmospheres*, 105, 14561-14574,  
1803 2000.

1804 Jorba, O., Dabdub, D., Blaszcak-Boxe, C., Pérez, C., Janjic, Z., Baldasano, J., Spada, M., Badia, A., and Gonçalves, M.:  
1805 Potential significance of photoexcited NO<sub>2</sub> on global air quality with the NMMB/BSC chemical transport model, *Journal of*  
1806 *Geophysical Research: Atmospheres*, 117, 2012.

1807 Kahnert, M.: Variational data analysis of aerosol species in a regional CTM: background error covariance constraint and  
1808 aerosol optical observation operators, *Tellus B: Chemical and Physical Meteorology*, 60, 753-770, 2008.

1809 Kain, J. S. and Fritsch, J. M.: A one-dimensional entraining/detraining plume model and its application in convective  
1810 parameterization, *Journal of Atmospheric Sciences*, 47, 2784-2802, 1990.

1811 Kaiser, J., Heil, A., Andreae, M., Benedetti, A., Chubarova, N., Jones, L., Morcrette, J.-J., Razinger, M., Schultz, M., and  
1812 Suttie, M.: Biomass burning emissions estimated with a global fire assimilation system based on observed fire radiative  
1813 power, *Biogeosciences*, 9, 527-554, 2012.

1814 Klose, M., Jorba, O., Gonçalves Ageitos, M., Escribano, J., Dawson, M. L., Obiso, V., Di Tomaso, E., Basart, S., Montané  
1815 Pinto, G., and Macchia, F.: Mineral dust cycle in the Multiscale Online Nonhydrostatic Atmosphere Chemistry model  
1816 (MONARCH) version 2.0, *Geoscientific Model Development*, 14, 6403-6444, 2021.

1817 Köble, R. and Seufert, G.: Novel maps for forest tree species in Europe, *Proceedings of the 8th European symposium on the*  
1818 *physico-chemical behaviour of air pollutants: “a changing atmosphere*, 17-20,

1819 Korhonen, H., Carslaw, K. S., Spracklen, D. V., Mann, G. W., and Woodhouse, M. T.: Influence of oceanic dimethyl sulfide  
1820 emissions on cloud condensation nuclei concentrations and seasonality over the remote Southern Hemisphere oceans: A  
1821 global model study, *Journal of Geophysical Research: Atmospheres*, 113, 2008.

1822 Kouznetsov, R. and Sofiev, M.: A methodology for evaluation of vertical dispersion and dry deposition of atmospheric  
1823 aerosols, *Journal of Geophysical Research: Atmospheres*, 117, 2012.

1824 Kouznetsov, R., Sofiev, M., Vira, J., and Stiller, G.: Simulating age of air and the distribution of SF 6 in the stratosphere  
1825 with the SILAM model, *Atmospheric Chemistry and Physics*, 20, 5837-5859, 2020.

1826 Kuenen, J., Visschedijk, A., Jozwicka, M., and Denier Van Der Gon, H.: TNO-MACC\_II emission inventory; a multi-year  
1827 (2003–2009) consistent high-resolution European emission inventory for air quality modelling, *Atmospheric Chemistry and*  
1828 *Physics*, 14, 10963-10976, 2014.

1829 Kuenen, J., Dellaert, S., Visschedijk, A., Jalkanen, J.-P., Super, I., and Denier van der Gon, H.: CAMS-REG-v4: a state-of-  
1830 the-art high-resolution European emission inventory for air quality modelling, *Earth System Science Data*, 14, 491-515,  
1831 2022.

1832 Kukkonen, J., Savolahti, M., Palamarchuk, Y., Lanki, T., Nurmi, V., Paunu, V.-V., Kangas, L., Sofiev, M., Karppinen, A.,  
1833 and Maragkidou, A.: Modelling of the public health costs of fine particulate matter and results for Finland in 2015,  
1834 *Atmospheric Chemistry and Physics*, 20, 9371-9391, 2020.

1835 Kylling, A., Stamnes, K., and Tsay, S.-C.: A reliable and efficient two-stream algorithm for spherical radiative transfer:  
1836 Documentation of accuracy in realistic layered media, *Journal of Atmospheric Chemistry*, 21, 115-150, 1995.

1837 Lahoz, W., Geer, A., Bekki, S., Bormann, N., Ceccherini, S., Elbern, H., Errera, Q., Eskes, H., Fonteyn, D., and Jackson, D.:  
1838 The Assimilation of Envisat data (ASSET) project, *Atmospheric Chemistry and Physics*, 7, 1773-1796, 2007.

1839 Lambert, J. D.: Numerical methods for ordinary differential systems, Wiley New York 1991.

1840 Lana, A., Bell, T., Simó, R., Vallina, S., Ballabrera-Poy, J., Kettle, A., Dachs, J., Bopp, L., Saltzman, E., and Stefels, J.: An  
1841 updated climatology of surface dimethylsulfide concentrations and emission fluxes in the global ocean, *Global*  
1842 *Biogeochemical Cycles*, 25, 2011.

1843 Landgraf, J. and Crutzen, P.: An efficient method for online calculations of photolysis and heating rates, *Journal of the*  
1844 *atmospheric sciences*, 55, 863-878, 1998.

1845 Lange, R.: Transferability of a three-dimensional air quality model between two different sites in complex terrain, *Journal of*  
1846 *Applied Meteorology and Climatology*, 28, 665-679, 1989.

1847 Langner, J., Bergström, R., and Pleijel, K.: European scale modeling of sulphur, oxidized nitrogen and photochemical  
1848 oxidants. Model development and evaluation for the 1994 growing season, *Swedish Met. and Hydrol. Inst., Norrköping,*  
1849 *Sweden*, 1998.

1850 Lansø, A. S., Smallman, T. L., Christensen, J. H., Williams, M., Pilegaard, K., Sørensen, L.-L., and Geels, C.: Simulating the  
1851 atmospheric CO 2 concentration across the heterogeneous landscape of Denmark using a coupled atmosphere–biosphere  
1852 mesoscale model system, *Biogeosciences*, 16, 1505-1524, 2019.

1853 Lefevre, F., Brasseur, G., Folkins, I., Smith, A., and Simon, P.: Chemistry of the 1991–1992 stratospheric winter: Three-  
1854 dimensional model simulations, *Journal of Geophysical Research: Atmospheres*, 99, 8183-8195, 1994.

1855 Lehtomäki, H., Korhonen, A., Asikainen, A., Karvosenoja, N., Kupiainen, K., Paunu, V.-V., Savolahti, M., Sofiev, M.,  
1856 Palamarchuk, Y., and Karppinen, A.: Health impacts of ambient air pollution in Finland, *International journal of*  
1857 *environmental research and public health*, 15, 736, 2018.

1858 Li, Y., Elbern, H., Lu, K., Friese, E., Kiendler-Scharr, A., Mentel, T. F., Wang, X., Wahner, A., and Zhang, Y.: Updated  
1859 aerosol module and its application to simulate secondary organic aerosols during IMPACT campaign May 2008,  
1860 *Atmospheric chemistry and physics*, 13, 6289-6304, 2013.

1861 Liu, D. C. and Nocedal, J.: On the limited memory BFGS method for large scale optimization, *Mathematical programming*,  
1862 45, 503-528, 1989.

1863 Louis, J.-F.: A parametric model of vertical eddy fluxes in the atmosphere, *Boundary-Layer Meteorology*, 17, 187-202,  
1864 1979.

1865 Lurmann, F. W., Lloyd, A. C., and Atkinson, R.: A chemical mechanism for use in long-range transport/acid deposition  
1866 computer modeling, *Journal of Geophysical Research: Atmospheres*, 91, 10905-10936, 1986.

1867 Maas, R. and Grennfelt, P.: Towards Cleaner Air - Scientific Assessment Report 2016, EMEP-Steering body and Working  
1868 Group on Effects - Convention on Long-Range Transboundary Air Pollution 2016.

1869 Madronich, S.: Photodissociation in the atmosphere: 1. Actinic flux and the effects of ground reflections and clouds, *Journal*  
1870 *of Geophysical Research: Atmospheres*, 92, 9740-9752, 1987.

1871 Madronich, S. and Weller, G.: Numerical integration errors in calculated tropospheric photodissociation rate coefficients,  
1872 *Journal of atmospheric chemistry*, 10, 289-300, 1990.

1873 Manders, A. M. M., Builtjes, P. J. H., Curier, L., Denier van der Gon, H. A. C., Hendriks, C., Jonkers, S., Kranenburg, R.,  
1874 Kuenen, J., Segers, A. J., Timmermans, R. M. A., Visschedijk, A., Wichink Kruit, R. J., Van Pul, W. A. J., Sauter, F. J., van  
1875 der Swaluw, E., Swart, D. P. J., Douros, J., Eskes, H., van Meijgaard, E., van Ulft, B., van Velthoven, P., Banzhaf, S., Mues,  
1876 A., Stern, R., Fu, G., Lu, S., Heemink, A., van Velzen, N., and Schaap, M.: Curriculum Vitae of the LOTOS-EUROS (v2.0)  
1877 chemistry transport model, *Geosci. Model Dev. Discuss.*, 2017, 1-53, 10.5194/gmd-2017-88, 2017.

1878 Marécal, V., Peuch, V. H., Andersson, C., Andersson, S., Arteta, J., Beekmann, M., Benedictow, A., Bergstrom, R.,  
1879 Bessagnet, B., Cansado, A., Chéroux, F., Colette, A., Coman, A., Curier, R. L., Denier van der Gon, H. A. C., Drouin, A.,  
1880 Elbern, H., Emili, E., Engelen, R. J., Eskes, H. J., Foret, G., Friese, E., Gauss, M., Giannaros, C., Guth, J., Joly, M.,  
1881 Jaumouilla, E., Josse, B., Kadyrov, N., Kaiser, J. W., Krajsek, K., Kuenen, J., Kumar, U., Liora, N., Lopez, E., Malherbe,  
1882 L., Martinez, I., Melas, D., Meleux, F., Menut, L., Moinat, P., Morales, T., Parmentier, J., Piacentini, A., Plu, M., Poupkou,  
1883 A., Queguiner, S., Robertson, L., Rouil, L., Schaap, M., Segers, A., Sofiev, M., Tarasson, L., Thomas, M., Timmermans, R.,  
1884 Valdebenito, A., van Velthoven, P., van Versendaal, R., Vira, J., and Ung, A.: A regional air quality forecasting system over  
1885 Europe: the MACC-II daily ensemble production, *Geosci. Model Dev.*, 8, 2777-2813, 2015.

1886 Mari, C., Jacob, D. J., and Bechtold, P.: Transport and scavenging of soluble gases in a deep convective cloud, *Journal of*  
1887 *Geophysical Research: Atmospheres*, 105, 22255-22267, 2000.



1888 Martensson, E., Nilsson, E., de Leeuw, G., Cohen, L., and Hansson, H.-C.: Laboratory simulations and parameterisation of  
1889 the primary marine aerosol production, *J. Geophys. Res.*, 108, 4297, doi:10.1029/2002JD002263, 2003.

1890 Martet, M., Peuch, V., Laurent, B., Marticorena, B., and Bergametti, G.: Evaluation of long-range transport and deposition  
1891 of desert dust with the CTM MOCAGE, *Tellus B: Chemical and Physical Meteorology*, 61, 449-463, 2009.

1892 Marticorena, B. and Bergametti, G.: Modeling the atmospheric dust cycle: 1. Design of a soil-derived dust emission scheme,  
1893 *Journal of geophysical research: atmospheres*, 100, 16415-16430, 1995.

1894 Marticorena, B., Bergametti, G., Aumont, B., Callot, Y., N'Doumé, C., and Legrand, M.: Modeling the atmospheric dust  
1895 cycle: 2. Simulation of Saharan dust sources, *Journal of Geophysical Research: Atmospheres*, 102, 4387-4404, 1997.

1896 Maul, P., Barber, F., and Martin, A.: Some observations of the meso-scale transport of sulphur compounds in the rural East  
1897 Midlands, *Atmospheric Environment* (1967), 14, 339-354, 1980.

1898 McRae, G. J., Goodin, W. R., and Seinfeld, J. H.: Numerical solution of the atmospheric diffusion equation for chemically  
1899 reacting flows, *Journal of Computational Physics*, 45, 1-42, 1982.

1900 Meleux, F., Solmon, F., and Giorgi, F.: Increase in summer European ozone amounts due to climate change, *Atmospheric  
1901 Environment*, 41, 7577-7587, 2007.

1902 Memmesheimer, M., Friese, E., Ebel, A., Jakobs, H., Feldmann, H., Kessler, C., and Piekorz, G.: Long-term simulations of  
1903 particulate matter in Europe on different scales using sequential nesting of a regional model, *International Journal of  
1904 Environment and Pollution*, 22, 108-132, 2004.

1905 Ménégoz, M., Salas y Melia, D., Legrand, M., Teyssèdre, H., Michou, M., Peuch, V.-H., Martet, M., Josse, B., and  
1906 Dombrowski-Etchevers, I.: Equilibrium of sinks and sources of sulphate over Europe: comparison between a six-year  
1907 simulation and EMEP observations, *Atmospheric Chemistry and Physics*, 9, 4505-4519, 2009.

1908 Menut, L., Bessagnet, B., Briant, R., Cholakian, A., Couvidat, F., Mailler, S., Pennel, R., Siour, G., Tuccella, P., and  
1909 Turquety, S.: The CHIMERE v2020r1 online chemistry-transport model, *Geoscientific Model Development*, 14, 6781-6811,  
1910 2021.

1911 Metzger, S., Dentener, F., Pandis, S., and Lelieveld, J.: Gas/aerosol partitioning: 1. A computationally efficient model, *J.  
1912 Geophys. Res.*, 107, 4312, 2002.

1913 Michou, M., Laville, P., Serça, D., Fotiadi, A., Bouchou, P., and Peuch, V.-H.: Measured and modeled dry deposition  
1914 velocities over the ESCOMPTE area, *Atmospheric Research*, 74, 89-116, 2005.

1915 Mircea, M., Ciancarella, L., Briganti, G., Calori, G., Cappelletti, A., Cionni, I., Costa, M., Cremona, G., D'Isidoro, M.,  
1916 Finardi, S., Pace, G., Piersanti, A., Righini, G., Silibello, C., Vitali, L., and Zanini, G.: Assessment of the AMS-MINNI  
1917 system capabilities to simulate air quality over Italy for the calendar year 2005, *Atmospheric Environment*, 84, 178-188,  
1918 <https://doi.org/10.1016/j.atmosenv.2013.11.006>, 2014.

1919 Miyoshi, T. and Yamane, S.: Local Ensemble Transform Kalman Filtering with an AGCM at a T159/L48 Resolution,  
1920 *Monthly Weather Review*, 135, 3841-3861, 10.1175/2007MWR1873.1, 2007.

- 1921 Monahan, E. C.: The ocean as a source of atmospheric particles, in: The Role of Air-Sea Exchange in Geochemical Cycling,  
1922 Kluwer Academic Publishers, Dordrecht, Holland, 129–163, 1986.
- 1923 Morcrette, J. J., Boucher, O., Jones, L., Salmond, D., Bechtold, P., Beljaars, A., Benedetti, A., Bonet, A., Kaiser, J., and  
1924 Razinger, M.: Aerosol analysis and forecast in the European Centre for medium-range weather forecasts integrated forecast  
1925 system: Forward modeling, *Journal of Geophysical Research: Atmospheres*, 114, 2009.
- 1926 Mozurkewich, M.: The dissociation constant of ammonium nitrate and its dependence on temperature, relative humidity and  
1927 particle size, *Atmospheric Environment. Part A. General Topics*, 27, 261-270, 1993.
- 1928 Nenes, A., Pandis, S., and Pilinis, C.: ISORROPIA: A New Thermodynamic Equilibrium Model for Multiphase  
1929 Multicomponent Inorganic Aerosols, *Aquatic Geochemistry*, 4, 123-152, 1998.
- 1930 Nho-Kim, E.-Y., Michou, M., and Peuch, V.-H.: Parameterization of size-dependent particle dry deposition velocities for  
1931 global modeling, *Atmospheric Environment*, 38, 1933-1942, 2004.
- 1932 Nho-Kim, E., Peuch, V., and Oh, S.: Estimation of the global distribution of Black Carbon aerosols with MOCAGE, the  
1933 CTM of Météo-France, *J. Korean Meteor. Soc*, 41, 587-598, 2005.
- 1934 Nieradzik, L.: Application of a high dimensional model representation on the atmospheric aerosol module MADE of the  
1935 EURAD-CTM, *Institut für Geophysik und Meteorologie der Universität zu Köln*, 2005.
- 1936 Nieuwstadt, F.: The steady-state height and resistance laws of the nocturnal boundary layer: Theory compared with Cabauw  
1937 observations, *Boundary-Layer Meteorology*, 20, 3-17, 1981.
- 1938 Nocedal, J.: Updating quasi-Newton matrices with limited storage, *Mathematics of computation*, 35, 773-782, 1980.
- 1939 Noilhan, J. and Planton, S.: A simple parameterization of land surface processes for meteorological models, *Monthly  
1940 weather review*, 117, 536-549, 1989.
- 1941 Omstedt, G., Bringfelt, B., and Johansson, C.: A model for vehicle-induced non-tailpipe emissions of particles along  
1942 Swedish roads, *Atmospheric environment*, 39, 6088-6097, 2005.
- 1943 Pai, S. J., Heald, C. L., Pierce, J. R., Farina, S. C., Marais, E. A., Jimenez, J. L., Campuzano-Jost, P., Nault, B. A.,  
1944 Middlebrook, A. M., Coe, H., Shilling, J. E., Bahreini, R., Dingle, J. H., and Vu, K.: An evaluation of global organic aerosol  
1945 schemes using airborne observations, *Atmos. Chem. Phys.*, 20, 2637-2665, 10.5194/acp-20-2637-2020, 2020.
- 1946 Parrish, D. F. and Derber, J. C.: The National Meteorological Center's spectral statistical-interpolation analysis system,  
1947 *Monthly Weather Review*, 120, 1747-1763, 1992.
- 1948 Passant, N.: Speciation of UK emissions of non-methane volatile organic compounds, *AEA Technology* 2002.
- 1949 Pepper, D., Kern, C., and Long Jr, P.: Modeling the dispersion of atmospheric pollution using cubic splines and chapeau  
1950 functions, *Atmospheric Environment (1967)*, 13, 223-237, 1979.
- 1951 Pérez, C., Haustein, K., Jorba, O., Janjic, Z., Huneeus, N., Baldasano, J. M., Black, T., Basart, S., Nickovic, S., Miller, R. L.,  
1952 Perlwitz, J., Schulz, M., and Thomson, M.: Atmospheric dust modeling from meso to global scales with the online

1953 NMMB/BSC-Dust model–Part 1: Model description, annual simulations and evaluation, *Atmospheric Chemistry and*  
1954 *Physics*, 11, 13001-13027, 2011.

1955 Petersen, A. K., Brasseur, G. P., Bouarar, I., Flemming, J., Gauss, M., Jiang, F., Kouznetsov, R., Kranenburg, R., Mijling,  
1956 B., and Peuch, V.-H.: Ensemble forecasts of air quality in eastern China–Part 2: Evaluation of the MarcoPolo–Panda  
1957 prediction system, version 1, *Geoscientific Model Development*, 12, 1241-1266, 2019.

1958 Peterson, J. T.: Calculated actinic fluxes (290-700 nm) for air pollution photochemistry applications, US Environmental  
1959 Protection Agency, Office of Research and Development ...1976.

1960 Petroff, A. and Zhang, L.: Development and validation of a size-resolved particle dry deposition scheme for application in  
1961 aerosol transport models, *Geoscientific Model Development*, 3, 753-769, 2010.

1962 Peuch, V.-H., Engelen, R., Rixen, M., Dee, D., Flemming, J., Suttie, M., Ades, M., Agustí-Panareda, A., Ananasso, C.,  
1963 Andersson, E., Armstrong, D., Barré, J., Bousserez, N., Dominguez, J. J., Garrigues, S., Inness, A., Jones, L., Kipling, Z.,  
1964 Letertre-Danczak, J., Parrington, M., Razinger, M., Ribas, R., Vermoote, S., Yang, X., Simmons, A., Garcés de Marcilla, J.,  
1965 and Thépaut, J.-N.: The Copernicus Atmosphere Monitoring Service: From Research to Operations, *Bulletin of the*  
1966 *American Meteorological Society*, 103, E2650-E2668, <https://doi.org/10.1175/BAMS-D-21-0314.1>, 2022.

1967 Peuch, V., Engelen, R., Simmons, A., Lahoz, W., Laj, P., and Galmarini, S.: Monitoring atmospheric composition and  
1968 climate, research in support of the Copernicus/GMES atmospheric service, Special Issue, *Atmos. Chem. Phys.*, [http://www.](http://www.atmos-chem-phys.net/special_issue310.html)  
1969 [atmos-chem-phys. net/special\\_issue310. html](http://www.atmos-chem-phys.net/special_issue310.html), 2014.

1970 Poupkou, A., Giannaros, T., Markakis, K., Kioutsoukis, I., Curci, G., Melas, D., and Zerefos, C.: A model for European  
1971 Biogenic Volatile Organic Compound emissions: Software development and first validation, *Environmental Modelling &*  
1972 *Software*, 25, 1845-1856, 2010.

1973 Prank, M., Chapman, D. S., Bullock, J. M., Belmonte, J., Berger, U., Dahl, A., Jäger, S., Kovtunenkov, I., Magyar, D., and  
1974 Niemelä, S.: An operational model for forecasting ragweed pollen release and dispersion in Europe, *Agricultural and forest*  
1975 *meteorology*, 182, 43-53, 2013.

1976 Price, C., Penner, J., and Prather, M.: NO<sub>x</sub> from lightning: 1. Global distribution based on lightning physics, *Journal of*  
1977 *Geophysical Research: Atmospheres*, 102, 5929-5941, 1997.

1978 Rabitz, H. and Aliş, Ö. F.: General foundations of high-dimensional model representations, *Journal of Mathematical*  
1979 *Chemistry*, 25, 197-233, 1999.

1980 Rappenglück, B., Lubertino, G., Alvarez, S., Golovko, J., Czader, B., and Ackermann, L.: Radical precursors and related  
1981 species from traffic as observed and modeled at an urban highway junction, *Journal of the Air & Waste Management*  
1982 *Association*, 63, 1270-1286, 2013.

1983 Rémy, S., Kipling, Z., Flemming, J., Boucher, O., Nabat, P., Michou, M., Bozzo, A., Ades, M., Huijnen, V., Benedetti, A.,  
1984 Engelen, R., Peuch, V. H., and Morcrette, J. J.: Description and evaluation of the tropospheric aerosol scheme in the  
1985 European Centre for Medium-Range Weather Forecasts (ECMWF) Integrated Forecasting System (IFS-AER, cycle 45R1),  
1986 *Geosci. Model Dev.*, 12, 4627-4659, [10.5194/gmd-12-4627-2019](https://doi.org/10.5194/gmd-12-4627-2019), 2019.

1987 Robertson, L., Langner, J., and Engardt, M.: An Eulerian limited-area atmospheric transport model, *Journal of Applied*  
1988 *Meteorology and Climatology*, 38, 190-210, 1999.

- 1989 Robichaud, A. and Ménard, R.: Multi-year objective analyses of warm season ground-level ozone and PM 2.5 over North  
1990 America using real-time observations and Canadian operational air quality models, *Atmospheric Chemistry and Physics*, 14,  
1991 1769-1800, 2014.
- 1992 Roselle, S. J. and Binkowski, F. S.: Cloud dynamics and chemistry, Science algorithms of the EPA Models-3 Community  
1993 multiscale air quality (CMAQ) modeling system, 1999.
- 1994 Rouil, L., Honore, C., Vautard, R., Beekmann, M., Bessagnet, B., Malherbe, L., Meleux, F., Dufour, A., Elichegaray, C.,  
1995 Flaud, J. M., Menut, L., Martin, D., Peuch, A., Peuch, V. H., and Poisson, N.: PREV'AIR An Operational Forecasting and  
1996 Mapping System for Air Quality in Europe, *Bulletin of the American Meteorological Society*, 90, 73-83,  
1997 10.1175/2008bams2390.1, 2009.
- 1998 Salameh, T., Drobinski, P., Menut, L., Bessagnet, B., Flamant, C., Hodzic, A., and Vautard, R.: Aerosol distribution over the  
1999 western Mediterranean basin during a Tramontane/Mistral event, *Annales Geophysicae*, 25, 2271-2291, 2007.
- 2000 Sander, S., Golden, D., Kurylo, M., Moortgat, G., Wine, P., Ravishankara, A., Kolb, C., Molina, M., Finlayson-Pitts, B., and  
2001 Huie, R.: Chemical kinetics and photochemical data for use in atmospheric studies evaluation number 15, Pasadena, CA: Jet  
2002 Propulsion Laboratory, National Aeronautics and Space ..., 2006.
- 2003 Sandu, A. and Sander, R.: Simulating chemical systems in Fortran90 and Matlab with the Kinetic PreProcessor KPP-2.1,  
2004 *Atmospheric Chemistry and Physics*, 6, 187-195, 2006.
- 2005 Sarwar, G., Simon, H., Bhave, P., and Yarwood, G.: Examining the impact of heterogeneous nitryl chloride production on  
2006 air quality across the United States, *Atmospheric Chemistry and Physics*, 12, 6455-6473, 2012.
- 2007 Schaap, M., Van Loon, M., Ten Brink, H., Dentener, F., and Bultjes, P.: Secondary inorganic aerosol simulations for Europe  
2008 with special attention to nitrate, *Atmospheric Chemistry and Physics*, 4, 857-874, 2004.
- 2009 Schaap, M., Kranenburg, R., Curier, L., Jozwicka, M., Dammers, E., and Timmermans, R.: Assessing the sensitivity of the  
2010 OMI-NO2 product to emission changes across Europe, *Remote Sensing*, 5, 4187-4208, 2013.
- 2011 Schaap, M., Manders, A. M. M., Hendriks, E. C. J., Cnossen, J. M., Segers, A. J. S., Denier van der Gon, H., Jozwicka, M.,  
2012 Sauter, F. J., Velders, G. J. M., Matthijsen, J., and Bultjes, P. J. H.: Regional Modelling of Particulate Matter for the  
2013 Netherlands Netherlands Research Program on Particulate Matter, ISSN: 1875-2314, 2009.
- 2014 Schell, B., Ackermann, I. J., Hass, H., Binkowski, F. S., and Ebel, A.: Modeling the formation of secondary organic aerosol  
2015 within a comprehensive air quality model system, *Journal of Geophysical Research: Atmospheres*, 106, 28275-28293,  
2016 2001a.
- 2017 Schell, B., Ackermann, I. J., Hass, H., Binkowski, F. S., and Ebel, A.: Modelling the formation of secondary organic within a  
2018 comprehensive air quality model system, *J. Geophys. Res.*, 106, 28275-28293, 2001b.
- 2019 Schultz, M. G., Backman, L., Balkanski, Y., Bjoerndalsaeter, S., Brand, R., Burrows, J. P., Dalsoeren, S., de Vasconcelos,  
2020 M., Grodtmann, B., Hauglustaine, D., Heil, A., Hoelzemann, J., Isaksen, I. S. A., Kaurola, J., Knorr, W., Ladstaetter-  
2021 Weißenmayer, A., Mota, B., Oom, D., Pacyna, J., Panasiuk, D., Pereira, J., Pulles, T., Pyle, J., Rast, S., Richter, A., Savage,  
2022 N., Schnadt, C., Schulz, M., Spessa, A., Staehelin, J., Sundet, J. K., Szopa, S., Thonicke, K., van het Bolscher, M., van  
2023 Noije, T., van Velthoven, P., Vik, A. F., and Wittrock F.: REanalysis of the TROpospheric chemical composition over the

2024 past 40 years (RETRO) — A long-term global modeling study of tropospheric chemistry Final Report, Max Planck Institute  
2025 for Meteorology, Jülich/Hamburg, Germany, , ISSN 1614-1199, 2007.

2026 Schutgens, N. A. J., Miyoshi, T., Takemura, T., and Nakajima, T.: Applying an ensemble Kalman filter to the assimilation of  
2027 AERONET observations in a global aerosol transport model, *Atmos. Chem. Phys.*, 10, 2561-2576, 10.5194/acp-10-2561-  
2028 2010, 2010.

2029 Seinfeld, J. H. and Pandis, S. N.: *Atmospheric Chemistry and Physics, From Air Pollution to Climate Change.*, New York,  
2030 USA.1998.

2031 Shaddick, G., Salter, J. M., Peuch, V.-H., Ruggeri, G., Thomas, M. L., Mudu, P., Tarasova, O., Baklanov, A., and Gumy, S.:  
2032 Global air quality: An inter-disciplinary approach to exposure assessment for burden of disease analyses, *Atmosphere*, 12,  
2033 48, 2020.

2034 Shrivastava, M. K., Lane, T. E., Donahue, N. M., Pandis, S. N., and Robinson, A. L.: Effects of gas particle partitioning and  
2035 aging of primary emissions on urban and regional organic aerosol concentrations, *Journal of Geophysical Research:*  
2036 *Atmospheres*, 113, 2008.

2037 Sič, B., El Amraoui, L., Marécal, V., Josse, B., Arteta, J., Guth, J., Joly, M., and Hamer, P.: Modelling of primary aerosols in  
2038 the chemical transport model MOCAGE: Development and evaluation of aerosol physical parameterizations, *Geoscientific*  
2039 *Model Development*, 8, 381-408, 2015.

2040 Silibello, C., Calori, G., Brusasca, G., Giudici, A., Angelino, E., Fossati, G., Peroni, E., and Buganza, E.: Modelling of  
2041 PM10 concentrations over Milano urban area using two aerosol modules, *Environmental Modelling & Software*, 23, 333-  
2042 343, 2008.

2043 Silver, J. D., Christensen, J. H., Kahnert, M., Robertson, L., Rayner, P. J., and Brandt, J.: Multi-species chemical data  
2044 assimilation with the Danish Eulerian hemispheric model: system description and verification, *Journal of Atmospheric*  
2045 *Chemistry*, 73, 261-302, 2016.

2046 Simpson, D., Benedictow, A., and Darras, S.: The CAMS soil emissions: CAMS-GLOB-SOIL, in: CAMS2\_61 – Global and  
2047 European emission inventories., 59–70, <https://doi.org/10.24380/q2si-ti6i>, 2023.

2048 Simpson, D., Guenther, A., Hewitt, C., and Steinbrecher, R.: Biogenic emissions in Europe 1. Estimates and uncertainties, *J.*  
2049 *Geophys. Res.*, 100, 22875–22890, 1995.

2050 Simpson, D., Fagerli, H., Jonson, J., Tsyro, S., Wind, P., and Tuovinen, J.-P.: The EMEP Unified Eulerian Model. Model  
2051 Description, The Norwegian Meteorological Institute, EMEP, Oslo, 2003.

2052 Simpson, D., Bergström, R., Briolat, A., Imhof, H., Johansson, J., Priestley, M., and Valdebenito, A.: GenChem v1. 0—a  
2053 chemical pre-processing and testing system for atmospheric modelling, *Geoscientific Model Development*, 13, 6447-6465,  
2054 2020a.

2055 Simpson, D., Benedictow, A., Berge, H., Bergstrom, R., Emberson, L. D., Fagerli, H., Flechard, C. R., Hayman, G. D.,  
2056 Gauss, M., Jonson, J. E., Jenkin, M. E., Nyiri, A., Richter, C., Semeena, V. S., Tsyro, S., Tuovinen, J. P., Valdebenito, A.,  
2057 and Wind, P.: The EMEP MSC-W chemical transport model - technical description, *Atmos. Chem. Phys.*, 12, 7825-7865,  
2058 2012.

2059 Simpson, D., Fagerli, H., Colette, A., Denier van der Gon, H., Dore, C., Hallquist, M., Hansson, H.-C., Maas, R., Rouil, L.,  
2060 Allemand, N., Bergström, B., Bessagnet, B., Couvidat, F., El Haddad, I., Genberg Safont, J., Goile, F., Grieshop, A.,  
2061 Fraboulet, I., Hallquist, A., Hamilton, J., Juhlich, K., Klimont, Z., Kregar, Z., Mawdsely, I., Megaritis, A., Ntziachristos, L.,  
2062 Pandis, S., Prévôt, A. S. H., Schindlbacher, S., Seljeskog, M., Sirina-Leboine, N., Sommers, J., and Åström, S.: How should  
2063 condensables be included in PM emission inventories reported to EMEP/CLRTAP?, EMEP, Oslo, 2020b.

2064 Sindelarova, K., Granier, C., Bouarar, I., Guenther, A., Tilmes, S., Stavrakou, T., Müller, J. F., Kuhn, U., Stefani, P., and  
2065 Knorr, W.: Global data set of biogenic VOC emissions calculated by the MEGAN model over the last 30 years, Atmos.  
2066 Chem. Phys., 14, 9317-9341, 10.5194/acp-14-9317-2014, 2014.

2067 Slinn, W., Hasse, L., Hicks, B., Hogan, A., Lal, D., Liss, P., Munnich, K., Sehmel, G., and Vittori, O.: Some aspects of the  
2068 transfer of atmospheric trace constituents past the air-sea interface, Atmospheric Environment (1967), 12, 2055-2087, 1978.

2069 Slinn, W. G. N.: Precipitation scavenging, US. Department of Energy, Washington, D.C., 1983.

2070 Smagorinsky, J.: General circulation experiments with the primitive equations: I. The basic experiment, Monthly weather  
2071 review, 91, 99-164, 1963.

2072 Soares, J., Sofiev, M., Geels, C., Christensen, J. H., Andersson, C., Tsyro, S., and Langner, J.: Impact of climate change on  
2073 the production and transport of sea salt aerosol on European seas, Atmospheric Chemistry and Physics, 16, 13081-13104,  
2074 2016.

2075 Sofiev, M.: A model for the evaluation of long-term airborne pollution transport at regional and continental scales,  
2076 Atmospheric Environment, 34, 2481-2493, 2000.

2077 Sofiev, M.: Extended resistance analogy for construction of the vertical diffusion scheme for dispersion models, Journal of  
2078 Geophysical Research: Atmospheres, 107, ACH 10-11-ACH 10-18, 2002.

2079 Sofiev, M.: On possibilities of assimilation of near-real-time pollen data by atmospheric composition models, Aerobiologia,  
2080 35, 523-531, 2019.

2081 Sofiev, M., Galperin, M., and Genikhovich, E.: Construction and evaluation of Eulerian dynamic core for the air quality and  
2082 emergency modelling system SILAM

2083 NATO Science for peace and security, Series C: Environmental Security, Air pollution modelling and its application, XIX,  
2084 Springer, 699-701 pp.2008.

2085 Sofiev, M., Genikhovich, E., Keronen, P., and Vesala, T.: Diagnosing the surface layer parameters for dispersion models  
2086 within the meteorological-to-dispersion modeling interface, Journal of applied meteorology and climatology, 49, 221-233,  
2087 2010.

2088 Sofiev, M., Soares, J., Prank, M., de Leeuw, G., and Kukkonen, J.: A regional-to-global model of emission and transport of  
2089 sea salt particles in the atmosphere, J. Geophys. Res., 116, doi:10.1029/2010JD014713, 2011.

2090 Sofiev, M., Vira, J., Kouznetsov, R., Prank, M., Soares, J., and Genikhovich, E.: Construction of an Eulerian atmospheric  
2091 dispersion model based on the advection algorithm of M. Galperin: dynamic cores v. 4 and 5 of SILAM v. 5.5, Geoscientific  
2092 Model Development Discussions, 8, 2015a.

2093 Sofiev, M., Siljamo, P., Ranta, H., Linkosalo, T., Jaeger, S., Rasmussen, A., Rantio-Lehtimäki, A., Severova, E., and  
2094 Kukkonen, J.: A numerical model of birch pollen emission and dispersion in the atmosphere. Description of the emission  
2095 module, *International journal of biometeorology*, 57, 45-58, 2013.

2096 Sofiev, M., Berger, U., Prank, M., Vira, J., Arteta, J., Belmonte, J., Bergmann, K. C., Chéroux, F., Elbern, H., Friese, E.,  
2097 Galan, C., Gehrig, R., Khvorostyanov, D., Kranenburg, R., Kumar, U., Marécal, V., Meleux, F., Menut, L., Pessi, A. M.,  
2098 Robertson, L., Rittenberga, O., Rodinkova, V., Saarto, A., Segers, A., Severova, E., Sauliene, I., Siljamo, P., Steensen, B. M.,  
2099 Teinmaa, E., Thibaudon, M., and Peuch, V. H.: MACC regional multi-model ensemble simulations of birch pollen  
2100 dispersion in Europe, *Atmos. Chem. Phys.*, 15, 8115-8130, 10.5194/acp-15-8115-2015, 2015b.

2101 Sofieva, S., Asmi, E., Atanasova, N. S., Heikkinen, A. E., Vidal, E., Duplissy, J., Romantschuk, M., Kouznetsov, R.,  
2102 Kukkonen, J., and Bamford, D. H.: Effects of temperature and salinity on sea-spray-aerosol formation simulated with a  
2103 bubble-generating chamber, *Atmospheric Measurement Techniques Discussions*, 2022, 1-40, 2022.

2104 Spada, M.: Development and evaluation of an atmospheric aerosol module implemented within the NMMB/BSC-CTM,  
2105 2015.

2106 Spada, M., Jorba, O., Pérez García-Pando, C., Janjic, Z., and Baldasano, J. M.: Modeling and evaluation of the global sea-  
2107 salt aerosol distribution: sensitivity to size-resolved and sea-surface temperature dependent emission schemes, *Atmos. Chem.*  
2108 *Phys.*, 13, 11735-11755, 10.5194/acp-13-11735-2013, 2013.

2109 Stadtler, S., Simpson, D., Schröder, S., Taraborrelli, D., Bott, A., and Schultz, M.: Ozone impacts of gas–aerosol uptake in  
2110 global chemistry transport models, *Atmospheric Chemistry and Physics*, 18, 3147-3171, 2018.

2111 Stockwell, W. R., Kirchner, F., Kuhn, M., and Seefeld, S.: A new mechanism for regional atmospheric chemistry modeling,  
2112 *Journal of Geophysical Research: Atmospheres*, 102, 25847-25879, 1997.

2113 Strand, A. and Hov, O.: A two-dimensional global study of tropospheric ozone production, *J Geophys Res* 99, 22877-22895,  
2114 1994.

2115 Struzewska, J. and Kaminski, J.: Formation and transport of photooxidants over Europe during the July 2006 heat wave–  
2116 observations and GEM-AQ model simulations, *Atmospheric Chemistry and Physics*, 8, 721-736, 2008.

2117 Struzewska, J. and Kaminski, J.: Impact of urban parameterization on high resolution air quality forecast with the GEM–AQ  
2118 model, *Atmospheric Chemistry and Physics*, 12, 10387-10404, 2012.

2119 Struzewska, J., Kaminski, J., and Jefimow, M.: Application of model output statistics to the GEM-AQ high resolution air  
2120 quality forecast, *Atmospheric Research*, 181, 186-199, 2016.

2121 Struzewska, J., Zdunek, M., Kaminski, J., Łobocki, L., Porebska, M., Jefimow, M., and Gawuc, L.: Evaluation of the GEM-  
2122 AQ model in the context of the AQMEII Phase 1 project, *Atmospheric Chemistry and Physics*, 15, 3971-3990, 2015.

2123 Thürkow, M., Kirchner, I., Kranenburg, R., Timmermans, R., and Schaap, M.: A multi-meteorological comparison for  
2124 episodes of PM10 concentrations in the Berlin agglomeration area in Germany with the LOTOS-EUROS CTM, *Atmospheric*  
2125 *Environment*, 244, 117946, 2021.

2126 Tie, X., Madronich, S., Walters, S., Zhang, R., Rasch, P., and Collins, W.: Effect of clouds on photolysis and oxidants in the  
2127 troposphere, *Journal of Geophysical Research: Atmospheres*, 108, 2003.

2128 Timmermans, R., van Pinxteren, D., Kranenburg, R., Hendriks, C., Fomba, K., Herrmann, H., and Schaap, M.: Evaluation of  
2129 modelled LOTOS-EUROS with observational based PM10 source attribution, *Atmospheric Environment: X*, 14, 100173,  
2130 2022.

2131 Troen, I. and Mahrt, L.: A simple model of the atmospheric boundary layer: Sensitivity to surface evaporation, *Bound.-Layer*  
2132 *Meteorol.*, 37, 129-148, 1986.

2133 Tsyro, S., Aas, W., Soares, J., Sofiev, M., Berge, H., and Spindler, G.: Modelling of sea salt concentrations over Europe: key  
2134 uncertainties and comparison with observations, *Atmos. Chem. Phys.*, 11, 10367–10388, doi:10.5194/acp-11-10367-2011,  
2135 2011.

2136 Tuovinen, J.-P., Ashmore, M., Emberson, L., and Simpson, D.: Testing and improving the EMEP ozone deposition module,  
2137 *Atmos. Environ.*, 38, 2373–2385, 2004.

2138 van Leer, B.: Multidimensional explicit difference schemes for hyperbolic conservation laws, in: *Computing Methods in*  
2139 *Applied Sciences and Engineering VI*, edited by: Lions, R. G. a. J. L., Elsevier, Amsterdam, 1984.

2140 Van Ulden, A. and Holtslag, A.: Estimation of atmospheric boundary layer parameters for diffusion applications, *Journal of*  
2141 *Applied Meteorology and Climatology*, 24, 1196-1207, 1985.

2142 Van Zanten, M., Sauter, F., RJ, W. K., Van Jaarsveld, J., and Van Pul, W.: Description of the DEPAC module: Dry  
2143 deposition modelling with DEPAC\_GCIN2010, RIVM rapport 680180001, 2010.

2144 Vautard, R., Bessagnet, B., Chin, M., and Menut, L.: On the contribution of natural Aeolian sources to particulate matter  
2145 concentrations in Europe: Testing hypotheses with a modelling approach, *Atmospheric Environment*, 39, 3291-3303,  
2146 <https://doi.org/10.1016/j.atmosenv.2005.01.051>, 2005.

2147 Venkatram, A.: Estimating the Monin-Obukhov length in the stable boundary layer for dispersion calculations, *Boundary-*  
2148 *Layer Meteorology*, 19, 481-485, 1980.

2149 Venkatram, A. and Pleim, J.: The electrical analogy does not apply to modelling dry deposition of particles, *Atmos.*  
2150 *Environ.*, 33, 3075-3076, 1999.

2151 Venkatram, A., Karamchandani, P., and Misra, P.: Testing a comprehensive acid deposition model, *Atmospheric*  
2152 *Environment* (1967), 22, 737-747, 1988.

2153 Vira, J. and Sofiev, M.: On variational data assimilation for estimating the model initial conditions and emission fluxes for  
2154 short-term forecasting of SOx concentrations, *Atmospheric environment*, 46, 318-328, 2012.

2155 Vira, J. and Sofiev, M.: Assimilation of surface NO<sub>2</sub> and O<sub>3</sub> observations into the SILAM chemistry transport model,  
2156 *Geoscientific Model Development*, 8, 191-203, 2015.

2157 Wang, X., Zhang, L., and Moran, M. D.: Development of a new semi-empirical parameterization for below-cloud  
2158 scavenging of size-resolved aerosol particles by both rain and snow, *Geoscientific Model Development*, 7, 799-819, 2014.

2159 Weaver, A. and Courtier, P.: Correlation modelling on the sphere using a generalized diffusion equation, *Quarterly Journal*  
2160 *of the Royal Meteorological Society*, 127, 1815-1846, 2001.



2161 Wesely, M. L.: Parameterization of surface resistances to gaseous dry deposition in regional-scale numerical models,  
 2162 Atmospheric Environment (1967), 23, 1293-1304, 1989.

2163 Wild, O., Zhu, X., and Prather, M. J.: Fast-J: Accurate Simulation of In- and Below-Cloud Photolysis in Tropospheric  
 2164 Chemical Models, Journal of Atmospheric Chemistry, 37, 245-282, 10.1023/A:1006415919030, 2000.

2165 Williams, E., Guenther, A., and Fehsenfeld, F.: An inventory of nitric oxide emissions from soils in the United States,  
 2166 Journal of Geophysical Research: Atmospheres, 97, 7511-7519, 1992.

2167 Williamson, D. L. and Rasch, P. J.: Two-dimensional semi-Lagrangian transport with shape-preserving interpolation,  
 2168 Monthly Weather Review, 117, 102-129, 1989.

2169 Willis, P. T. and Tattelman, P.: Drop-size distributions associated with intense rainfall, Journal of Applied Meteorology and  
 2170 Climatology, 28, 3-15, 1989.

2171 Xian, P., Reid, J. S., Hyer, E. J., Sampson, C. R., Rubin, J. I., Ades, M., Asencio, N., Basart, S., Benedetti, A., and  
 2172 Bhattacharjee, P. S.: Current state of the global operational aerosol multi-model ensemble: An update from the International  
 2173 Cooperative for Aerosol Prediction (ICAP), Quarterly Journal of the Royal Meteorological Society, 145, 176-209, 2019.

2174 Yamartino, R., Scire, J., Carmichael, G., and Chang, Y.: The CALGRID mesoscale photochemical grid model—I. Model  
 2175 formulation, Atmospheric Environment. Part A. General Topics, 26, 1493-1512, 1992.

2176 Yamartino, R. J., Flemming, J., and Stern, R.: Adaptation of analytic diffusivity formulations to Eulerian grid model layers  
 2177 of finite thickness, in: Air Pollution Modeling and Its Application XVII, Springer, 468-477, 2007.

2178 Yarwood, G., Rao, S., Yocke, M., and Whitten, G. Z.: Updates to the Carbon Bond chemical mechanism: CB05,  
 2179 [http://www.camx.com/publ/pdfs/CB05\\_Final\\_Report\\_120805.pdf](http://www.camx.com/publ/pdfs/CB05_Final_Report_120805.pdf), 2005.

2180 Yienger, J. and Levy, H.: Empirical model of global soil-biogenic NO<sub>x</sub> emissions, Journal of Geophysical Research:  
 2181 Atmospheres, 100, 11447-11464, 1995.

2182 Yuan, H., Dai, Y., Xiao, Z., Ji, D., and Shangguan, W.: Reprocessing the MODIS Leaf Area Index Products for Land  
 2183 Surface and Climate Modelling, Remote Sensing of Environment, 155, 1171–1187, doi:10.1016/j.rse.2011.01.001, 2011.

2184 Zare, A., Christensen, J., Irannejad, P., and Brandt, J.: Evaluation of two isoprene emission models for use in a long-range  
 2185 air pollution model, Atmospheric Chemistry and Physics, 12, 7399-7412, 2012.

2186 Zare, A., Christensen, J., Gross, A., Irannejad, P., Glasius, M., and Brandt, J.: Quantifying the contributions of natural  
 2187 emissions to ozone and total fine PM concentrations in the Northern Hemisphere, Atmospheric Chemistry and Physics, 14,  
 2188 2735-2756, 2014.

2189 Zender, C. S., Bian, H., and Newman, D.: Mineral Dust Entrainment and Deposition (DEAD) model: Description and 1990s  
 2190 dust climatology, Journal of Geophysical Research: Atmospheres, 108, 10.1029/2002jd002775, 2003.

2191 Zhang, K. M., Knipping, E. M., Wexler, A. S., Bhawe, P. V., and Tonnesen, G. S.: Size distribution of sea-salt emissions as a  
 2192 function of relative humidity, Atmospheric Environment, 39, 3373-3379, <https://doi.org/10.1016/j.atmosenv.2005.02.032>,  
 2193 2005.

2194 Zhang, L., Brook, J. R., and Vet, R.: A revised parameterization for gaseous dry deposition in air-quality models, *Atmos.*  
2195 *Chem. Phys.*, 3, 2067–2082, 2003.

2196 Zhang, L., Gong, S., Padro, J., and Barrie, L.: A size-segregated particle dry deposition scheme for an atmospheric aerosol  
2197 module, *Atmospheric Environment*, 35, 549-560, 2001.

2198 Zhang, Y., Bocquet, M., Mallet, V., Seigneur, C., and Baklanov, A.: Real-time air quality forecasting, part I: History,  
2199 techniques, and current status, *Atmospheric Environment*, 60, 632-655, 2012a.

2200 Zhang, Y., Bocquet, M., Mallet, V., Seigneur, C., and Baklanov, A.: Real-time air quality forecasting, part II: State of the  
2201 science, current research needs, and future prospects, *Atmospheric Environment*, 60, 656-676,  
2202 <https://doi.org/10.1016/j.atmosenv.2012.02.041>, 2012b.

2203 Zilitinkevich, S. and Mironov, D. V.: A multi-limit formulation for the equilibrium depth of a stably stratified boundary  
2204 layer, *Boundary-Layer Meteorology*, 81, 325-351, 1996.  
2205